KfK 5027
Mai 1992

Annual Report on Nuclear Physics Activities

January 1, 1991 – December 31, 1991

Editors:
J. Knapp, H. Rebel
Institut für Kernphysik

Kernforschungszentrum Karlsruhe

KERNFORSCHUNGSZENTRUM KARLSRUHE

Institut für Kernphysik

KfK 5027

ANNUAL REPORT

on

NUCLEAR PHYSICS ACTIVITIES

January 1, 1991 - December 31, 1991

Editors:

J. Knapp and H. Rebel

Kernforschungszentrum Karlsruhe GmbH, Karlsruhe

Kernforschungszentrum Karlsruhe GmbH
Postfach 3640, 7500 Karlsruhe 1

ISSN 0303-4003

ABSTRACT

This annual report surveys the research activities from January 1, to December 31, 1991 at the Institute of Nuclear Physics (IK) of the Kernforschungszentrum Karlsruhe. The research program comprises experimental investigations of cosmic rays, neutrino physics with the KARMEN detector, nuclear astrophysics and nuclear reactions, laser spectroscopy of radioactive species and applications of nuclear methods. The presentation includes a status report of the KASCADE project.

ZUSAMMENFASSUNG

Der vorliegende Jahresbericht gibt einen Überblick über die Forschungsarbeiten am Institut für Kernphysik (IK) des Kernforschungszentrums Karlsruhe im Zeitraum vom 1. Januar bis 31. Dezember 1991. Das Forschungsprogramm umfaßt experimentelle Untersuchungen der kosmischen Strahlung, Neutrino-Physik am KARMEN-Detektor, nukleare Astrophysik und Kernreaktionen, Laserspektroskopie radioaktiver Isotope sowie praktische Anwendungen nuklearer Methoden. Der Report beinhaltet einen Status-Bericht des KASCADE-Projektes.

PREFACE

The annual report gives a survey on current nuclear physics and astrophysics activities at the Kernforschungszentrum Karlsruhe and it describes the studies carried out in the Institut für Kernphysik. Our department is divided in two sections, labelled, for historical reasons, IK I and IK III.

The report covers the following subjects :

- **Astrophysics with Extensive Air Showers** : A joint project of both sections is KASCADE (KArlsruhe Shower Core and Array DEtector), a large detector system for experimental studies of cosmic rays, presently under development and construction at the site of the Kernforschungszentrum Karlsruhe. The experiment aims at information on the elemental composition of the primary cosmic ray particles by observation and analysis of the electromagnetic, muonic and hadronic components of extensive air showers. In addition, the measurements will contribute to clarifications of the question of cosmic ray point sources for which enigmatic features are observed.

Construction of the detector system and installation of various components have started, accompanied by comprehensive prototype and detector development studies. Extensive Monte-Carlo simulations of the passage of cosmic rays through the atmosphere try to explore the relation between the experimental shower parameters and the nature of the primary cosmic rays.

Additional activities of Section IK I are concentrated in the field :

- **Neutrino Physics** : The KArlsruhe Rutherford interMediate Energy Neutrino experiment KARMEN makes use of the pulsed 'beam stop' neutrinos ν_μ, ν_e and $\bar{\nu}_\mu$ produced at the spallation neutron source ISIS of the Rutherford Appleton Laboratory (England). The program involves experimental studies of fundamental questions in the fields of particle physics (ν-oscillations) and nuclear physics (ν-nucleus interactions).

First results of the measurements of the charged current and neutral current neutrino-nucleus interactions on ^{12}C with their implications for weak interaction physics are reported and the status of the search for neutrino oscillations is discussed.

Section IK III is additionally working in following fields :

- **Nuclear Astrophysics** : Capture cross sections of fast neutrons in the keV range are measured in order to understand in detail the synthesis of heavy elements in stars. In this work, a considerable increase in accuracy has been achieved by use of a novel 4π scintillation counter made of BaF_2. Results with this detector demonstrate a level of accuracy not attained before. Further experiments deal with the measurement of very small neutron capture cross sections by activation and with nuclear spectroscopy to obtain nuclear structure information required for the astrophysical interpretation of the data.

- **Nuclear Reactions** : Experiments in this field had been performed earlier using the 156 MeV ^{6}Li beam from the Karlsruhe Isochronous Cyclotron. They have now been terminated in favour of the KASCADE experiment. A number of results have only been published recently and are reported.

- **Laser Spectroscopy** : This technique is applied to sub-ng amounts of radioactive atoms in order to determine hyperfine structure and isotopic shifts of atomic transitions. The results yield information on nuclear moments and on the change of nuclear charge radii due to varying neutron number. Work at present concentrates on hafnium ions stored in a Paul ion trap.

- **Applied Gamma-Ray Spectroscopy** : Here instruments are developed to determine concentration and isotopic composition of fissile materials. The instruments make use either of the intrinsic radioactivity or of X-ray absorption and fluorescence. Their main applications are in the safeguards of nuclear fuel and in process control during fabrication and reprocessing.

(B. Zeitnitz)

(G. Schatz)

CONTENT

1. ASTROPHYSICS WITH EXTENDED AIR SHOWERS

1.1 STATUS REVIEW OF THE KASCADE PROJECT

J. ENGLER, H.J. GILS, H.O. KLAGES, H. REBEL, G. SCHATZ, B. ZEITNITZ

KASCADE, the KArlsruhe Shower Core and Array DEtektor being under construction at the KfK site, is an experimental set-up for measuring various observables of extensive air showers (EAS) induced in the atmosphere by ultra high energy cosmic rays. The motivation for the experiment is the great astrophysical interest in reliable information on the elemental composition of the cosmic ray primaries at energies above 10^{14} eV [1]. For that purpose KASCADE is designed to observe the electromagnetic, muonic, and hadronic components of extensive air showers in the primary energy range 10^{14} - 10^{17} eV.

The KASCADE set-up consists of mainly two components, an array of about 300 detector stations positioned on a rectangular grid of 13 m grid size and a central detector of 16x20 m^2 lateral size. The detector array will measure the density and lateral distribution of the widely extended electromagnetic (e/γ) and muonic components of air showers, whereas the central detector will analyze the hadron and high energetic muon component in the narrow shower core. More details of the experimental set-up have previously been reported [2] and are given in the following contributions.

During the period covered by this report the efforts for KASCADE have been concentrated on the following subjects, which are more detailed in further contributions of this report :

Detector array : Measurements of EAS were performed with the prototype cluster of the array. Following the experience with this cluster, improvements and modifications were made for the e/γ and μ detectors. The analog and digital frontend electronics is being designed and prototypes of some components were tested. Detector and control stations of two further clusters were mounted. Various equipment was provided for producing and testing large numbers of detector components. The laser system for relative-time calibration of the detector stations was brought into operation.

Central calorimeter : Construction of the basement for the central detector was completed. It is shown in fig.1 together with the detector array stations. Nearly

All the iron absorber slabs have been cast and delivered. A detailed mechanical design for stacking the iron slabs was made. Stacking will start in May '92 and is expected to end in July '92. A number of about 1000 liquid ionisation chambers were produced and partly tested with a secondary triton beam at the cyclotron. Production rate will be increased by providing new tools and, in particular, an additional filling station for the ionization liquid. The design of the digitizing electronics was finished. First experimental studies on secondary hadrons from cosmic rays have been started with a prototype calorimeter.

Fig. 1 : View of the KASCADE-site by end of 1991. The picture shows three clusters of array detector stations in the foreground and the basement for the central detector and central electronic stations in the background.

Muon chambers in the central detector : The frames and rails for mounting the multiwire proportional chambers for muon detection in the basement of the central detector have been designed and partly constructed. Prototype parts of the new frontend electronics have been tested. The microprocessor-controlled multiplexers have been designed and a first prototype is in test operation [3].

Experimental studies with a prototype set-up consisting of a stack of 4 muon chambers were continued.

Trigger : Design studies of the layout of the trigger detector plane in the central detector have been performed and prototype modules are under construction. The corresponding trigger electronics is also being designed.

Central data acquisition : A concept for the central data acquisition system has been worked out including a special microprocessor array which links the interrelated experimental data. Software concepts adapted to the computer hardware configuration are being developed.

[1] P. Doll et al., KfK Report 4686 (1990), Kernforschungszentrum Karlsruhe

[2] J. Engler et al., KfK Report 4875 (1991), eds. H. Beer, J. Wochele, Kernforschungszentrum Karlsruhe, p.59
F. Bauer et al., ibid, p. 62

[3] D. Bormann, Internal Note, HPE des Kernforschungszentrums Karlsruhe (1991)

1.2 THE KASCADE ARRAY

1.2.1 STATUS AND PROGRESS OF THE KASCADE ARRAY

F. BAUER, B. BODMANN*, F.P. BRADY**, P. DOLL,
R. GLASSTETTER, R. GUMBSHEIMER, D. HAUNSCHILD,
H. HUCKER, H. KERN, H.O. KLAGES, A. KRETSCHMANN***,
W. KRIEGLEDER, F. KRÖNER, H.LEICH***, H.-J. MAYER,
U. MEYER***, G. MONDRY, H. MÜLLER, C. RÄMER,
A. SCHALLER*, H. SCHIELER, G. SCHMALZ, H.J. SIMONIS,
H. SKACEL, T. STOLLA*, G. VÖLKER, P. WEGNER***,
Y. WETZEL, J. ZABIEROWSKI****

Measurements with the prototype cluster : The installation of the first cluster of 16 detector stations of the KASCADE array has been completed in February, 1991. Using a preliminary NIM- and CAMAC-based electronics 64 detectors for the electron/photon component and 16 detectors for the muon component of extensive air showers were put into operation. Details of the detector design, indicated in fig.1, are given in previous reports [1]. With penetrating cosmic muons the detector properties were studied, adjusting the individual high voltage operation values to equalize the muon energy loss spectra for all modules. No variation was observed for temperature changes between 0°C and 30°C. This corresponds to the cancellation of the (small) changes of the scintillator light output and of the photomultiplier gain with temperature. All signal cables are of equal length and put in tubes underground as indicated in the schematic layout of a cluster in fig.2. In a further step, the operational conditions of the detectors have been kept fixed. A simple hardware multiplicity trigger was put into operation to measure the response of the prototype cluster to extensive air showers. Details of the trigger and the electronics are given in refs.[2,3].

The pulse heights of all detectors and the relative arrival times for about 10^6 showers were measured in a multi-parameter listmode experiment and written on tape by a LSI 11/73 online computer. The distribution of measured pulse heights enabled the reconstruction of the air showers only insofar as to classify two categories: (i) core inside the cluster and (ii) core outside (the majority of events). The comparatively small area of the prototype cluster (~ 40x40 m^2) does not allow a detailed reconstruction of shower size and age. However, simplified Monte-Carlo simulations of the response of one cluster to a 'typical' set of air showers show

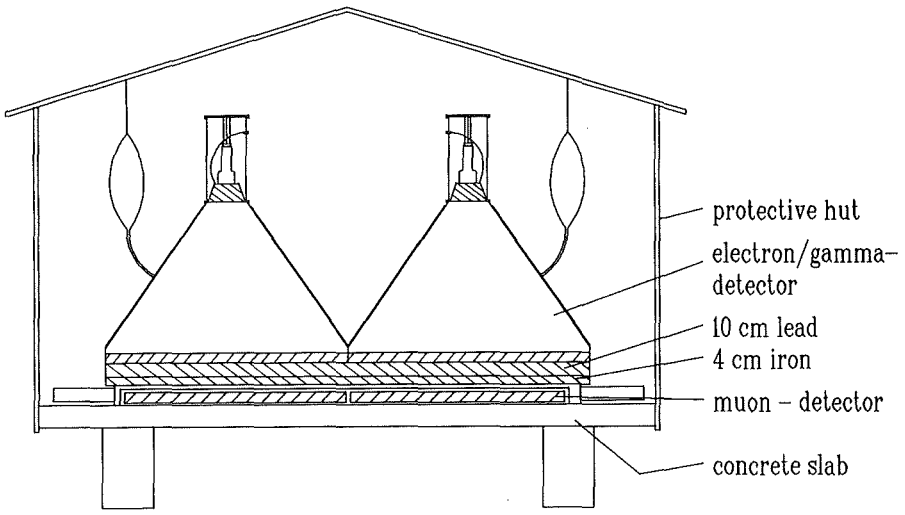

Fig.1 : Schematic view of a detector station of the KASCADE array.

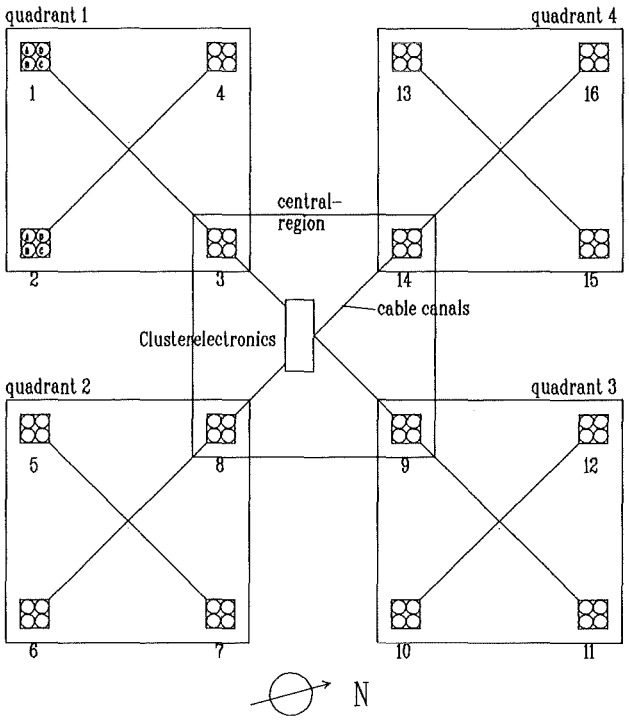

Fig.2 : Sixteen detector stations grouped as a cluster.

remarkable agreement with the measured data. In order to enable the reconstruction of the shower direction from the measured arrival time differences, the time delays of the individual detectors are determined experimentally. For this purpose, a pulsed laser was used together with a fiber optic light distribution system [1]. The individual delays were measured with a typical accuracy of 100 ps.

The results are consistent with the measurements on low-energy air showers. The trigger rate is assumed to stem mainly from vertically incident showers.

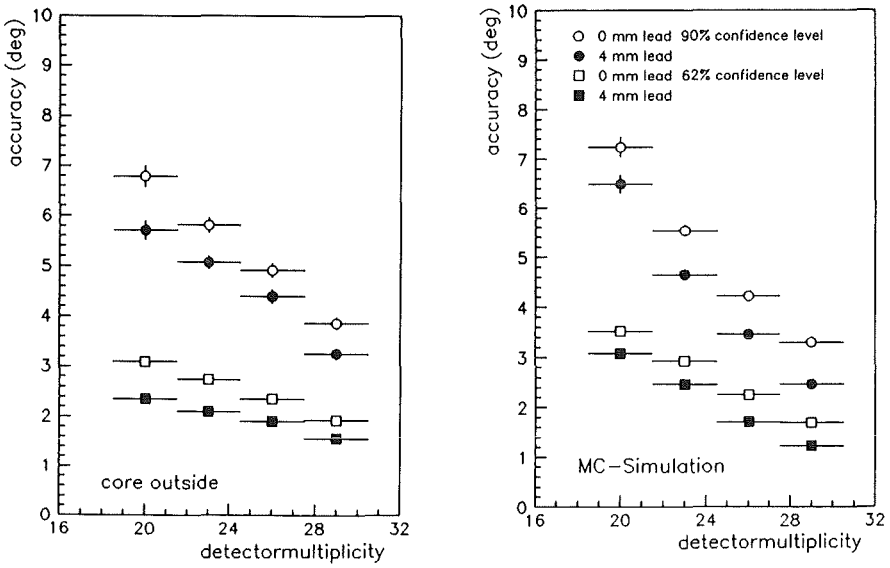

Fig.3 : Angular reconstruction error for subarrays.

For studies of the angular resolution of the clusters, the 64 e/γ detectors were divided in 4 groups of 16, forming subarrays shifted by ~ 1 m. The shower direction was determined independently in the subarrays. The results were compared and differences analyzed statistically. In this way, the influence on the angular resolution of a 4 mm Pb converter foil above the scintillator could be experimentally studied. The results are in very good agreement with the predictions of detailed Monte-Carlo calculations of the array response (fig.3). The angular resolution of the array is improved by about 30% by the lead converter. The improvement reveals a clear dependence on the distance from the shower core, as shown in fig.4 for the accuracy of single clusters. The angular measurements indicate that the results of the Monte-Carlo simulations for the angular resolution of the full KASCADE array are slightly conservative. We expect to achieve an angular reconstruction accuracy of better than 0.15° at $N_e = 10^5$.

The second effect of the lead sheet on top of the detectors is the hardening of the spectrum of detected shower particles [3]. Lead acts as an absorber for low-energy (< 20 MeV) electrons and as converter for higher-energy electrons and photons. Thus, the single particle Landau peak in the energy loss spectra is diminished, and the determination of the electron lateral distribution is more complicated. The Monte-Carlo simulations show that the lateral energy correction function becomes more important if a lead converter is used.

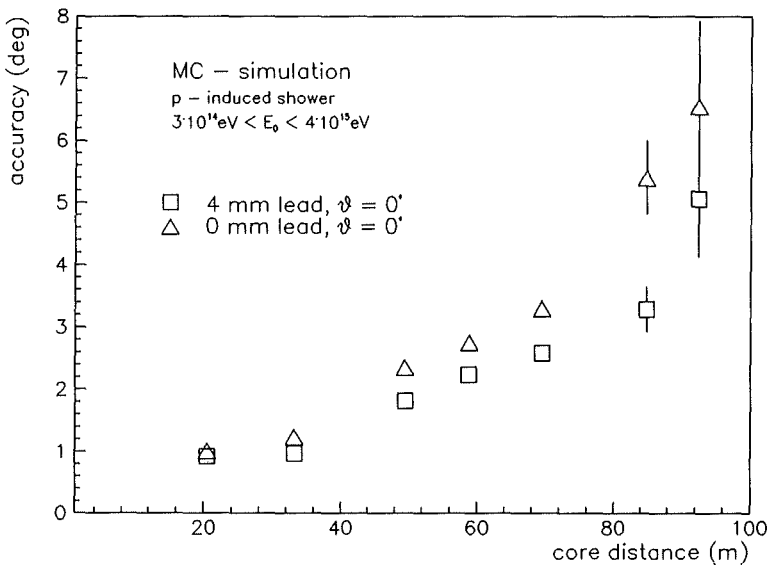

Fig.4 : Angular resolution of single clusters.

For the measurement of the muon component of the extensive air showers a scintillator detector is used below a heavy shielding (10 cm of lead and 4 cm of iron) corresponding to 20 radiation lengths. The high energy photons and electrons near the shower core have a nonnegligible probability to generate fake signals of the muon detector. This 'punch through effect' has been studied by extensive Monte Carlo calculations and experimentally in the shower measurements. It turns out that the 'simple muon counting' approach overestimates the true muon number mainly because of 'punch through' at small core distances and due to the high energy tail of the Landau distribution at all distances. Both effects can be corrected for core distances greater than 30 m with good reliability as shown in fig.5 (triangles). The information of the energy deposit in the e/γ detectors above the shielding was used together with the (low) granularity of the muon detector which consists of 4 scintillator segments. Fig.6 shows a pulse height spectrum of a muon detector for about 300 000 air shower events. At low pulse heights, the 'punch through' is dominating. The dashed line indicates the shape of the 'single muon' distribution.

The measurements with the prototype cluster have been used to check the predictions of the detailed Monte-Carlo simulations of the detector response and the event reconstruction accuracy which were performed in 1991.

The determination of the muon content of the extensive air showers is of particular importance for the KASCADE experiment. According to fig.5 the number of muons hitting the detectors can be determined with an accuracy ~ 6%. The reconstruction of the total muon number of an individual shower depends on the adopted functional form of the lateral distribution and on the sampling density

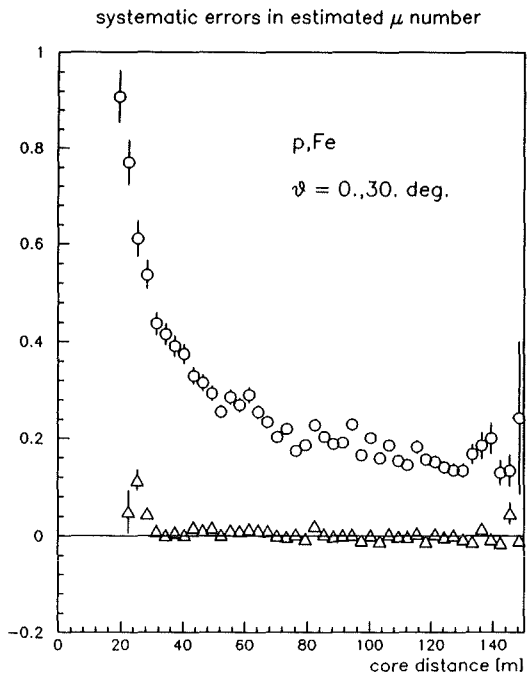

Fig.5 : Reconstruction accuracy of the muon content.

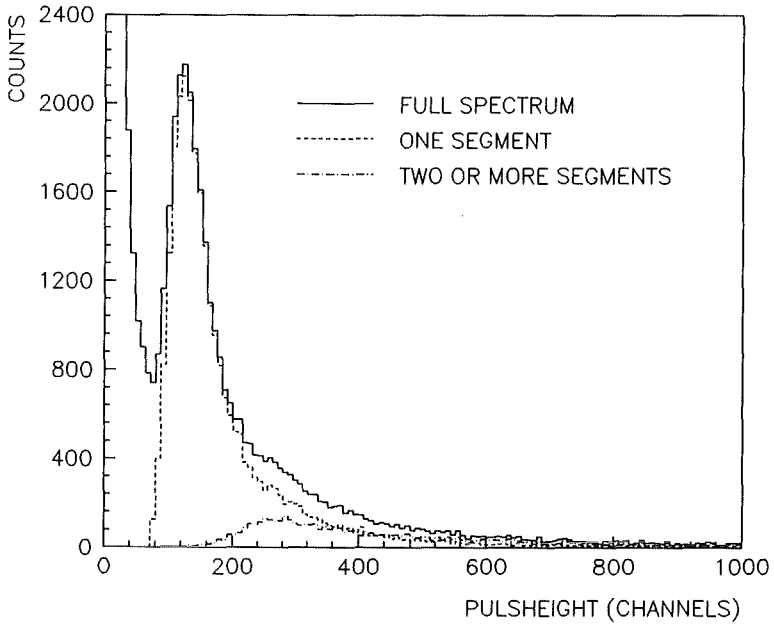

Fig.6 : Muon detector spectrum for air shower events.

(2.5% for KASCADE). Details of the reconstruction accuracy can be found in ref. [5].

During the ten months of operation the technical details of the detectors have been tested under realistic field conditions. The experiences led to a number of (mostly small) technical changes for the final detector design. The photomultipliers of the muon detectors will be coupled to the WLS-light guide system by flexible transparent silicon pads to improve the light transport

efficiency. The most important change is the use of a different liquid scintillator material improving the long term stability of the light output. A 2:1 mixture of mineral oil and pseudocumene will be used as scintillator base.

Layout of the frontend electronics : The development of the readout electronics for the array detectors has been continued and a prototype for the local trigger logic has been set up.

The frontend electronics is based on the general philosophy that each cluster of the KASCADE array acts as an independent air shower experiment. Data from different clusters are correlated by use of a common clock (time label) running synchronously in each cluster. All detector signals above the hardware threshold are converted into temporary data containing the time label. An 'event' is defined by a certain multiplicity condition which has to be fulfilled at least in one cluster, subsequently generating a trigger signal. The data with corresponding time labels are collected from all clusters. For the trigger information and detector readout within one cluster two VME crates are used, both equipped with special VME boards and controlled by TVC modules (fig.7).

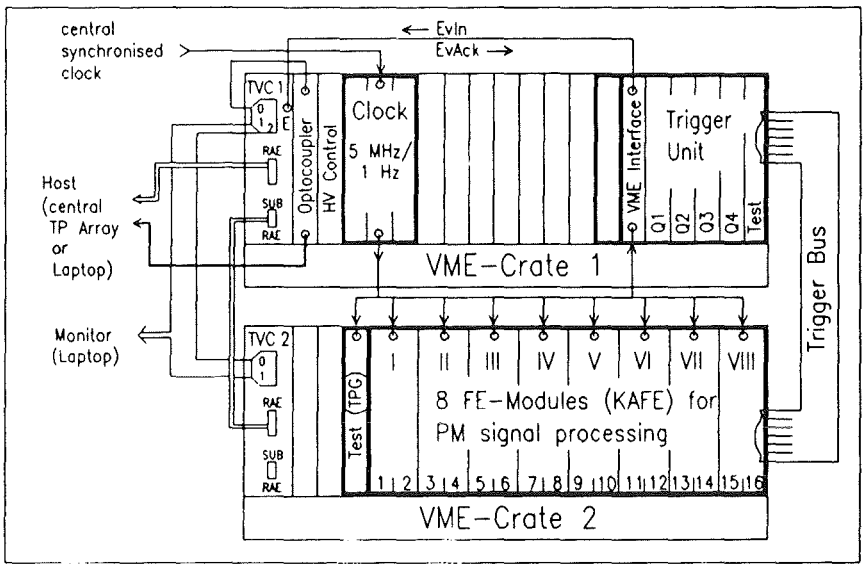

Fig.7 : Structure of the frontend electronics

Together with the high voltage control module and the clock modules, the modules of the trigger unit are located in VME-crate 1. The required modules of the frontend electronics - 8 KAFE (KASCADE Array Frondend Electronics) modules and the Test-Pulse-Generator (TPG) - are located in VME-Crate 2. The test pulses from the TPG to each KAFE module, as well as the 5 MHz and 1 Hz timing pulses from the clock to each of the FE modules and to the trigger unit, are

distributed simultaneously via coaxial cables. Trigger unit and KAFE modules are connected via flat band cables (Trigger Bus).

A single KAFE module contains all the electronics for 2 detector stations. Every access via VME happens in the operating mode A24/D16. The VME module, with a depth of 220 mm and a front panel width of 2 VME units, is equipped with a piggy back board where the analog parts are located. Thus, only one VME interface and one time label counter (TLC) is necessary for two detector stations. Each of the photomultiplier input signals passes through an input amplifier circuit and a discriminator. By writing on registers of the board's VME interface and by an 8-bit DAC conversion, it is possible to preset the discriminator thresholds for the 3 input signal groups separately. The signals exceeding the thresholds pass through pulse formers and leave the module as digital comparator outputs to the trigger unit. They will be stored in an output register as busy-bits.

All digital informations reach a logic array via a branch in front of the pulse former. In the area of e/γ signals their logical OR will start a time measurement, whereas in the muon area a logical OR of 4 previously requested coincidences (12,23,34,41) are necessary. The time measurement is stopped by the next and the second following 5 MHz pulses (TL).

As TDC we use an application specific integrated circuit (ASIC). The ASIC contains 4 independent channels and each channel is able to measure up to 4 hits simultaneously. With the function mode 'Common Start' we are able to get an on-line calibration for the particular channel. The resolution in one channel is about 300 ps. The start signals of the TDC measurements are also used as gate pulses for three e/γ-ADCs and two muon-ADCs, respectively .

In addition, all input signals of the 4 e/γ-photomultiplier are branched behind the input amplifiers, added in a summation circuit, delayed and given to different main amplifiers. One of them only serves as an analog output. The two others amplify the signal in the ratio of 1:16. After an integration time of 200 ns a fast 8-Bit ADC (Datel ADC-305, 20 MHz) in each branch converts in about 150 ns and writes the result into an output register. A logic array identifies the possible overflows, which are stored in another output register as overflow bits of the respective ADCs. The signal processing applies analogously to the signals of the muon detector photomultipliers. The dynodes signal in the e/γ-part is amplified such that a total ratio of about 1:16:256 between the values of the three ADC branches is achieved. In this way a dynamic range of about 1:5000 is realized.

Subsequently, a global module control decides on the basis of present overflow bits which two of the three possible e/γ-ADC registers will be read into

the FIFO, together with all the other output registers. Other tasks of the global module control are to block all discriminator outputs after the integration as well as the output of the TLC after its readout to the output register and their re-opening after finishing the readout of all output registers to the FIFO.

In the case of test measurements, which are triggered via the TPG module, we detect the incoming test pulses. The processing corresponds to that of normal physical events, with the exception that the test signal is switched to the e/γ- and the muon-summation circuits to test all present ADCs. For such an event a test-bit is set in the same output register where we also can find the ADC overflow bits and the address (cluster, station) of the data block.

The VME interface allows the access to the FIFO as well as to the threshold registers and to the status-control register. While the FIFO is of the type 'read-only' from VME, the others are read-write registers. The threshold registers contain the present comparator threshold which can be changed by a write access.

The status-control register contains the present condition of the FIFO (full, empty), of the service button (on/off) and of the whole module (inhibit ON/OFF). The module, with the exception of the TLC, can be reset and inactivated (selective reset) or only inactivated (inhibit ON) and activated (inhibit OFF) by write accesses. Experiment startup (power ON) or a VME-reset also produces a selective reset.

The hardware trigger unit has three functions: (i) multiplicity trigger decisions on various levels, generating a programmable event interrupt to TVC 1 and finally to the host computer system, (ii) low-priority interrupts for calibration and monitoring purposes in the cluster by single-muon data, and (iii) time control, i.e. a UT (or Julian Time) clock with 200 nsec resolution, correlating data from different parts of the experiment. The trigger unit is controlled and read out via the VME bus.

Status and further developements : At present 3 clusters of detector stations are set up on the experimental site (see fig.1 of contr. 1.1).

- Six additional clusters will be installed in 1992. Serial detector production has been prepared.

- Serial production of KAFE-modules and of the modules of the trigger unit is planned to start in autumn 1992.

- Prototype studies have shown the feasibility of alternative techniques for muon detection in the area close to the central detector of the KASCADE experiment. A detailed technical design study has been started for a medium size - (~20 m^2) - 3 layer-muon tracking detector using limited streamer tubes. In a first stage 12 of these detectors are planned, covered by ~ 10 r.l. shielding of concrete and sand.

- Test measurements have been performed concerning the determination of the time profile of extensive air showers as a function of core distance. The first results are in good agreement with the time dispersion of the particles of simulated air showers. The shower thickness may be used as a measure of the core distance, and the reconstruction of high energy showers with cores outside the array can be improved. In addition, further interesting information on characteristic properties of extended air showers may be derived from such measurements.

[1] F. Bauer et al., Report KfK 4875 (1991), eds. H. Beer, J. Wochele, Kernforschungszentrum Karlsruhe, p. 62 ff

[2] G. Völker, Report KfK 4983 (1992), Kernforschungszentrum Karlsruhe

[3] W. Kriegleder, Report KfK 5023 (1992), Kernforschungszentrum Karlsruhe

[4] H.J. Mayer, Nucl. Instr. Meth. A 294 (1990) 651

[5] H.J. Mayer, Nucl. Instr. Meth. A 311 (1992) 327

* Physikalisches Institut, Universität Erlangen-Nürnberg

** University of California, Davis, USA

*** DESY-Zeuthen

**** INS Lodz, Poland

1.2.2 A NEURAL NETWORK ALGORITHM FOR CORE LOCATION ANALYSIS AT LARGE EXTENDED AIR SHOWER ARRAYS

H.J. MAYER

The application of neural network algorithms to shower reconstruction has been examined. As a first result a Hopefield-Tank type network for core location analysis was constructed and tested successfully. The algorithm combines high efficiency for the identification of the shower core with good rejection capability for showers that fall outside the array. In addition it offers an easy possibility to identify events with subcores. The algorithm is fast and can be used in an online pre-analysis procedure. Details are given in ref.[1]. Simulated KASCADE data covering the full expected range of the experiment were used to test the algorithm. The efficiency of the algorithm, i.e. the probability for finding the core when it lies truly inside the array is shown in fig.1 as a function of shower size and for two different core criteria. Application of the weaker criterium gives better results for the efficiency at expense of a reduced rejection capability. About 90% efficiency are reached at $N_e = 10^4$ and full efficiency is obtained at shower sizes of $N_e \sim 2 \cdot 10^4$. An average resolution of roughly 2.8 m (63% confidence radius) is found. While slightly diminishing the efficiency, the rejection capability for showers outside the array considerably benefits from the so-called strong core condition (fig.2). From

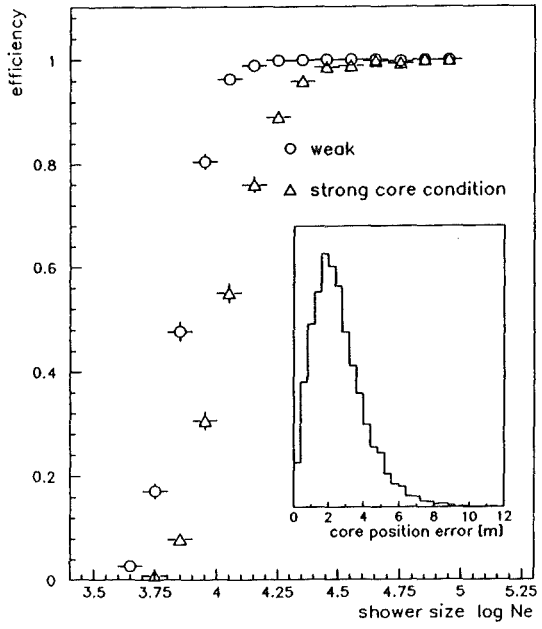

Fig.1 : Efficiency of the network for core finding. The inset gives the error distribution of the core positions (weak condition).

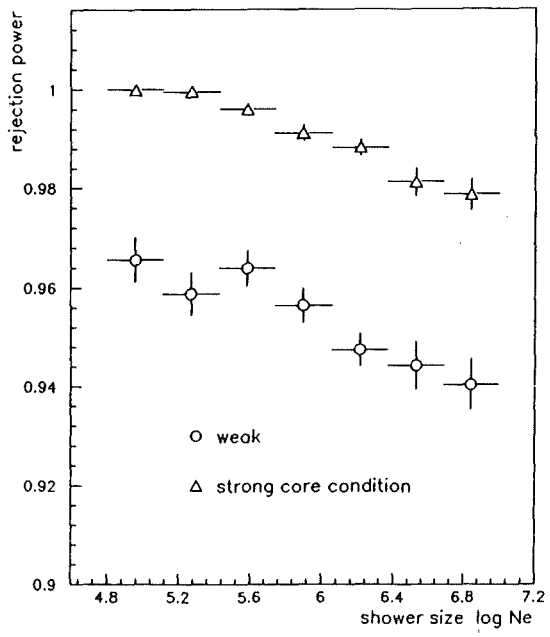

Fig.2 : Rejection capability of the network.

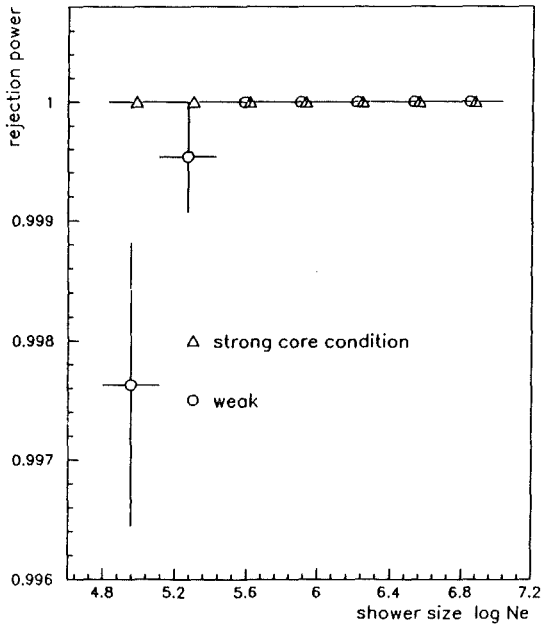

Fig.3 : Rejection capability of the network with an additional energy criterium applied.

simulated showers with core position truly outside the array, the rejection capability, given as $(N - N_{fc})/N$, is evaluated from the number of fake core events N_{fc} and the total number of accepted events N. An event is accepted for analysis if at least 40 detectors are hit, this number corresponding to the efficiency threshold of the network for events with the shower core hitting the array. The weak core

condition reduces the rejection capability from 97% at $N_e = 10^5$ to about 94% at $N_e = 10^7$. Larger showers have a better chance to fake a core due to their larger spatial extension. Application of the strong core condition yields a rejection capability of almost 100% for small showers and still about 98% at $N_e = 10^7$.

The network does not make use of information on the absolute values of the observed detector pulse heights. This leaves room for additional criteria to discriminate fake shower cores from real ones. Fig.3 shows that the application of an additional energy criterium enables the use of the weak core condition without loss of rejection power. One obtains an almost complete suppression of events with shower core position outside the array boundaries, at the same time conserving maximum efficiency.

[1] H.J. Mayer, Nucl. Instr. Meth. A 311 (1992) 327

1.2.3 STREAMER MODE STUDIES FOR KASCADE MUON DETECTORS

P. DOLL, K. DAUMILLER, H.O. KLAGES

Preparational studies of streamer tubes for the air shower experiment KASCADE motivated the investigation of some features of the self-quenching streamer (SQS) mode for various argon-isobutane gas settings and operation voltages with respect to its behaviour along and beyond the plateau region and increasing light yield [1]. We employed a pulse shape analyzing technique and the spectroscopy of the light escaping from the SQS mode in the 370 to 500 nm wave length region.

Fig.1 shows derived from an event matrix the pulse height for 434 ± 10 nm photons observed in the photo tube versus the charge amplitude of the corresponding streamer event for two gas setting MIX 1 and MIX 2 and 6.4 kV anode voltage. Because of the erratic behaviour of the SQS avalanches (no spatial constraint on the position of the charge centroid has been applied sofar) we must expect a rather broad distribution in each parameter. Since the anode charge has been calibrated, we can relate a charge of about 200 pC to the most frequent streamers (around channel 350) which corresponds to about 10^9 electrons hitting the anode wire.

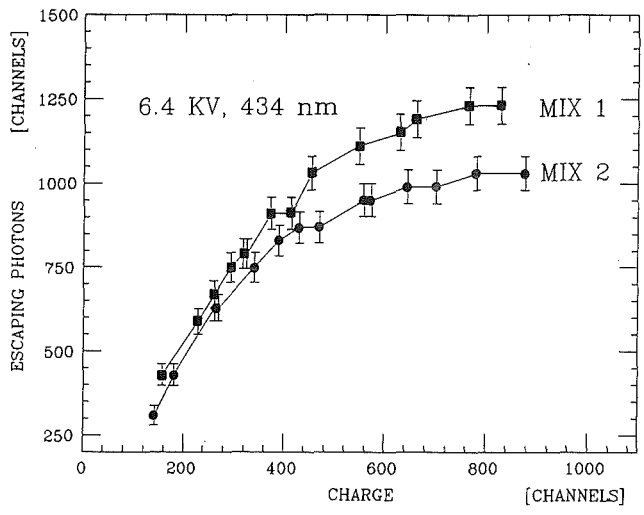

Fig.1 : Photon yields versus charge yields of SQS events for 434 ± 10 nm photons recorded for two gas mixtures MIX 1 and MIX 2 and 6.4 kV operation voltage. MIX 1: 37.5% argon, 62.5% isobutane; MIX 2 : 32% argon, 68% isobutane. The error bars represent statistical errors only.

On the other hand, fig. 1 exhibits an interesting correlation.The streamers which occur with larger electron charges release less visible photons, a behaviour very much reminiscent of the counter-correlation observed for the ionization-scintillation mode. This is even more the case for a larger isobutane content in the gas mixture. Since isobutane is almost fully transparent for wave lengths larger than 175 nm [2], the attenuation mechanism by means of isobutane must work in the UV wave length range. The average number of photons derived from the photon spectra on the basis of Poisson statistics indicates to about 5 orders of magnitude less photons in the 370 to 500 nm wave length range than electrons recorded on the anode wire. This drastic reduction of visible photons is preceded by a drastic quenching of UV photons, the natural feature of the SQS mode.

The study of the streamer discharge mechanism by means of a pulse shape analyzing technique and a spectroscopy of escaping light [3] may help to support the clarification of the mechanism of the (SQS) mode especially when pushed to high light yield.

[1] P. Doll, K. Daumiller, H.O. Klages, Report KfK 4875 (1991) eds. H.Beer, J.Wochele, Kernforschungszentrum Karlsruhe, p. 136

[2] D. Anderson, Nucl. Instr. and Meth. 178 (1980) 125

[3] P. Doll, K. Daumiller, H.O. Klages, Proceed. VI Int.Wire Chamber Conference, Vienna, Austria (1992), eds. W. Bartl, G. Neuhofer (in press)

1.3 THE CENTRAL DETECTOR OF KASCADE

1.3.1 STATUS OF THE CENTRAL DETECTOR

E. BOLLMANN, J. ENGLER, P. GABRIEL, M. GETTERT, H.J. GILS, A. HANSER, F. HERM, H. KEIM, J. KNAPP, H.J. MATHES, H.H. MIELKE, H. REBEL, G. VÖLKER, J. WENTZ, J. WOCHELE, S. ZAGROMSKI, P. ZIEGLER

The principal lay-out of the central detector is shown in fig.1. The absorber block of the calorimeter is sliced into 8 layers starting with iron slabs of 12 cm thickness at the top and ending in the concrete ceiling of the foundations.

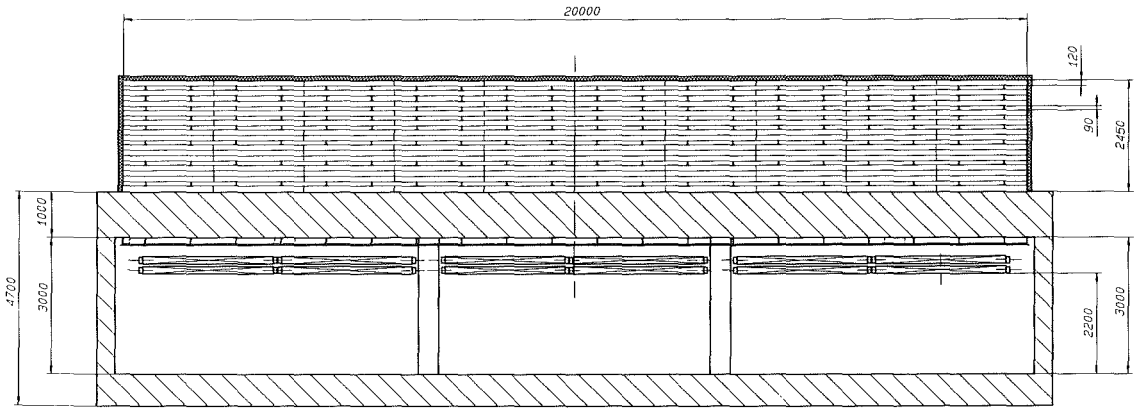

Fig.1 Principal lay-out of the central detector with a sampling calorimeter of iron absorbers and multiwire propotional chambers for muon detection in the basement.

All the absorber slabs have been cast and are ready for mounting. The concrete foundations have been finished and the iron stacking is scheduled for summer 1992. The equipment for charging the slots in the iron absorber with the active elements has been built by Forschungszentrum Rossendorf, and it is ready to be used.

Active Layers : Ionization chambers using the liquid TMS (tetramethylsilane) as medium have been developed at the institute and are taken as active elements for the sampling calorimeter. 1000 chambers have been built at the time of writing, and 500 of them have been tested at the Karlsruhe Cyclotron with 96 MeV tritons.

Meanwhile a first statement on long time stability of the chamber signal can be made, since the first chambers had been filled and closed end of 1990. Fig. 2 shows the mean signal of the first 8 chambers at a voltage of 2 kV. We observe a signal stability of (0.7 ± 6.5) % per year, i.e. we have no evidence for a signal decrease. This is a very important aspect in view of a stable operation of the calorimeter during its anticipated lifetime of about 10 years.

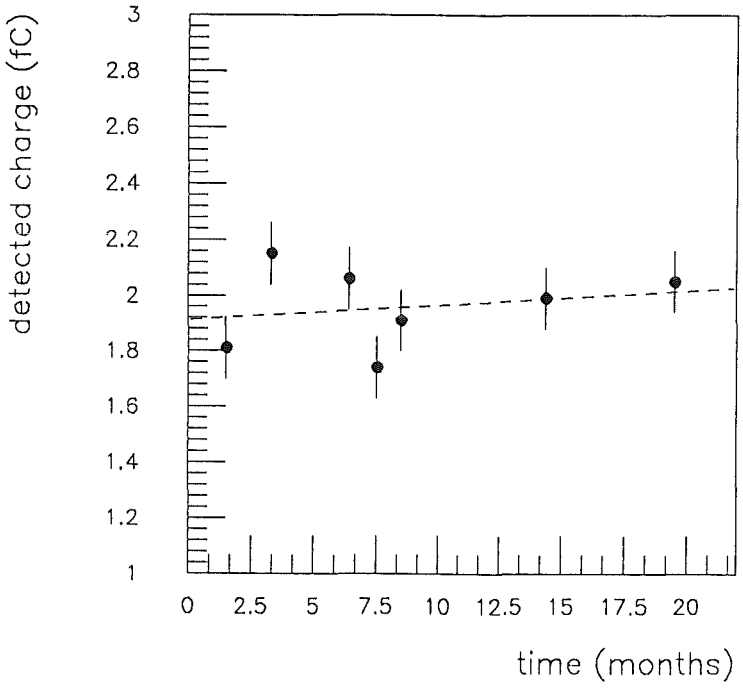

Fig.2: Signal yield of the first 8 KASCADE ionization chambers at 2 kV detector voltage with respect to the time elapsed since pinch-off.

Therefore, we are considering the idea to use the ionization chambers not only for hadron detection but also for measurements of the penetrating muons. The signal rise for relativistic muons and the radiation due to direct pair production may be used for a rough estimation of the energy.

As an example, fig.3 shows a simulation of three 10 TeV muons passing through the central detector. The bursts are clearly distinguishable.

For a good muon detection the signal should be measured with a precision comparable to the intrinsic Landau fluctuations of energy loss. These amount to about 25%, and all errors in the measurement should be lower than this figure.

In this respect the electronic noise is of major importance. We have investigated the noise performance in the prototype calorimeter. A ratio of signal/noise = 3.5 has been obtained. This is nearly the figure of 4.0 which had been found in the ideal environment of an electronic laboratory. These encouraging results demonstrate that problems of transient und pick-up noise in the final set-up can be sufficently well mastered. A second aspect concerns the chamber geometry. In order to minimize contributions, which add to the Landau

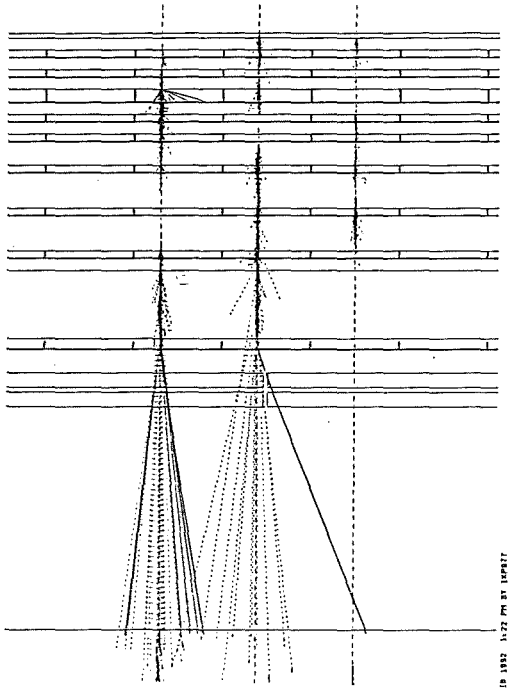

Fig.3 : Three muons of 10 TeV passing through the central detector, simulated by the code Geant 3.

Straight lines represent electrons, dotted lines indicate photons.

fluctuations, the chamber has to be sufficiently flat, and the thickness has to be known to an accuracy better than 10%. For a sample of channels the mean thickness has been measured with a micrometric screw.

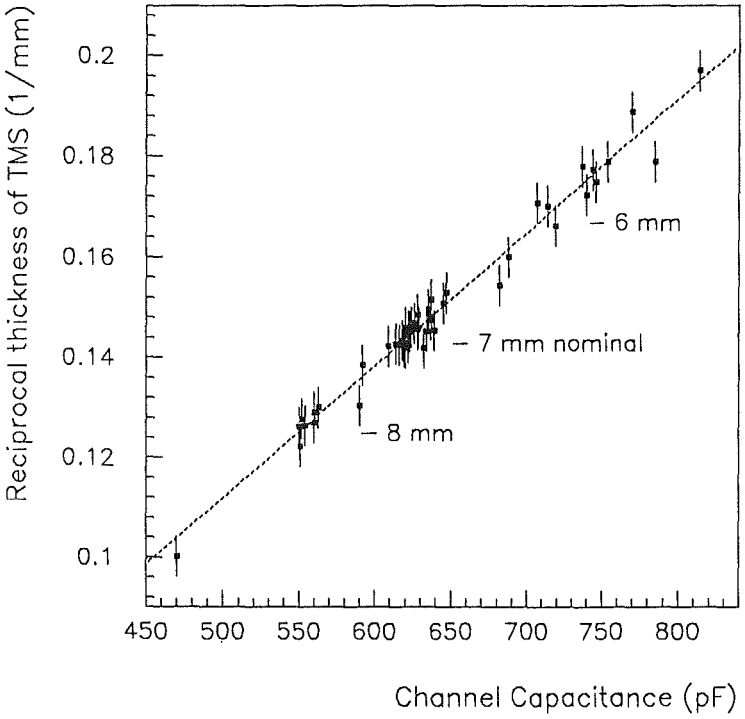

Fig.4 : Mean thickness of the TMS liquid in various chambers with respect to the measured capacitance of the particular channel [1].

Fig.4 shows the correlation of the mean thickness with the capacitance of that particular channel. The latter can be measured very easily. The scattering of the points correspond to an 'rms' value for the measured thickness of $\sigma = 0.39$ mm or 5.6%. This means that the capacitance gives a reliable value for the thickness of each individual channel. The measurements also proved that the chambers are

resonably flat to about 2 %. This flatness could be achieved by a careful adjustment of the TMS vapour pressure during filling.

It is very promising that muons passing through the iron absorber can be clearly detected and their energy loss be measured with a reasonable precision.

Prototyp Calorimeter : In order to study in detail the performance of the central detector, a prototype calorimeter has been set up using the original iron slabs.

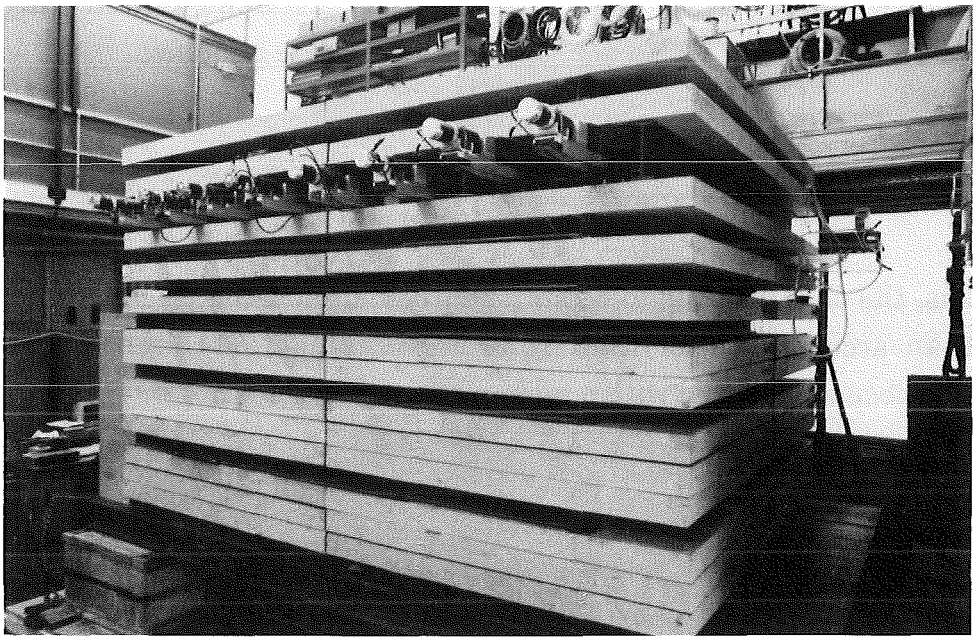

Fig.5 : Photograph of the prototype calorimeter.

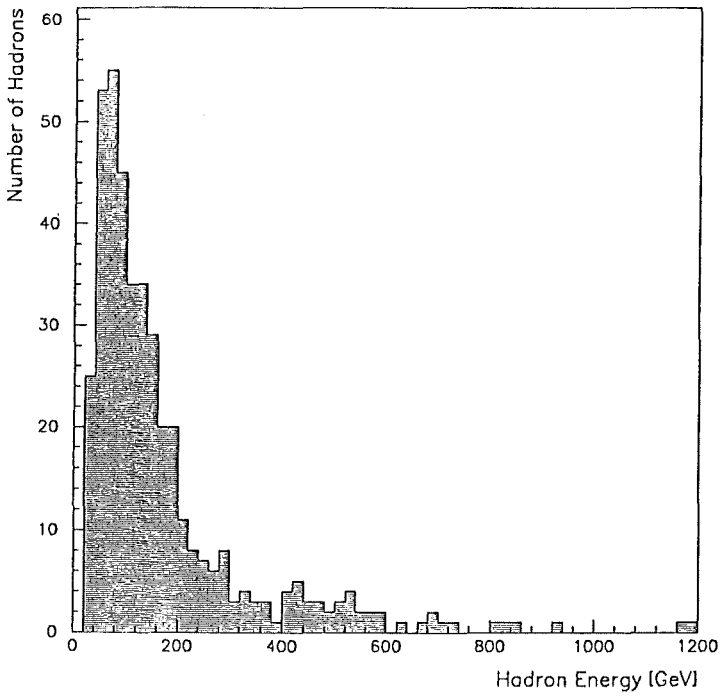

Fig.6 : Energy spectrum of hadrons observed in the prototype calorimeter (not normalized).

It is equipped with KASCADE ionization chambers, and became operational in 1991. Fig.5 shows a photograph of the set-up. First hadrons with an energy of up to 1 TeV have been detected.

A preliminary spectrum is shown in fig.6. Detailed acceptance calculations to normalize the yield are currently under way.

Muon Chambers : The operation of the multiwire proportional muon chambers (MWPC) is currently studied by a special test set-up [2] consisting of a stack of four chambers. An additional chamber is operated with the prototype new frontend electronics in order to adjust the electronic and readout conditions to the actual requirements of the experiment.

In addition to the activities around the test set-up, the installation of the MWPC detectors in the basement of the central detector building (fig.1) has been prepared:

- The mechanical mounting elements have been constructed and a first prototype is ready.
- The detector gas supply system has been extended by implementing a gas recycling device in order to reduce drastically the isobutane consumption and to meet safety requirements [3].
- For reconditioning all muon chambers a repair-station has been built-up as a large tent with mechanical equipment for opening and cleaning in a dust free environment. The station is connected with a small arrangement for routine checks and localizing malfunctions of the detectors.

Trigger System : The TMS and MWPC detectors are not equipped with a self-trigger system and need fast external triggering. After a careful consideration of various options the third active layer of the calorimeter is forseen as a 'trigger level' by scintillator pads. Prototype elements are in the test procedure [4].

[1] K. van Nuland, Internal Report, Kernforschungszentrum Karlsruhe (1991), unpublished

[2] H. Mathes, S. Zagromski, H. Rebel, H.J. Gils, A. Grill, M. Kretschmer, O. Schoeps, T. Thouw, J. Wentz. contribut. 1.3.2 of this report

[3] V. Masuch, M. Petcu, S. Zagromski, Internal Report, Kernforschungszentrum Karlsruhe (1992), unpublished

[4] M. Brendle, A. Hanser, H. Rebel, G. Völker, contribution 1.3.5 of this report

1.3.2 OPERATION AND MEASUREMENTS WITH THE KASCADE MUON CHAMBER TEST SET-UP

H.J. MATHES, S. ZAGROMSKI, H. REBEL, H.J. GILS, A. GRILL, M. KRETSCHMER, O.SCHOEPS, T. THOUW, J.WENTZ

For muon detection with the KASCADE multiwire proportional chambers the test set-up described in [1] has been extended.

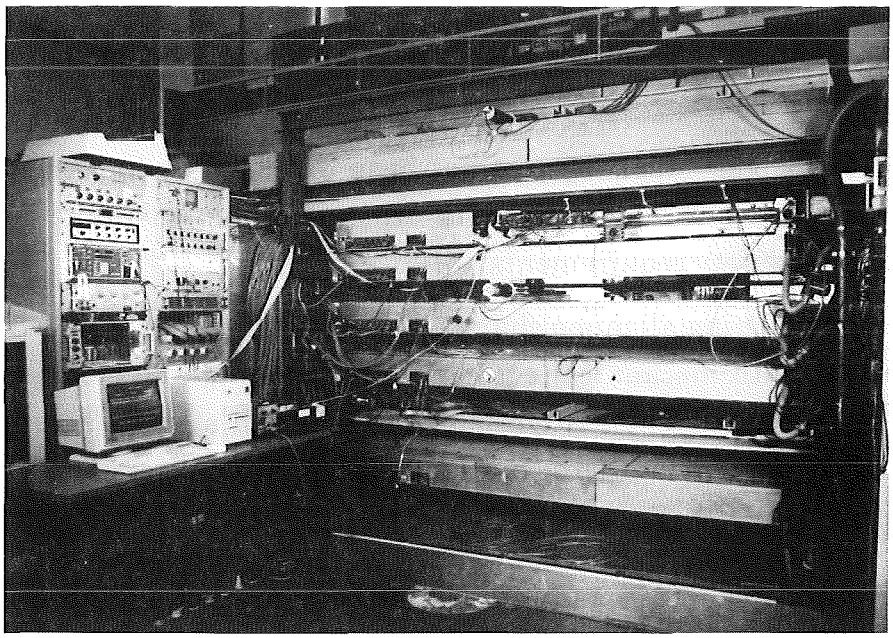

Fig.1 : Photograph showing the front view of the test set-up.

The investigation of some properties of the muon component originating from EAS needed some modifications which have been installed during the last year (fig.1).

In order to increase the sensitive area of muon chambers between the trigger planes, the trigger size has been enlarged. The lower, segmented trigger scintillator allows to measure the arrival time of a single particle by use of the mean-timing principle.

The investigation of high multiplicity events near EAS cores required to reduce the background originating from the electromagnetic cascade. Therefore a 24 radiation length thick lead-iron-absorber layer (12 cm iron + 10 cm lead) was put between the upmost chamber and the upper trigger plane. With this absorber the punch-through from electrons and photons up to about 10 Gev particle energy is drastically reduced which leads to a sufficient reduction of the shower correlated electromagnetic background. A further effect is a cut-off in the muons momentum spectrum at 0.45 GeV/c.

The described local trigger system reacts mainly on single muons. With some additional electronics and the use of a segmented trigger the fraction of events with higher track multiplicities is increased. This class of events includes also such cases where a particle interacts with the absorber and produces secondaries.

Nevertheless, the selection criteria do no indicate EAS initiated tracks. Thus, a simple mini-array (4 detectors with 0.3 m^2 each) installed outside the hall is used to inform about the presence of an EAS event. By making use of a simple geometric algorithm the results allow to determine the shower direction and the shower front arrival time at the place of the muon detectors with moderate accuracy.

The signals of this array scintillators are fed into a majority logic whose output starts the readout of the chambers and all associated readout channels. The extenstion of the mini-array and the measured rate of events implies a cut of the primary energy spectrum around 10^{14} eV.

Each array detector has an additional scintillator burried under 11.6 radiation lengths of lead. There are current feasibility studies to use the punch-through of the highly energetic electromagnetic component of the core to select showers with cores near to the prototype set-ups.

The extended trigger system and the additional readout-channels (ADC, TDC, clock etc.) demanded a redesign of the data acquisition software. To deal with online-spectra filling and representation for all channels extended use was made of the multitasking capability of the PDP 11/73. The acquisition system includes also the monitoring of the gas flow and the high voltages.

After rearranging the chambers mechanical support they had to be brought in operation again. Their equipment with the original CELLO-electronics implied a very time-consuming adjustment procedure. Problems with the HV-stability, caused by the gas-mixing system, delayed the start of the data-taking phase.

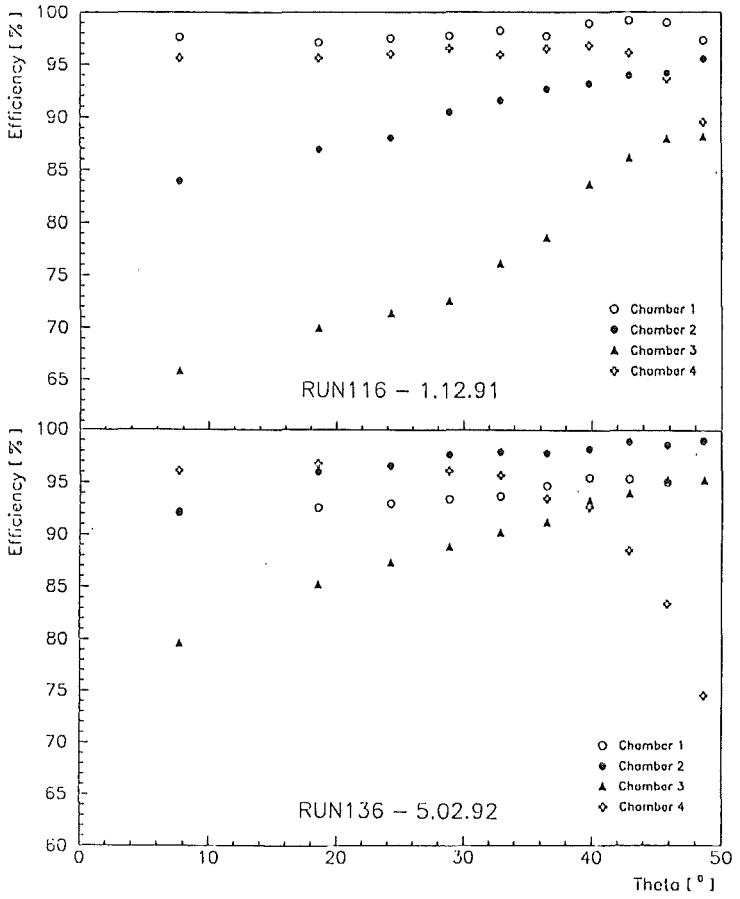

Fig.2 : Angle dependent efficiencies of all 4 chambers for two different runs. The theta-bins chosen include the same solid-angle.

The complete detector started to take data in the beginning of december 1991 without considerable operation failures.

By first step the data analysis attempts to identify the tracks of single muons in order to understand and characterize the operational properties of the muon chambers and of the trigger scintillators. In every trigger configuration a large fraction of such events is observed. High and uniform detection efficiencies, i.e. independent from the incident angle and the position are aimed at. Individual characterization of every muon chamber channel by efficiency and noise values is planned.

	Chamber 1	Chamber 2	Chamber 3	Chamber 4
Run116	97.9 %	89.4 %	74.5 %	95.8 %
Run136	93.1 %	95.7 %	86.0 %	95.5 %

Table 1 : Table of integral efficiencies for two different runs.

The efficiencies for two different runs are shown in tab. 1 and fig.2. The efficiency calculation is somewhat influenced by the reconstruction algorithm. The differences of chamber efficiencies between the two runs are not fully understood yet, as for both runs high voltage and the gas flow had been kept at the same values. The only reason seen so far is a possible dependence from temperature or pressure of the gas and of the surrounding atmosphere. For further studies of these effects these parameters will be monitored in future.

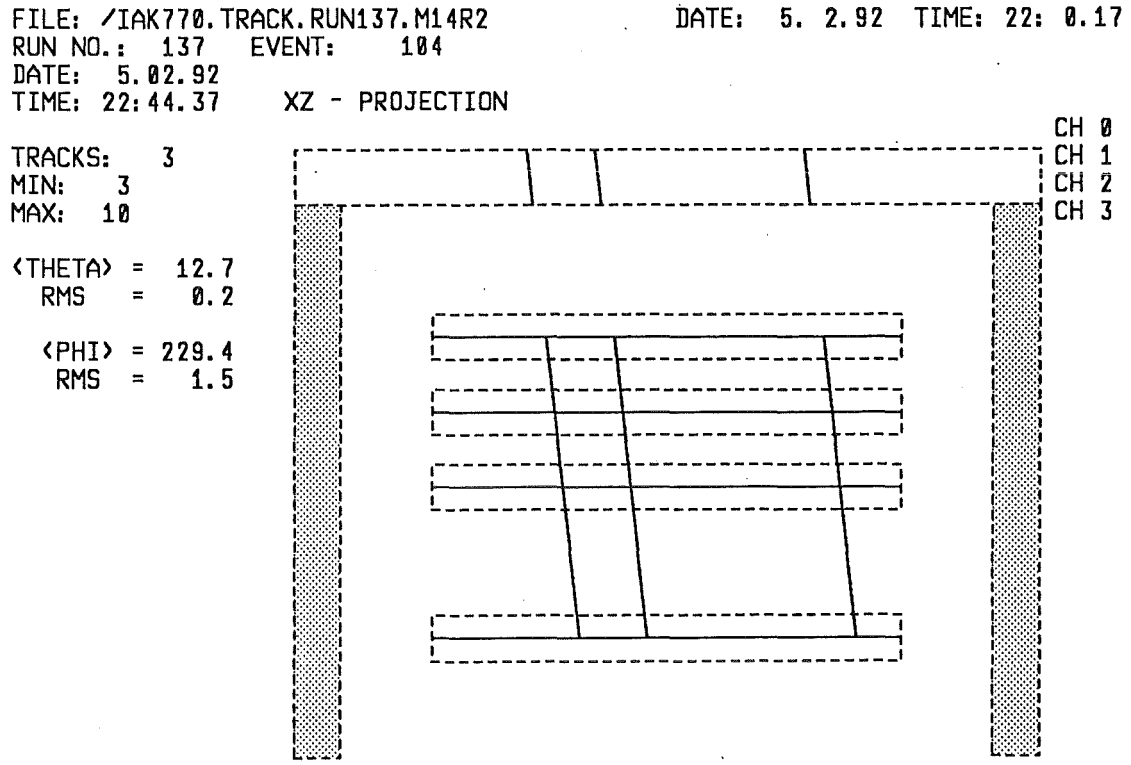

Fig.3: Display of an event with quasi parallel tracks.

A further result of the data analysis is the requirement to control small displacements of the chambers relative to each other very precisely. These displacements influence the number of reconstructed tracks and the integral efficiency. Corrections for these effects are worked out.

Even though the track reconstruction works well with single tracks in the case of low noise, this is not always the case for multiple track events. From a preliminary study of such events via an event-display program it is obvious that the algorithm fails for events when secondaries have been produced. In case of events with several quasi-parallel tracks (fig.3) the effect of phantom hits which lead to phantom tracks needs further discussion.

[1] J. Horzel, Report KfK 4815 (1990), Kernforschungszentrum Karlsruhe

1.3.3 THE NEW FRONTEND ELECTRONICS OF THE MULTIWIRE PROPORTIONAL CHAMBERS FOR MUON DETECTION

H. KOEPERNIK*, D. PROEHL*, A. WOLF*, S. ZAGROMSKI, H. REBEL

Tests measurements with the multiwire proportional chambers, forseen for muon detection with the central detector of KASCADE have shown that the original frontend electronics for reading out the ca. 32 000 channels, does not meet the requirements of a long-term operation.

The reasons [1] to replace the old electronics are the unsufficient reliability (by physical wear and great power consumption), and the instability of parameter values like trigger level and delay time. Furthermore, there is no possibility of computer aided adjustment of the parameters.

In principle each chamber consists of three planes of electrodes as shown in fig.1, which allow the determination of the coordinates of a hit. The anode wires are in the middle plane and two cathode planes are mounted in a distance of 8 mm from the wires. The cathode planes consist of stripes which are oriented at ± 34 degrees with respect to the anode wires. Concerning the spatial dimensions there are three different types of chambers. The largest one consists of 208 anode wires and 2 x 336 cathode strips.

The frontend electronics of the chambers is arranged on anode - and cathode motherboards, which are directly connected to the contacts of chamber electrodes and contains 32 channels each (fig.2).

The motherboards of each plane are connected together and to a transputer-controlled multiplexer by a parallel bus for controlling the trigger level, delay and data readout. The serial transputerlink provides the communication with the superior computer.

The chamber output signal of each channel is captured by a high-speed charge sensitive amplifier. Its output signals are used to generate a high-speed timing trigger signal. A muon event is expected to deposite a typical charge of

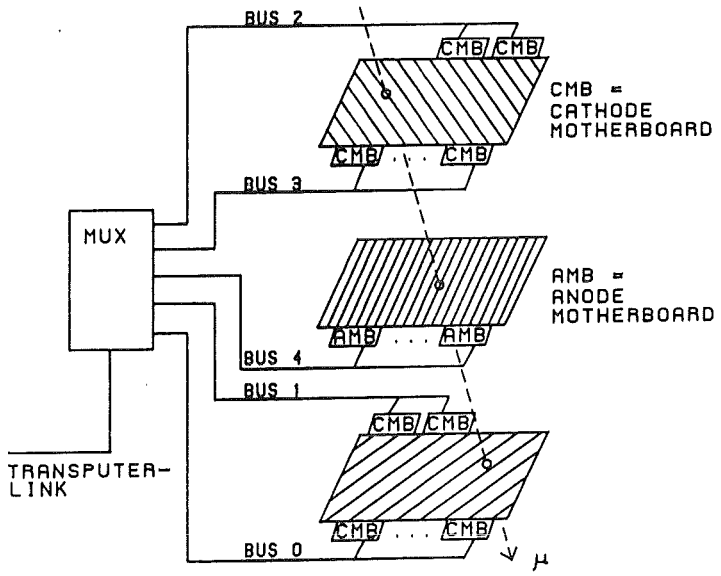

Fig.1 : Schematic view of frontend electronics of one chamber.

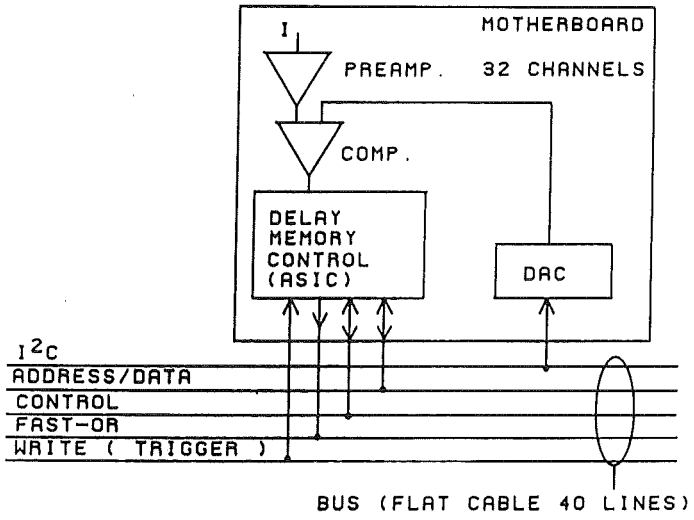

Fig.2 : Principal diagram of a motherboard.

about 100 fC [2]. The required high input sensitivity, and also a short rise time and low power consumption of amplifier, in consideration of the small space available, could be only achieved by applying a special hybrid circuit technique. For adjusting the trigger level the comparator of each channel is supplied with a computer controlled threshold voltage. The output signal of the comparator is passing a computer controlled delay. To select the real muon events from underground, the delayed signal is correlated with a fast trigger signal derived from layers of plastic scintillators (200 ns coincidence width).

Therefore, the computer controlled digital delay lines (programmable in steps of 25 ns to max 3 μs) and the memory registers to latch the selected muon events of all 32 channels are integrated in an integrated circuit (ASIC), developed

for this purpose. This ASIC contains also the required interface circuit to link the motherboard with the parallel bus. In consideration of the channels high spatial density at the multiwire chambers the solution of this problem was on the one hand only possible by using a large scale integrated ASIC, on the other hand the application of ASIC contributes essentially to the reduction of costs.

In 1991 the first test setup with the prototyp of electronics was assembled, PC-aided checked on a chamber area of 300x300mm^2 and the distribution of muon events was measured and evaluated [3]. The first complete chamber is scheduled to be equipped in March 1992. The aim is to finalize the equipment of all 32 chambers of the central detector until the end of 1992.

[1] H. Koepernik, S. Zagromski, Internal Report, Kernforschungszentrum Karlsruhe (1991), unpublished

[2] J. Horzel, KfK Report 4814 (1990), Kernforschungszentrum Karlsruhe

[3] H. Koepernik, Internal Reports, Kernforschungszentrum Karlsruhe (1991), unpublished

* Forschungszentrum Rossendorf, Dresden

1.3.4 INVESTIGATION OF THE SIGNAL PRODUCTION IN LIQUID-IONIZATION-CHAMBERS BY THE PASSAGE OF STRONGLY IONIZING PARTICLES AND A NEW THEORETICAL DESCRIPTION OF RECOMBINATION[1)]

R. SUPPER

Starting from the original Onsager-theory an extended theory is presented describing the recombination of charge carriers and of signal production in TMS-liquid ionization chambers. The shielding by the impurities of the liquid is explicitly taken into account. By dedicated measurements various parameter dependencies of the theory are checked and the parameter values are experimentally determined. The studies comprise test procedures of the TMS chamber operation and are in context of a hadron calorimeter set-up of the cosmic ray experiment KASCADE.

1) published as KfK Report 4966 (1991)

1.3.5 STATUS OF THE TRIGGER SYSTEM IN THE KASCADE CALORIMETER

M. BRENDLE*, A. HANSER, G. VÖLKER, H. REBEL

For a discrimination of the useful true events from background and noise an efficient trigger system is indispensable for the operation of the central detector of KASCADE. For this purpose fast detectors - e. g. scintillation detectors - are needed. Consequently in addition to triggering, measurements of arrival time distributions of the incoming particles may be accessible. An interesting shower event is recognized by coincidence of several particles. However, single high energy hadrons are also of interest because they enable to test the conditions of the liquid ionization chambers permanently. To recognize these single hadrons and to record the arrival times of single particles a system of many detectors having a relatively small sensitive area and a sufficient time and energy resolution is required. The detectors must be placed below adequate absorber layers to ensure sufficient local shower creation by the high energy hadrons and to suppress the disturbing electromagnetic component. The third active layers in the calorimeter is thought to be the best position for the trigger and timing system, i.e. below 5 cm Pb + 36 cm Fe.

A first study [1] showed the suitability of trigger and timing detectors consisting of one plastic scintillator with an area of 0.5 m x 0.5 m and one photomultiplier coupled to the scintillator via a simple inexpensive slab light guide. Because of the high number of such detectors needed for the trigger system and because of their large portion of insensitive area the usability of larger detectors is studied. Light-readout by wave length shifter (WLS) bars is preferred for larger detectors with respect to the demanded flat and compact set-up, inspite of some losses in time resolution. Two detector types were put in the short list of our investigation, both fitting the dimensions of the liquid ionization chambers:

A: Two plastic scintillator sheets with dimensions 0.5 m x 0.5 m x 3 cm with a WLS bar positioned between them and one photomultiplier at one end of the WLS bar.

B: Two plastic scintillator sheets with dimensions 1 m x 0.5 m x 3cm with a WLS bar of 1 m length positioned between them and two photo-multipliers, one at each end of the WLS bar.

Tests of detector type A using diverse scintillator materials and multiplier types showed an energy resolution better than needed and a time resolution with σ of 1.7 - 1.8 ns, the latter value obtained using more inexpensive materials. Detector type B promises better time resolution, especially if meantimers are employed. However, particle densities which can be processed in timing measurements are lower by a factor of two due to the larger area. Tests of detectors type B have been started. Identical types of light-proof boxes can be used for both detector types; in the case of type A two detectors can be placed in one of such boxes, whose design is finalized. Twelve prototypes are under construction.

Several concepts for the front end electronics and the trigger circuit are in current discussion.

[1] B. Schulze, Internal Report, Kernforschungszentrum Karlsruhe (1991), unpublished - Diploma Thesis, University Karlsruhe 1992

* Physikalisches Institut, Universität Tübingen

1.4 SIMULATION OF COSMIC RAY INTERACTIONS IN THE ATMOSPHERE

1.4.1 STATUS OF THE AIR SHOWER MONTE-CARLO SIMULATION STUDIES

J.N. CAPDEVIELLE*, P. GABRIEL, H.J. GILS, P.K.F. GRIEDER**, D. HECK, J. KNAPP, H.J. MAYER, J. OEHLSCHLÄGER, H. REBEL, G. SCHATZ, T. THOUW

The simulation code CORSIKA [1] has been further improved in many respects with the aim of obtaining a better agreement with experimental data. In all modifications we tried to achieve a better transparency of the program structure for easier use and to accelerate the calculations.

Considering the photonuclear reaction a gamma-ray may not only produce a single pion (subroutine PIGEN1), but also - in dependence on the gamma-ray energy - two pions (subroutine PIGEN2), or at energies above 2 GeV even many more hadrons (modified subroutine HDPM). In addition the angular distributions of the secondary particles have been adjusted to the experimental values [2] by approximating dipole and quadrupole radiation characteristics for the resonances at 0.3 GeV, 0.7 GeV and 1.0 GeV.

The subroutine NIHILA, which describes the annihilation of anti-nucleons has been rewritten to improve the kinematics of the secondary pions. All momenta and the energies are conserved for each individual annihilation event. This leads to a considerably better agreement with experimental data, especially for the longitudinal momenta and the angular distributions. In earlier versions of CORSIKA [1,3] the mean free paths of particles with finite life times have been calculated by approximations, which are only valid for path lengths shorter than the barometric constant of 8 km. We introduced a path length calculation [4] by an exact formula (muons) or by an iterative procedure with fast convergence (pions and kaons). All interaction lengths are now based on experimental cross sections [5].

For studies of the influence of fragmentation of a heavy primary nucleus in the first collision, total fragmentation or successive abrasion of the primary may be optionally used by a steering flag procedure.

All these modifications did not drastically change our previous results [6]; the main effect is an increase of the muon numbers by up to ca.10%, and hence a

slightly improved separation of the primary particles in the mass spectrum. In comparison with results of the program SHOWERSIM [7], there is now good agreement.

[1] J.N. Capdevielle et al., Report KfK 4875 (1991), eds. H. Beer, J. Wochele, Kernforschungszentrum Karlsruhe, p. 78.

[2] H. Genzel et al., in Landolt-Börnstein (new series) I/8 (Springer Verlag, Berlin, 1973)

[3] P. Doll et al., Report KfK 4686, Kernforschungszentrum Karlsruhe (1990)

[4] D. Heck, G. Schatz, Internal Report (1991), unpublished

[5] A. Baldini et al., in Landolt-Börnstein (new series) I/12 (Springer Verlag, Berlin, 1987)

[6] P. Gabriel, Thesis University Karlsruhe (1992)

[7] A. Wrotniak, Report 85-191, University of Maryland (1985), unpublished

* Laboratoire de Physique Théorique, Université de Bordeaux, Gradignan, France

** Physikalisches Institut, Universität Bern, Switzerland

1.4.2 TREATMENT OF NUCLEUS-NUCLEUS INTERACTIONS IN EAS SIMULATIONS

G. SCHATZ

In extensive air showers (EAS) initiated by complex nuclei interactions between the primary nucleus and air nuclei occur. In the energy range of interest for KASCADE ($>10^{14}$ eV) experimental data of nucleus-nucleus collisions are not available. The quantities relevant for nucleus-nucleus collisions, i.e.

- inelastic cross sections,
- the number of projectile nucleons interacting inelastically and
- the number of target nucleons hit by a projectile nucleon

have to be calculated from the only available information, the proton-antiproton inelastic cross section. The latter is considered to be identical to the nucleon-nucleon cross section. Here and in the following the term inelastic is used to indicate an interaction with particle production, i.e. in the sense of high energy physics, not nuclear physics. Excitation and fragmentation of the interacting nuclei without particle production are disregarded.

Glauber theory allows to calculate the quantities mentioned above from the inelastic nucleon-nucleon cross section and the distribution of nucleons in the two nuclei participating in the collision. The nucleon distributions can be obtained from measured charge distributions compiled by de Vries et al. [1]. The charge distributions differ from the nucleon distributions required due to the finite extent of the proton with a rms charge radius of 0.862 fm. Unfolding the proton charge distribution is very simple if the nuclear charge distribution can be described by a Gaussian. The following relation holds between the mean square charge and nucleon radii

$$<r^2>_n = <r^2>_{ch} - <r^2>_P$$

Here $<r^2>_P$ denotes the mean square radius of the proton. Nuclei below mass number 20 can be sufficiently well described by Gaussian charge distributions. For heavier nuclei a (one or two parameter) Fermi distribution was used. Here the situation is more complicated because folding a Fermi distribution with a Gaussian does not result in a Fermi distribution again. Therefore the following procedure was adopted : A (one or two parameter) Fermi distribution was folded with the Gaussian charge distribution of the proton and the parameters varied until the radius parameter c and the slope of the charge distribution at $r=c$ were reproduced. This resulted in a reduction of the diffuseness by 20 to 25% whereas the radius parameter did not change very much as compared to the charge distribution.

Detailed calculations were performed for 40 nuclei with mass numbers between $A=1$ and 56 for which empirical charge distributions are given in [1], for three values of the inelastic nucleon-nucleon cross section (30, 45 and 60 mb) and the three target nuclei ^{14}N, ^{16}O and ^{40}Ar. For the remaining mass numbers between 1 and 56 the data were interpolated (except for $A=5$ and 8 for which no stable nuclei exist). The results are the inelastic nucleus-nucleus cross sections, the probabilities of n projectile nucleons interacting inelastically and the probalilities of a projectile nucleon hitting m target nucleons.

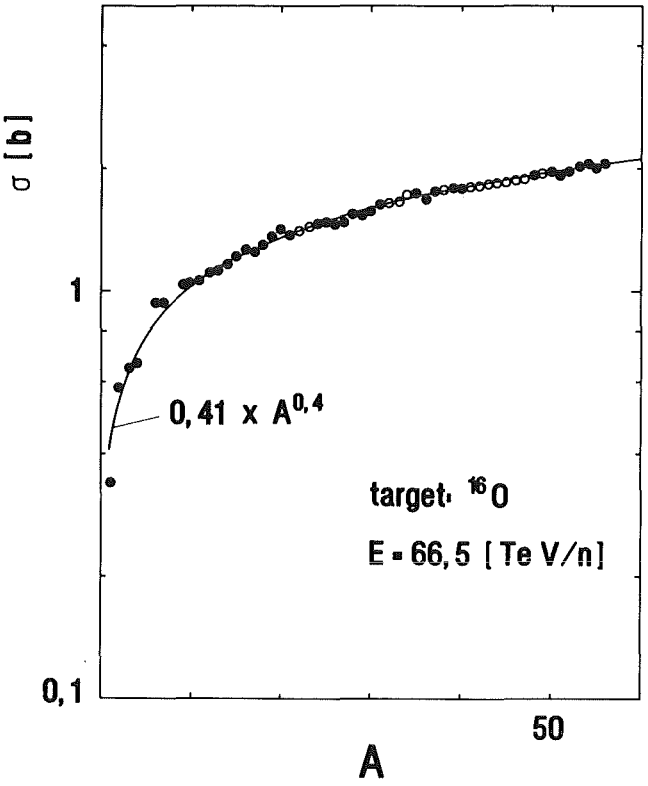

Fig.1: Inelastic nucleus nucleus cross sections for a ^{16}O target and with an inelastic nucleon-nucleon cross section of 45 mb. Full circles represent values which have been calculated individually, open circles are interpolated. The smooth curve is an empirical fit to the data.

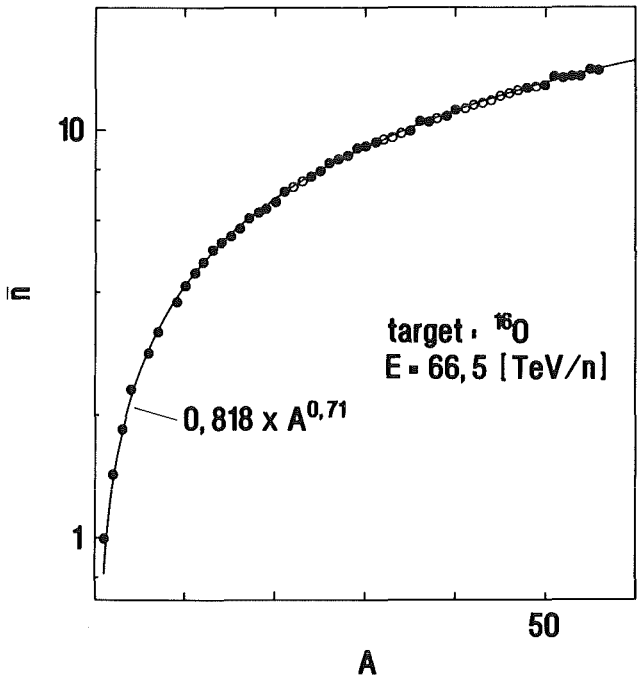

Fig.2: Average number of projectile nucleons participating in a collision of a mass A nucleus with ^{16}O. Full circles represent values which have been calculated individually, open circles are interpolated. The smooth curve is an empirical fit to the data.

Samples of the results are shown in Figs. 1 and 2. Most of the irregularities probably result from the inaccuracies of the input parameters except for the lightest nuclei where they may well show the influence of specific nuclear structure. The comparatively large cross sections for A = 2, 6 and 7 correlate with a large radius and the small value for A = 4 probably reflects the comparatively small radius of the alpha particle. As can be seen from Figs. 1 and 2 most data can be well approximated by a power law.

The three values of the inelastic cross section correspond to laboratory energies of 120 GeV, 66.5 TeV and 5.87 PeV in nucleon-nucleon collisions. Since the calculations do not make use of any specific properties of the projectile except for the cross section the results obtained for A = 1 can also be used for determining the meson-nucleus cross sections.

The resulting cross sections and probabilities are inserted into the CORSIKA program (versions 3.04 and later) as tables which can be interpolated quadratically with respect to the inelastic nucleon-nucleon cross section.

[1] H. de Vries, C.W. de Jager, C. de Vries, Atomic Nucl. Data Tables **36** (1987) 495

1.4.3 INFLUENCE OF NUCLEAR FRAGMENTATION ON EAS DEVELOPMENT

D. HECK, G. SCHATZ

A contribution [1] of this report describes the calculation of nucleus-nucleus cross sections and other data relevant for the simulation of nuclear interactions in extensive air showers (EAS). The results allow for a description of particle production in nucleus-nucleus collisions. In such a collision several of the projectile nucleons will interact inelastically, i.e. producing secondary elementary particles. The remaining ones will proceed at the same velocity, i.e. the same energy per nucleon. The question arises as to whether they will remain bound in one nucleus or travel on as free nucleons (or some intermediate situation will prevail). Since the mean free path of a heavy nucleus is much shorter than that of a nucleon of the same velocity the longitudinal development of EAS may be expected to depend on the degree of nuclear fragmentation.

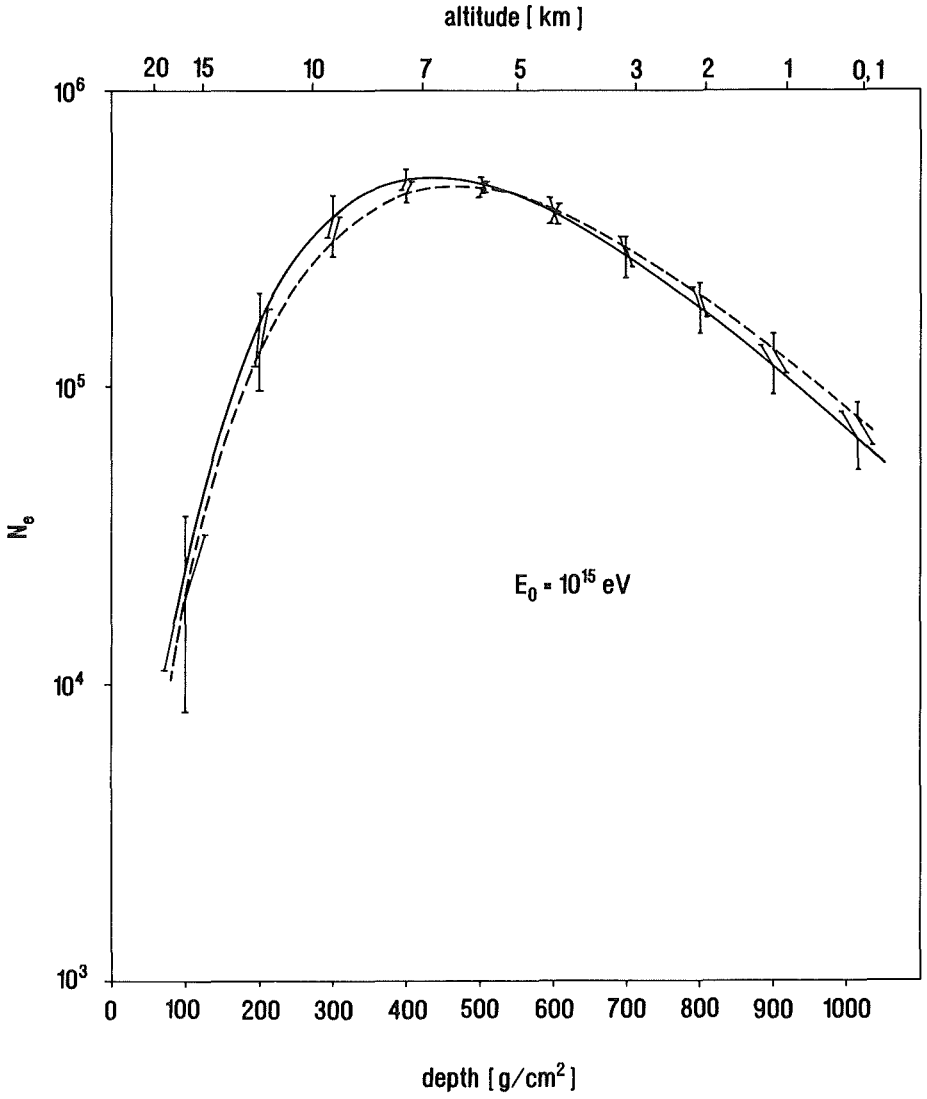

Fig.1 : Longitudinal development of extensive air showers initiated by iron nuclei of 10^{15} eV calculated by assuming complete (full line) or no fragmentation (dashed line).

The two cases mentioned (i) all non-interacting nucleons proceed as free particles (complete fragmentation) or (ii) all non-interacting nucleons stay bound in one nucleus (no fragmentation) clearly represent the two limiting cases embracing the real situation in which most frequently a larger nuclear fragment and several free nucleons and/or alpha particles will emerge from the collision. In order to study the possible influence of nuclear fragmentation on EAS development detailed simulations of EAS induced by iron nuclei were performed for the two limiting cases using the cross sections and probabilities calculated in ref. [1]. The calculations used the CORSIKA program version 3.04. Results of the longitudinal shower development are shown in fig.1. The difference between 'no' and 'complete'

fragmentation turns out to be very small. The same holds for all other shower properties examined in detail. At first sight this may appear very surprising in view of the large differences in mean free path between nuclei and nucleons which amounts to 12.5 g/cm^2 for an iron nucleus of 10^{15} eV energy and to 71 g/cm^2 for a free nucleon of the energy $10^{15}/56$ eV. Since the average number of interacting nucleons is 13 for an iron nucleus of the quoted energy (Fig.2 of ref.[1]) a nucleus of an average mass 43 will emerge from the collision in the 'no fragmentation' case whose mean free path equals 14.2 g/cm^2. So one might expect a large difference in longitudinal shower development for the two cases under consideration. The solution to this seeming paradox lies in the fact that during the collision of the cosmic ray nucleus with an air nucleus only the fraction n/A of the projectile nucleons interacts. The effective mean free path of projectile nucleons in air is therefore given by

$$\lambda_{eff} = \lambda \cdot A/n$$

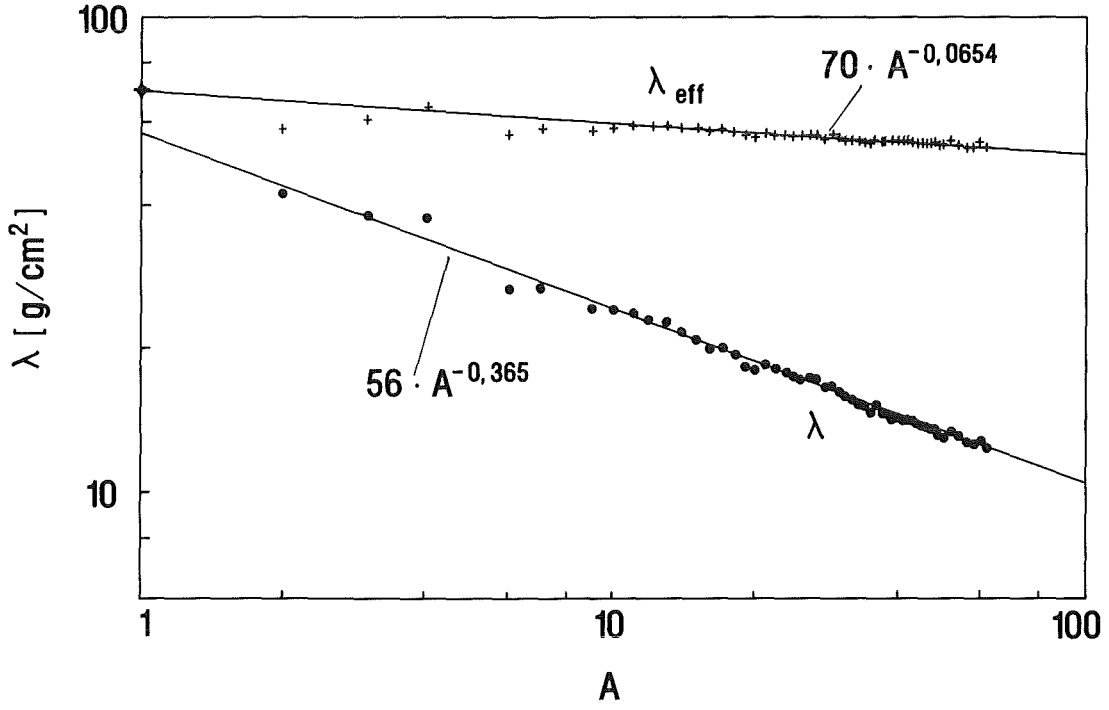

Fig.2 : Mean free path λ of nuclei in the atmosphere at fixed total energy of 10^{15} eV and effective mean free path λ_{eff} obtained by dividing λ by the fraction of projectile nucleons interacting inelastically.

Fig.2 compares the mean free path λ to its effective counterpart λ_{eff}. It shows that λ_{eff} is almost independent of the nuclear mass number A. This observation implies that the average path a nucleon in a primary cosmic ray nucleus travels in

the atmosphere before undergoing its first inelastic interaction does not depend very much on the mass of the nucleus. A further consequence of the weak mass dependence of λ_{eff} is the fact that the depth distributions of energy loss of protons and nuclei do not differ very much. This sheds some light on the argument frequently brought forward that a major difference between showers induced by protons and nuclei lies in the height of the first interaction. While this is of course correct one should also realize that the average energy loss by the first interaction is much lower for a heavy nucleus. When only 13 of 56 nucleons interact and each one loses 50% of its energy the total loss only amounts to 12%. A primary proton would interact deeper but lose half of its energy during the first collision.

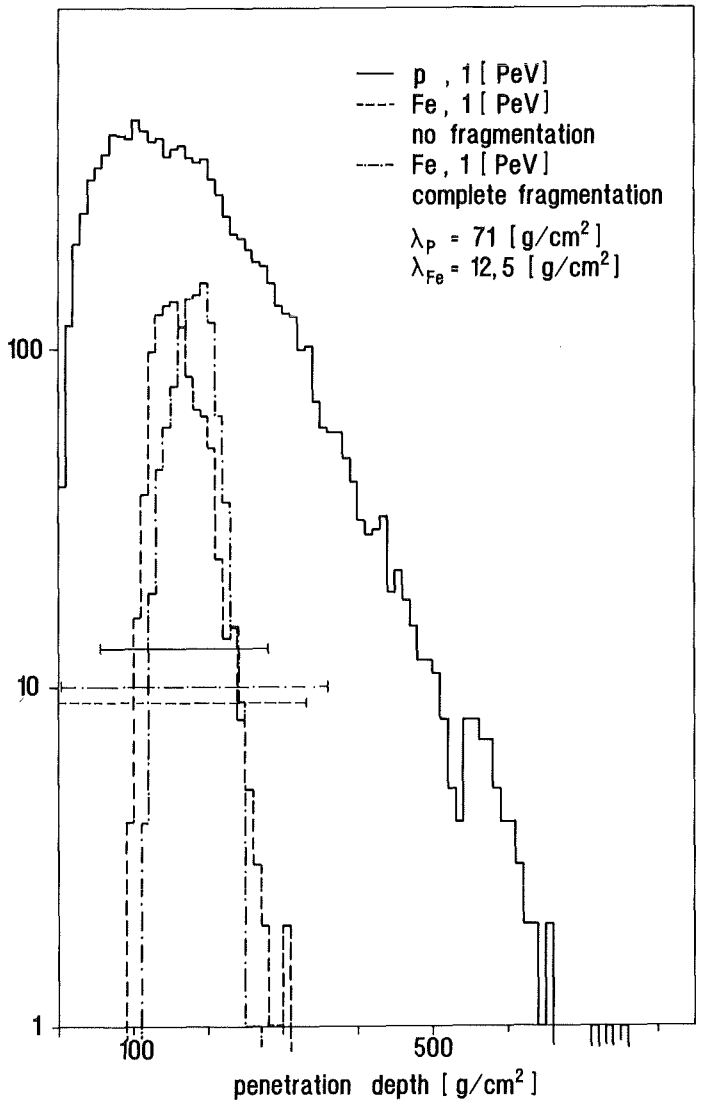

Fig.3 : Distribution of energy penetration depths for proton and iron primaries of 10^{15} eV. For the latter the two limiting cases of no and complete fragmentation have been calculated. The data are based on a simplified model calculation.

The latter aspect was studied in more detail by a simple model calculation. The energy loss of primary protons and iron nuclei was calculated by the Monte-Carlo method using the cross sections of ref.[1] and assuming a distribution of energy loss constant between 0 and 100% (as proposed by Cocconi et al., [2]) Each particle was followed through a number of successive collisions until the particle or its fragments reached ground level. For each event the average depth of energy loss was calculated as the mean depth of collisions weighted by the fraction of the primary energy dissipated at the respective interaction point. We will call this quantity the (energy) penetration depth. In addition, for each event the variance of distribution of the individual depth distribution of the energy loss was calculated. The distribution of penetration depths is shown in fig.3 for protons and iron nuclei of 10^{15} eV. The horizontal bars are centered at the mean values of the distributions and represent the average of the variances, i.e. the depth range in which most of the energy is lost. As can be seen from fig.3 the mean penetration depths hardly differ. The main difference between protons and iron nuclei is in the width of the depth distribution. The penetration depths of showers initiated by protons of the same energy scatter considerably whereas the width of the corresponding distribution for iron induced showers is much smaller. This is of course to be expected because of the averaging of 56 subshowers in the latter case. The difference between the distributions with 'no' and 'complete' fragmentation is again much smaller than the width of the respective distributions. The fact that proton induced showers attain their maxima deeper in the atmosphere then has to be attributed to the higher energy of secondary particles, especially gamma rays from the decay of neutral pions. It is well known from the analytical theory of electromagnetic showers that their maxima lie the deeper the higher their energy.

[1] G. Schatz, contribution 1.4.2 of this report

[2] G. Cocconi, L.J. Koesters, D.H. Perkins, UCRL-10022 (1961) 167
G. Coccconi, Nucl. Phys. B28 (1971) 341

1.4.4 ANALYSIS OF THE ARRIVAL TIME DISTRIBUTION OF MUONS IN AIR SHOWERS SIMULATED WITH CORSIKA

H. REBEL, V. CORCALCIUC*, G. VÖLKER, W. ZIMMER*

In principle the history of the cascade development of extensive air showers (EAS) is reflected by the time structure of incidence. In particular, the longitudinal structure of the *muonic* component is expected to be sensitive to the geometrical structure of the air shower as well as to the Lorentz factors of the secondary particles [1,2]. Thus, especially at larger distances from the shower axis where the geometric factor is dominating, the arrival time distributions map the longitudinal development of the shower in the atmosphere and may inform on early stages of the shower. As the longitudinal development is again determined by the multiplicity of the secondary particles from collisions with the primary cosmic rays by the mean free path and the cross sections of interaction with air nuclei, the measurement of muon arrival time distributions and the time dispersion of the muon front may provide signatures for the elemental composition of the primary cosmic rays. In order to get more quantitative insight in these features and in the experimental requirements of such measurements we analysed the data from EAS Monte-Carlo simulations with the CORSIKA code (see ref.[3]) for muons produced by proton and iron-nuclei initiated showers at energies of $5 \cdot 10^{14}$, $2 \cdot 10^{15}$ eV and to $1 \cdot 10^{16}$ eV.

We studied the influence of various observation parameters on the distributions of the arrival time (defined as delay time with respect to the arrival of the electromagnetic front) and the mean muon time dispersal, respectively. They are dependent on the threshold energy of muon detectors, the primary energy and the shower core distance (and the zenith angle of incidence). In general, as far as a comparison is possible, the results agree with the few data given in literature. Significant discrepancies are indicated with results of Khristiansen at al. [4] who found a remarkably small time dispersion at larger distances from the shower core.

Fig.1 displays results inferred from the simulation of 200 showers of vertical incidence at sea level for each projectile type and energy. The distributions at small distances (regime of Lorentz effects) where measurements would less suffer from intensity problems, are rather insensitive to the nature of the primary particles. Visible effects show up at larger core distances due to the dominance of path length effects of the travelling muons. However, there the low density of the

muons does not allow to study fluctuations between single showers. The features are more pronounced for larger threshold energies of the muon detection while higher primary energies shift the effects to larger core distances. It is interesting to note that a simple geometrical reasoning, taking into account the average difference of the maximum positions for proton and Fe induced showers, is able to explain differences in the arrival time distributions at larger core distances.

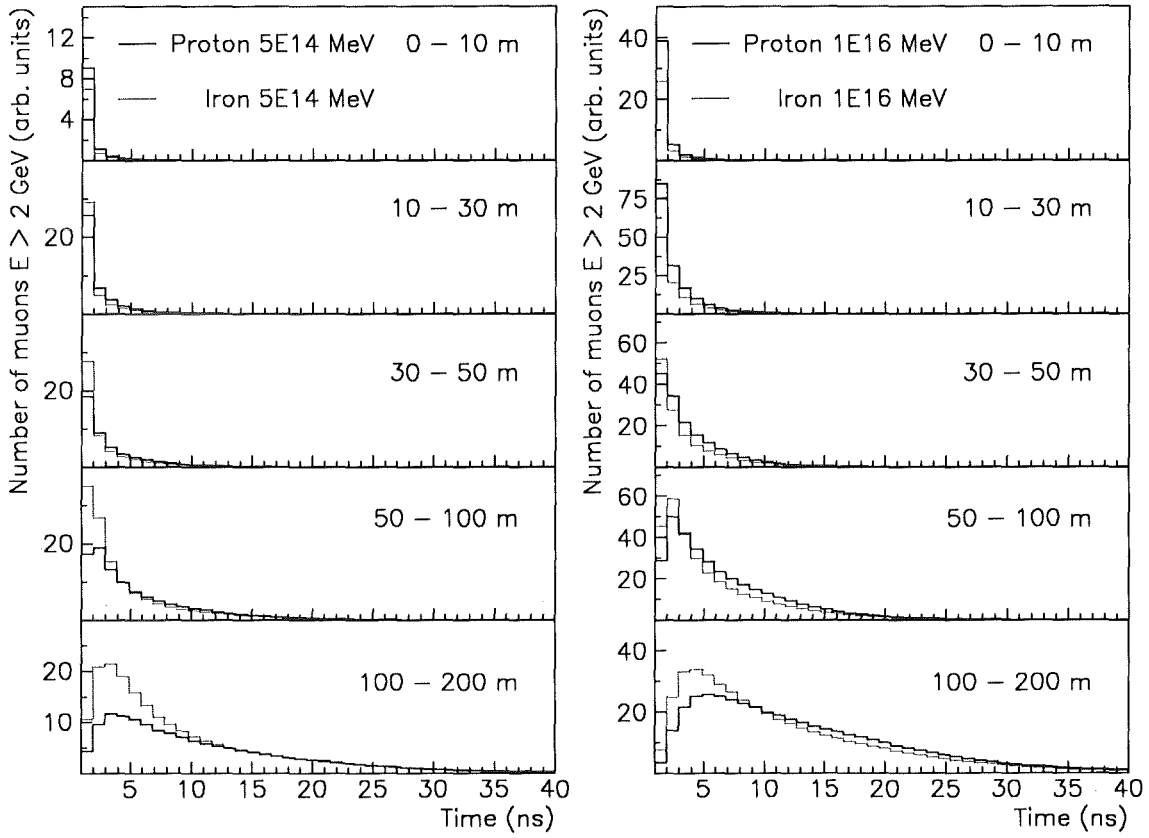

Fig.1 : Arrival time distributions of muons ($E_\mu \geq 2$ GeV) for proton and Fe induced air showers ($E_0 = 5 \cdot 10^{14}$ eV and $1 \cdot 10^{16}$ eV) and various distances from the shower core.

[1] P.K.F. Grieder, Proc. 17th Int. Conf. on Cosmic Rays, Paris 6 (1981) 288

[2] F. Kakimoto, T. Tamura, Y. Matsumoto, T. Enoki, I. Tsuchimoto, K. Nishi and K. Suga, Journ. Physics G : Nucl. Phys. 12 (1986) 151

[3] J.N. Capdevielle et al., Report KfK 4875 (1991), eds. H. Beer, J. Wochele, Kernforschungszentrum Karlsruhe, p. 78

[4] G.B. Khristiansen et al., Proc. 21st Int. Conf. on Cosmic Rays, Adelaide (Australia) 9 (1990) 150

* Institute of Atomic Physics, Bucharest, Romania

2. NEUTRINOPHYSICS

T. CSABO, G. DREXLIN, V. EBERHARD, K. EITEL, H. GEMMEKE, W. GRANDEGGER, R. GUMBSHEIMER, H. HUCKER, L. HUSSON, J. KLEIN-FELLER, M. KLEIFGES, R. MASCHUW, CH. MITSCHKE, P. PLISCHKE, J. RAPP, G. SPOHRER, J. WOCHELE, S. WÖLFLE, J. WOLF, B. ZEITNITZ, D. BLASER*, B. BODMANN*, A. DIRSCHBACHER*, E. FINCKH*, T. HANIKA*, J. HÖßL*, W. KRETSCHMER*, R. MEYER*, F. SCHILLING*, J.A. EDGINGTON**, A. MALIK**, B. SELIGMANN**, A. DODD***, A.G. D.PAYNE***, N.E. BOOTH****.

2.1 INTRODUCTION

The neutrino experiment **KARMEN** (KArlsruhe Rutherford interMediate Energy Neutrino experiment) is performed at the neutron spallation facility **ISIS** of the Rutherford Appleton Laboratory. From the decay of stopped pions produced in the UD_2O 'beam dump' of the pulsed 800 MeV proton beam of ISIS, equal numbers of ν_μ, ν_e and $\bar{\nu}_\mu$ are emitted isotropically with energies up to 52.8 MeV. Due to the short lifetime of π^+ (26 ns) there is a prompt burst of ν_μ within the first 0.5 µs after proton beam-on-target whereas the subsequent μ^+-decay provides a $(\nu_e,\bar{\nu}_\mu)$-pulse in the later time window of 0.5 - 8 µs where ν_μ are no longer present. Both ν_e and $\bar{\nu}_\mu$ show the characteristic exponential time dependence determined by the μ^+-lifetime of 2.2 µs. This time structure after a 20 ms interval between neutrino pulses is repeated with the ISIS proton extraction frequency of 50 Hz. The resulting duty factor of the order of 10^{-4} allows effective suppression of cosmic background.

Neutrinos are detected with a 56 t-liquid scintillation calorimeter, located at a mean distance of 17.5 m from the neutrino source and housed in a 6000 tonne shielding blockhouse. A total thickness of 7.2 m of steel shields the calorimeter against neutrons from the spallation source. The detector consists of a large rectangular vessel filled with 65,000 l of mineral oil based scintillator **PPP** (paraffin, pseudocumene, **PMP**-fluor). An optical segmentation divides the central detector volume into 512 optically separated modules. Each module of 18 x 18 cm^2 cross section and 350 cm length is viewed by two 3" phototubes on either end. The 96% active mass of the detector in combination with its high energy resolution of $\sigma(E)/E = 11.5\%/\sqrt{E(MeV)}$ provides good calorimetric properties for low energy particles.

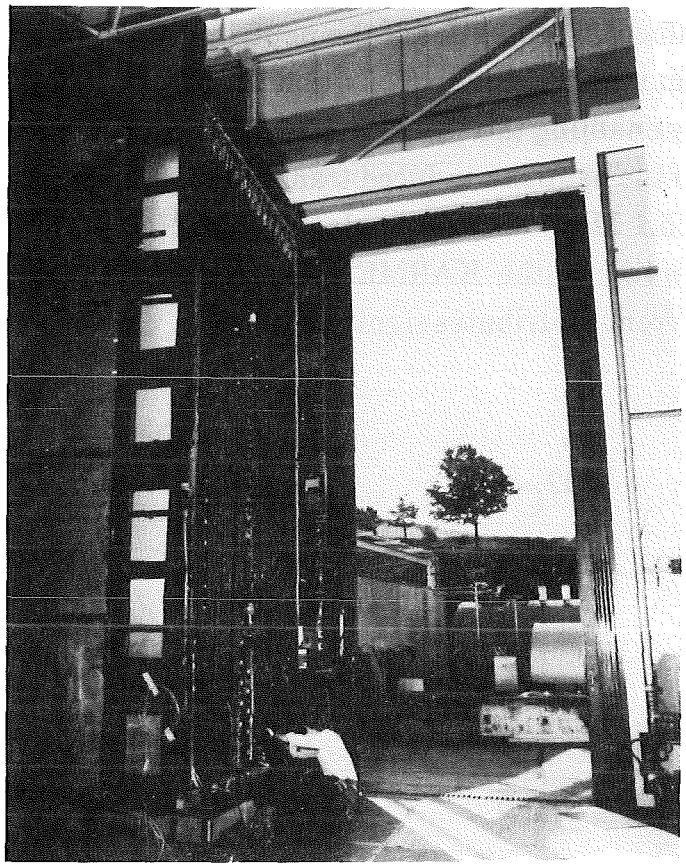

Fig.1: View on one end of KARMEN with its cabling and the scintillator storage tank outside (1989).

An anticounter system surrounding the central detector serves as active shield against μ-induced background reactions from cosmic rays. The calorimeter in its final stage of assembly is shown in fig.1.

Major physics aims of the experiment are the search for neutrino oscillations and the investigation of charged (CC) and neutral current (NC) nuclear interactions with their implications for specific weak couplings, flavor universality and weak interaction nuclear formfactors.

KARMEN started taking data in November 1989. Since then a number of improvements on ISIS performance, slow and fast neutron shielding as well as on trigger and readout electronics have been installed. This enabled the KARMEN experiment after two years of continous operation to deduce its first quantitative results on ν-^{12}C interactions and ν-oscillations.

2.2 RESULTS FROM ν-^{12}C REACTIONS

The observation of neutrino-induced transitions between discrete nuclear states is an ideal tool to study in detail the structure of the weak hadronic current as well as to investigate fundamental properties of the neutrino itself. Due to the well defined change of quantum numbers in the transition the target nucleus acts as a 'spin-isospin' filter thereby enabling the selection of specific parts of the weak hadronic current. In the case of the neutrino-induced transitions from $^{12}C_{g.s.}$ (0^+0) to the excited state $^{12}C^*(1^+1,15.1$ MeV) and the analogue state $^{12}N_{g.s.}$ (1^+1), see fig.2, both of which are observed in the KARMEN experiment [1], only the isovector - axialvector weak current contributes significantly.

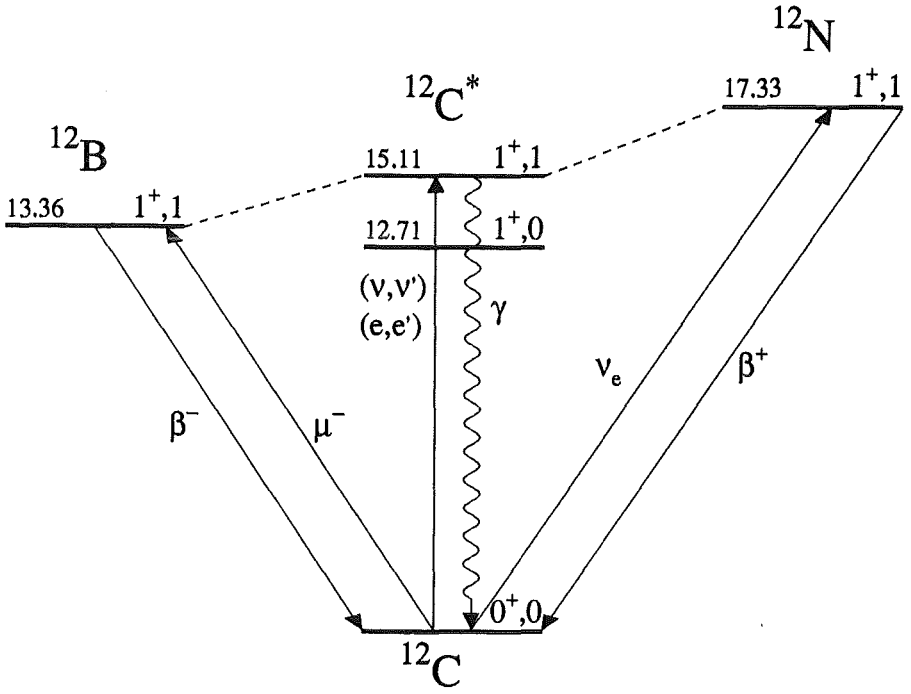

Fig.2 : Isospin-triplet A = 12 and its isovector-axialvector weak transitions.

Classical weak processes with the same change of spin, parity and isospin such as the β-decays of the mirror nuclei ^{12}N and ^{12}B and the muon capture reaction $^{12}C(\mu^-,\nu_\mu)^{12}B$ explore the structure of the weak current only at fixed values of momentum transfer q^2. The inverse β-decay $\nu_e + {}^{12}C \rightarrow {}^{12}N_{g.s.} + e^-$ is, in contrast, a weak interaction where a range of q^2 can be investigated, allowing thereby the study of the q^2-dependence of the axial form factor of the weak hadronic current.

Investigation of the NC nuclear excitation $^{12}C(\nu,\nu')^{12}C^*(1^+1,15.1\ MeV)$ induced by neutrinos of different flavour i.e. ν_e and $\bar{\nu}_\mu$ or ν_μ provides a test of the μ-e universality of the ν-Z^0 coupling.

2.2.1 CHARGED CURRENT REACTION $^{12}C(\nu_e,e^-)^{12}N_{g.s.}$

Detection of the exclusive $^{12}C(\nu_e,e^-)^{12}N_{g.s.}$ reaction [3] is based on a spatially correlated coincidence between an electron from the inverse β-decay on ^{12}C in the ν_e-time window and a positron at the same position from the subsequent $^{12}N \rightarrow \nu_e + e^+ + ^{12}C$ decay.The ^{12}N decay uniquely identifies the neutrino-induced transition to the ground state of ^{12}N and is characterized by a lifetime of $\tau = 15.9$ ms with an endpoint energy of $E_0 = 16.3$ MeV.

The data sample used for the present analysis was taken from December 1989 to December 1991 corresponding to 2260 Coulombs of protons on target. Only events fully contained within the fiducial volume which had no activity in the 20 μs pretrigger interval were scanned for delayed coincidences with the signature of a $^{12}C(\nu_e,e^-)^{12}N_{gs}$ reaction. Straight forward energy and time cuts on the prompt as well as on the delayed signal requiring spatial correlation eliminated all but 112 coincidence events from the data sample.

Fig. 3a-d shows the distributions of visible energies and times after beam-on-target for these candidate $^{12}C(\nu_e,e^-)^{12}N_{g.s.}$ events, as well as for background events taken in an 80 μs window before beam-on-target (shaded area). The visible energies of the prompt and delayed parts of the coincidence are compared to Monte Carlo simulations, whereas the time spectra are shown with the decay curves of μ^+ ($\tau = 2.2$ μs) and $^{12}N_{g.s.}$ ($\tau = 15.9$ ms) superimposed.

The time distribution of prompt events (fig. 3b) clearly demonstrates that the delayed coincidences are due to neutrinos from μ^+-decay at rest. For the first time neutrinos have been identified almost without any background, indicated by the high signal to background ratio of 30:1, which highlights the significant advantages of operating a high resolution calorimeter at a pulsed neutrino source.

The distribution of the time differences between prompt electrons and delayed positrons, shown in fig. 3d, agrees well with the ^{12}N-lifetime. Due to the fixed readout cycle of the experiment from 15.8-19.8 ms no data are collected in the corresponding time interval.

From these data the integral flux-averaged cross section for ν_e from μ^+-decay at rest has been deduced to be $<\sigma_{cc}>^{exp}=[8.0\pm0.8(stat.)\pm0.75(syst.)]\cdot10^{-42}$ cm^2.

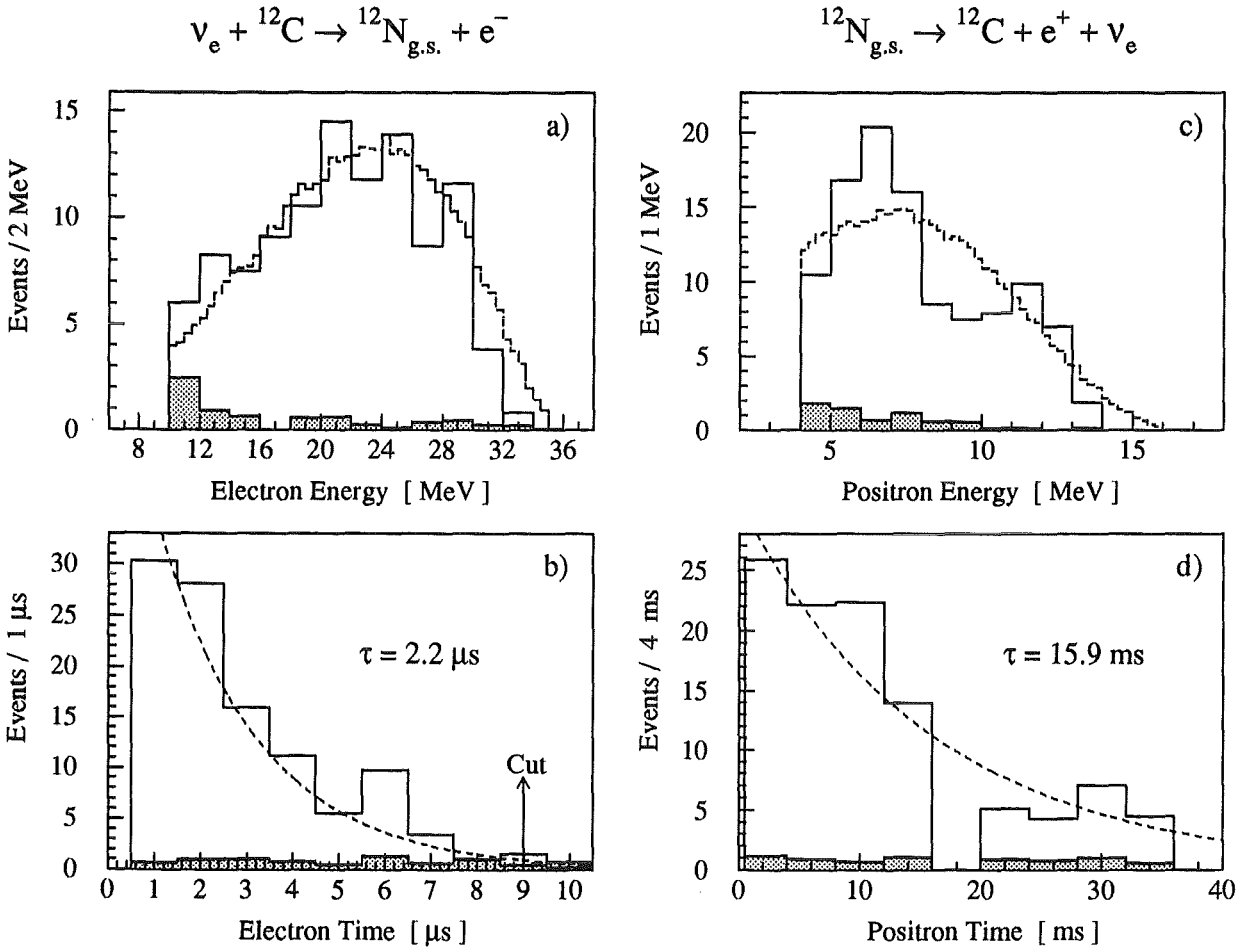

Fig.3: Delayed $^{12}C(\nu_e,e^-)^{12}N_{gs} \rightarrow {}^{12}C + e^+ + \nu_e$ coincidences. The energy spectra of prompt electrons (a) and delayed positrons (c) are compared to GEANT simulations (broken line). The corresponding time distributions are shown in (b) and (d) with the decay curves of μ^+ and ^{12}N being superimposed. The normalized 'beam off' background is shown as shaded area.

This result is in good agreement with recent theoretical calculations [4] yielding values between 8 and $9.4\cdot10^{-42}$ cm^2 with a 10 % uncertainty.

The high energy resolution of the KARMEN detector also allowed a measurement of the energy dependence of the $^{12}C(\nu_e,e^-)^{12}N_{g.s.}$ cross section. As the recoil energy transferred to the ^{12}N-nucleus is negligible, the neutrino energy

E_ν is related to the electron kinetic energy E_{e^-} by the relation $E_\nu = E_{e^-} + 17.3$ MeV. Thus a precise measurement of the electron kinetic energy determines the primary neutrino energy. Due to the good calorimetric properties of the KARMEN detector an unfolding procedure allows to transform visible energies into primary kinetic energies by applying the experimental detector response function. The resulting neutrino energy spectrum was subdivided into four energy intervals, fig.4 shows the resulting energy dependence of the cross section which was measured for the first time ever and is in good agreement with theoretical predictions.

This agreement makes the $^{12}C(\nu_e,e^-)^{12}N_{g.s.}$ reaction a useful flux normalization for all other neutrino-induced reactions in this experiment, i.e. the inclusive charged current channel $^{12}C(\nu_e,e^-)X$, the neutral current reaction $^{12}C(\nu,\nu')^{12}C^*(1^+1)$ and neutrino oscillations of the appearance type $\nu_\mu \rightarrow \nu_e$.

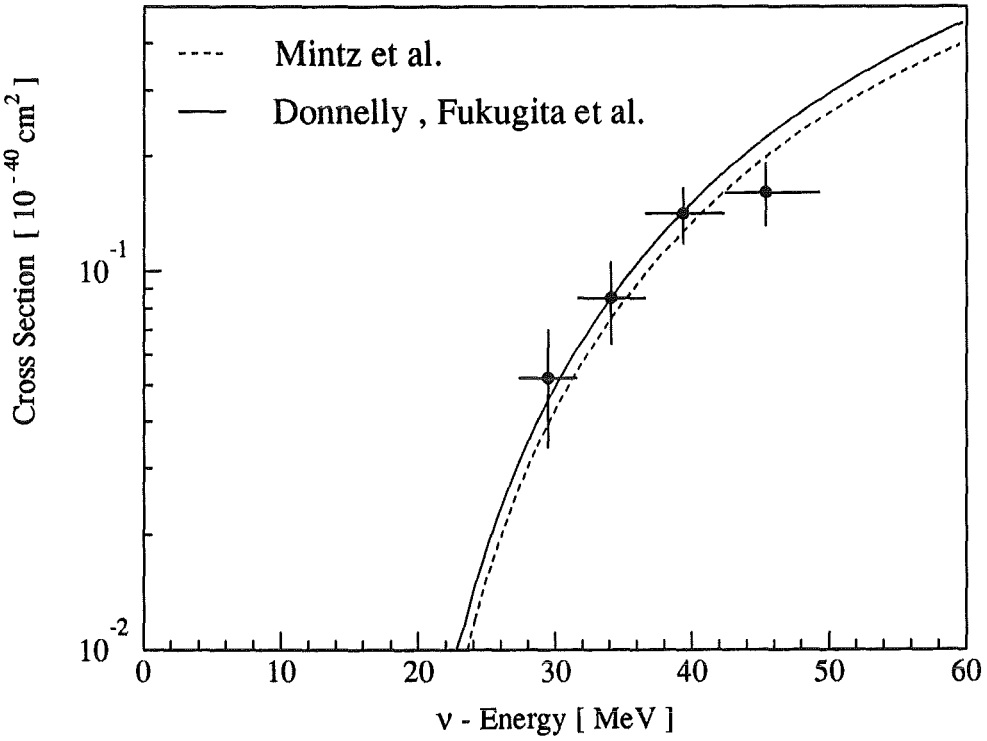

Fig.4 : Energy dependence of the $^{12}C(\nu_e,e^-)^{12}N_{g.s.}$ cross section for neutrino energies up to 50 MeV. The experimental data points are compared to theoretical calculations [4].

2.2.2 NEUTRAL CURRENT REACTION $^{12}C(\nu,\nu')^{12}C^*(1^+1,15.1\ MeV)$

Since summer 1990 an improved experiment shielding and optimized trigger conditions allowed to evaluate the data for neutral current events of the type $\nu + {}^{12}C \rightarrow \nu' + {}^{12}C^*(1^+1,15.1\ MeV)$ [2].

The signal for the inelastic ν-scattering process is the detection of a localized scintillation event of a 15 MeV photon emitted from the $(T=1,J^\pi=1^+)$ analogue state of ^{12}C. Evaluation has again been restricted to the time window of ν_e and $\bar{\nu}_\mu$. After subtraction of the beam off and beam correlated background 70 candidate events for the NC-reactions survive in the range of visible energies between 11 and 16 MeV, as shown in fig.5. The time characteristic of these events, shown in fig. 6a, is in good agreement with the 2.2 μs decay curve as expected for neutrinos from the decay $\mu^+ \rightarrow e^+ + \bar{\nu}_\mu + \nu_e$ in the beam stop. Furthermore these events cannot be faked by an extension of low energy background as the time behaviour of events with 8-11 MeV visible energy (fig. 6b) indicates a completely different origin. In fact this background is increasing with time due to the presence of beam correlated slow neutrons which won't cause a detector signal with visible energy above 10 MeV. The energy distribution above 11 MeV is within the statistics well reproduced by a Monte Carlo simulation including the inclusive charged current reactions an ^{12}C and ^{13}C.

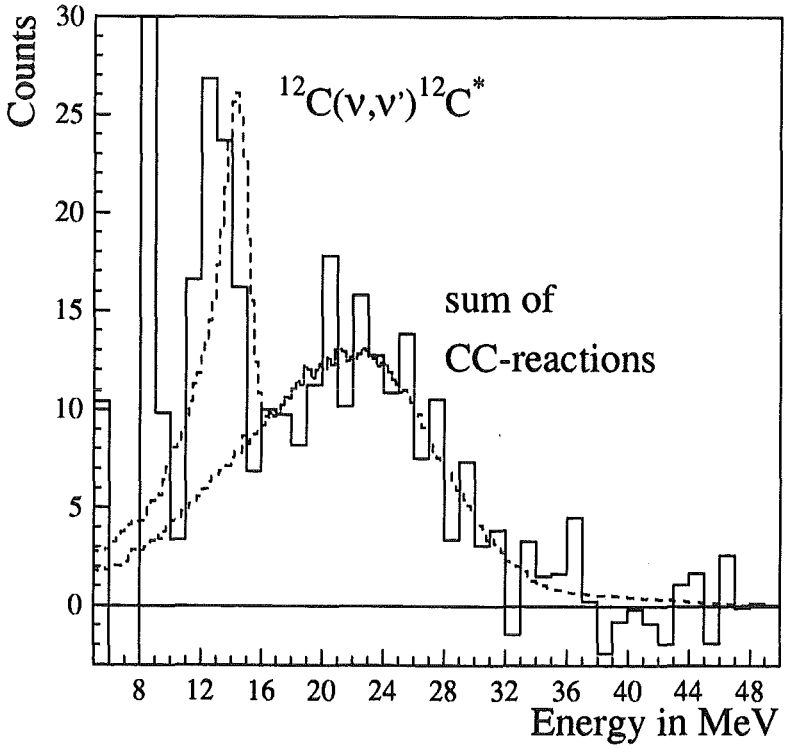

Fig.5 : Visible energy spectrum of single prong events during the $(\nu_e,\bar{\nu}_\mu)$-time window with background subtracted. The dotted line corresponds to the Monte Carlo distributions for inclusive charged current reactions and the neutral current $^{12}C(\nu,\nu')^{12}C^*(1^+1,15MeV)$ reaction, respectively.

From the evaluation of the data between 11 and 16 MeV it is possible to extract for the first time a neutral current cross section for neutrino nucleus

scattering. The summed cross section for $\bar{\nu}_\mu$ and ν_e averaged over their energy distribution was determined to be $<\sigma(\nu_e+\bar{\nu}_\mu)>^{exp}=[9.1\pm2.3(stat.)\pm1.5(syst.)]\cdot10^{-42}$ cm^2. This result agrees well with recent calculations for the neutral current excitation of the $^{12}C(1^+1)$ state using standard model weak interaction couplings as performed by several authors [4] : $<\sigma(\nu_e+\bar{\nu}_\mu)>^{theo}=[9.9\pm1.0]\cdot10^{-42}$ cm^2.

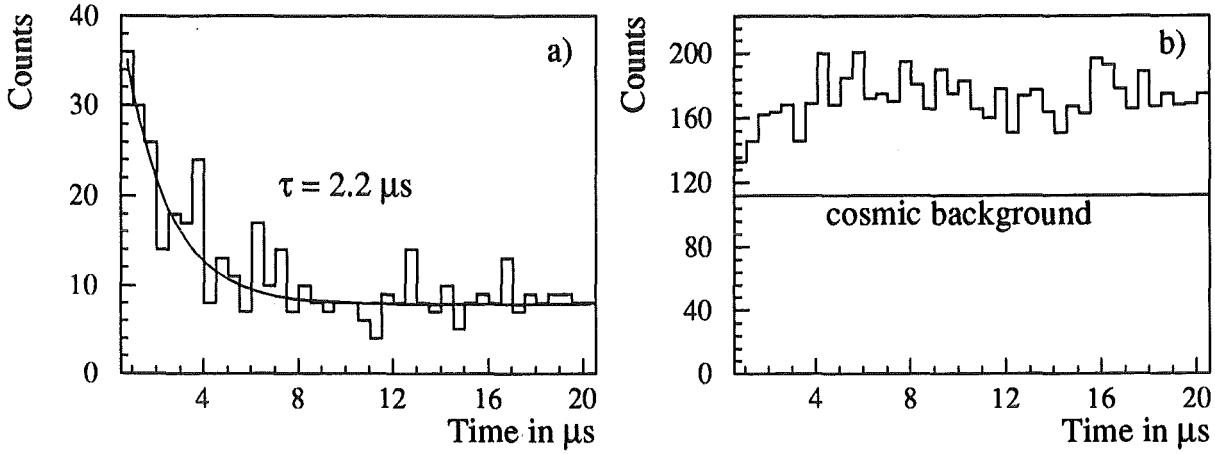

Fig.6 : Event time with respect to beam-on-target for neutrino induced events (a) in the NC-energy window (E=11-16 MeV) and background events (b) (E=8-11 MeV).

Provided the neutrino has a non-vanishing magnetic moment the same transition can be mediated by the electromagnetic interaction. However, even for $\mu_\nu=4\cdot10^{-10}\mu_{Bohr}$, the current upper laboratory limit for a neutrino magnetic moment, its contribution to the $^{12}C(1^+1)$ excitation is negligible [5].

2.2.3 INCLUSIVE CHARGED CURRENT REACTIONS $^{12,13}C(\nu_e,e^-)^{12,13}N$

The single prong events of neutral current reactions are superimposed by a broad distribution of charged current reactions of the type $^{12}C(\nu_e,e^-)^{12}N^*$ and $^{12}C(\nu_e,e^-)^{12}N_{g.s.}$ centered around 22 MeV. The contribution of other reactions as ν-e-scattering and $^{13}C(\nu_e,e^-)^{13}N$ is negligible due to the low cross section [4] or low ^{13}C content, respectively. The $^{12}C(\nu_e,e^-)^{12}N_{g.s.}$ cross section is fixed by our exclusive measurement [3] described above.

If the excess countrate above 16 MeV visible energy is thus assigned to inclusive CC transitions to excited states of ^{12}N the measured data indicate a

significantly higher cross section for the ^{12}C $(\nu_e,e^-)^{12}N^*$ reaction than theoretically expected [4]. Currently there is no conclusive argument for this deviation which survives all carefully applied experimental checks; a more elaborated theoretical investigation of inelastic inclusive reactions seems to be necessary.

2.4 SEARCH FOR NEUTRINO OSCILLATIONS

Although the statistics after only two years of data taking is still quite low analysis of the data has been extended to the search for ν oscillations of the type $\nu_\mu \rightarrow \nu_e$ and $\bar{\nu}_\mu \rightarrow \bar{\nu}_e$. Appearance oscillations $\nu_\mu \rightarrow \nu_e$ require the detection of 30 MeV electron neutrinos during the time window of muon neutrinos with the delayed coincidence signature of the ^{12}C $(\nu_e,e^-)^{12}N_{g.s.}$ reaction. Until now no event has been found whereas 56 would have been expected for an oscillation probability of 1 (full oscillation). With an expected background from ν_e-contamination (μ^+-decay) and cosmics of 0.7 events the exclusion limit for oscillations is currently $P\nu_\mu \rightarrow \nu_e < 4.1 \cdot 10^{-2}$ at a 90 % confidence level (CL).

$\bar{\nu}_\mu \rightarrow \bar{\nu}_e$ oscillations will be identified in KARMEN by another delayed coincidence signal caused by the inverse β-decay of the $\bar{\nu}_e$ on protons i.e. $^1H(\bar{\nu}_e,e^+)n$, where the positron is looked for during the time slot of $\bar{\nu}_\mu$ and the neutron will be detected by the Gd(n,γ) ($\Sigma E \leq 8$MeV) reaction about 100 μs later. Four events of that type have been found where 206 events could have been expected for full oscillation. With an expected background of 2.15 events the exclusion limit for $\nu_\mu \rightarrow \nu_e$ is $P\bar{\nu}_\mu \rightarrow \bar{\nu}_e < 2.8 \cdot 10^{-2}$ at 90 % CL.

These limits are about an order of magnitude away from the currently published oscillation limits on this cannel. After four more years of data taking KARMEN will have proven these limits with great reliability because of its good resolution figures, clear ν-signatures and well understood background conditions.

[1] G. Drexlin et al. (KARMEN Collaboration), Nucl. Instr. & Meth. **A289** (1990) 490;
B. Bodmann et al., Nucl. Instr. & Meth. **A286** (1990) 214

[2] B. Bodmann et al. (KARMEN Coll.), Phys. Lett. **B267** (1991) 321

[3] G.Drexlin et al. (KARMEN Coll.), Phys. Lett. B (in press)

[4] T.W. Donnelly, Phys. Lett. 43B (1973) 93
T.W. Donnelly and R.D. Peccei, Phys. Rep. **50** (1979) 1
M. Fukugita, Y. Kohyama and K. Kubodera, Phys. Lett. **B212** (1988) 139
S.L. Mintz and M. Pourkaviani, Phys. Rev. **C40** (1989) 2458;
J. Phys. G : Nucl. Part. Phys. **16** (1990) 569
E. Kolbe et al., KFA-Report IKP(TH)-48 (1991)

[5] A. Dodd, E. Papageorgiu, S. Ranfone, Phys. Lett. **B266** (1991) 434

* Physikalisches Institut, Universität Erlangen-Nürnberg

** Queen Mary and Westfield College, London, UK

*** Rutherford Appleton Laboratory, Chilton, Didcot, UK

**** Oxford University, Oxford, UK

3. NUCLEAR PHYSICS

3.1 NUCLEAR ASTROPHYSICS

3.1.1 MEASUREMENT OF THE $^{14}C(n,\gamma)^{15}C$ CROSS SECTION AT A STELLAR TEMPERATURE OF kT = 23.3 keV

H. BEER, M. WIESCHER*, F. KÄPPELER, J. GÖRRES*,
P.E. KOEHLER**

Nonstandard big bang nucleosynthesis leads to the production of ^{14}C ($t_{1/2}$ = 5730 yr) via the reaction sequence $^{7}Li(n,\gamma)^{8}Li(\alpha,n)^{11}B(n,\gamma)^{12}B(\beta^-)$ ^{12}C (n,γ) $^{13}C(n,\gamma)^{14}C$. The further reaction path for the synthesis of heavier elements depends on the depletion of ^{14}C by either (p, γ), (d, n), (α, γ) or (n, γ) reactions. We have investigated the neutron capture channel. The capture cross section of ^{14}C has been determined by a fast cyclic activation technique. The measurements were carried out at the 3.75 MV Van de Graaff accelerator using the $^{7}Li(p,n)$ reaction close to the reaction threshold. The activation sample consisted of 605 mg carbon powder enriched to 98% in ^{14}C. The ^{14}C capture cross section was measured relative to the ^{197}Au standard cross section. The resulting ^{15}C activity ($t_{1/2}$ = 2.45s) was counted with a HPGe-detector via the characteristic 5297.79 keV γ-ray line. The detector efficiency was determined via the γ ray lines of the 992 keV resonance in the $^{27}Al(p,\gamma)$ reaction and with a calibrated ^{238}Pu-^{13}C source with a line at 6.13 MeV. The activity measurement was severely hampered since the nickel canning of the sample was activated ($^{56,57,58}Co$) in previous experiments with a 500 MeV proton beam. To reduce pile-up (especially from the ^{56}Co lines) a 28 mm thick tungsten shielding was placed between sample and HPGe detector. Dead time effects in the ADC were reduced by an electronic threshold at 685 keV. The overall deadtime of the system was determined by means of a research pulser signal of definite frequency (50 Hz) that was registered in the γ-ray spectrum during the whole measurement. Five individual runs of typically 5 days measuring time were performed. The data in fig.1 represent the total sum spectrum. The single escape peak of the 5297.79 keV line lies already in the background region from pile-up events and cannot be used in the analysis. From the full energy peak we deduced a total number of 333 ± 78 counts, leading to a capture cross section of 1.72 ± 0.43 μb. This value is by a factor of 5 smaller than predicted by theoretical calculations, resulting in a significant reduction of the reaction flow via the $^{14}C(n,\gamma)^{15}C(\beta^-)^{15}N$ sequence. Therefore, the main depletion

mechanism of ^{14}C in the inhomogeneous big bang nucleosynthesis remains either $^{14}C(p, \gamma)^{15}N$ or $^{14}C(d, n)^{15}N$ depending on the hydrogen abundances in the neutron rich zones as discussed by Kawano, Fowler, Kavanagh, Malaney [1].

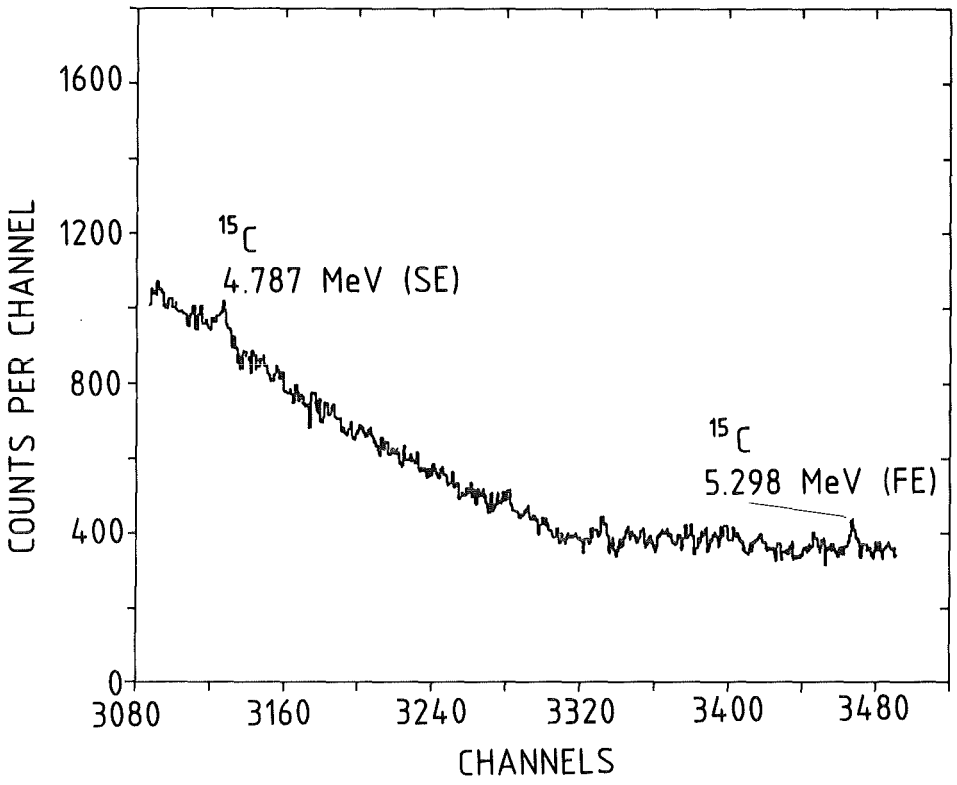

Fig. 1 : The total accumulated data of the measurements. The single escape (SE) and full energy peak (PE) of the 5.298 MeV line are shown.

[1] L. Kawano, W.A. Fowler, R.W. Kavanagh, R.A. Malaney, Astrophysical Journal 1992 (in press)

* University of Notre Dame, Notre Dame, Indiana

** Los Alamos National Laboratory, New Mexico

3.1.2 CAPTURE REACTIONS ON ^{14}C IN INHOMOGENEOUS BIG BANG NUCLEOSYNTHESIS[1)]

J. GÖRRES*, M. WIESCHER*, R.E. AZUMA**, C.A. BARNES***, H. BEER, F. KÄPPELER, F.K. THIELEMANN****

The alpha and neutron capture reactions on ^{14}C, important in a nonstandard big bang scenario, have been studied experimentally. The results will be presented and the relative importance of all reactions, leading to the destruction of ^{14}C, will be discussed

1) published in Radioactive Nuclear Beams, ed. Th. Delbar, Adam Hilger, Bristol 1991, Philadelphia - New York, p. 293

* University of Notre Dame, Notre Dame, Indiana

** University of Toronto, Canada

*** W.K. Kellogg Radiation Laboratory, Caltech, California

**** Harvard Smithsonian Center for Astrophysics, Cambridge, Massachusetts

3.1.3 $^{17}O(n,\alpha)^{14}C$ - BOTTLE NECK FOR PRIMORDIAL NUCLEOSYNTHESIS ?

H. SCHATZ, F. KÄPPELER, P.E. KOEHLER*, M. WIESCHER**, H.P. TRAUTVETTER***

In the standard model, the expansion in the big bang is considered as homogeneous and isotropic. Hence, the nucleosynthesis is characterized by a sequence of neutron and proton capture reactions that is restricted to the mass range $A<5$ with only a marginal outbreak to the $A=6$-7 region via the $^{3}He(\alpha,\gamma)^{7}Be$ reaction. An alternative scenario, that would allow for bridging the second instability gap at $A=8$ has been proposed by treating the formation of hadrons from the primeval quark-gluon plasma as a first order phase transition [1] around $kT\sim100$ MeV. In this model, one obtains strong density fluctuations.

After the freeze-out of the weak interactions, these fluctuations give rise to proton-rich high density zones embedded in neutron-rich regions of low density.

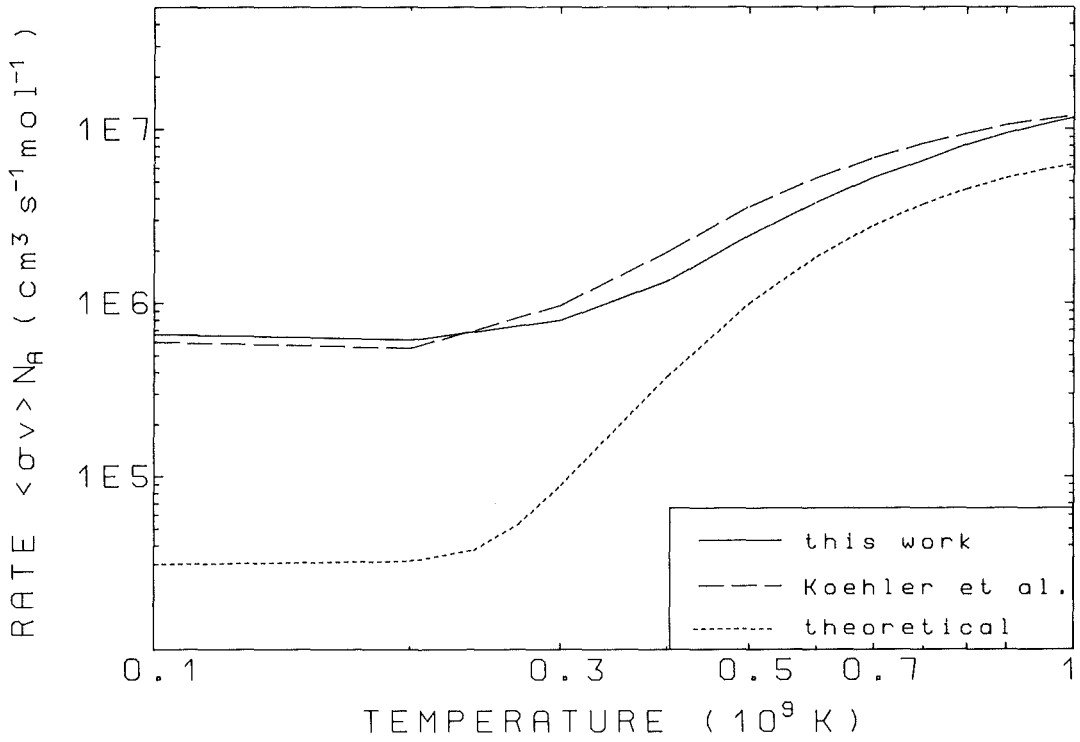

Fig.1 : The astrophysical rate of the $^{17}O(n,\alpha)$ reaction : present results (solid line) and previous experimental values (dashed line) as compared to a calculation based on resonance parameters.

The nucleosynthesis in this model occurs via reaction sequences that allow for an outbreak from the mass range $A<8$, thus offering - in contrast to the standard model - a possibility for the formation of heavier elements already in the big bang [1]. Hence, the inhomogeneous big bang could explain the observation of small abundances of carbon and other light elements in even the oldest stars in a natural way. Similar to the reactions on ^{14}C, also ^{17}O is one of the critical points in the nuclear reaction network, where the main reaction flow to heavier nuclei has to pass. Therefore, the competition of the $^{17}O(n,\alpha)^{14}C$ reaction - which recycles the mass flow back to ^{14}C - with the (n,γ) - and other reactions leading to the region beyond oxygen emplies an important problem for the successful production of heavier elements.

We have investigated this reaction at the Karlsruhe 3.75 MV Van de Graaff accelerator in the energy range up to 250 keV, and at thermal energies at the Munich research reactor, using a gridded ionization chamber for detection of the α-particles. By operating the chamber in a twin mode, backward-forward anisotropies were measured over the full energy range in order to correct for

angular distribution effects resulting from the interference between resonances. Though our studies led to a qualitative confirmation of a recent measurement [2], the latter corrections were found significant, ranging between 10 and 50%. In fig.1 the resulting temperature dependence of the reaction rate is compared with the data of Koehler and Graff [2] and with a previous calculation based on available resonance parameters.

In any case, the experimental cross section of the $^{17}O(n,\alpha)$ reaction was found to be two to three times larger in the relevant temperature range than it had been predicted by theoretical calculations. This implies that ^{17}O represents, indeed, a bottle neck for the build-up of still heavier elements.

[1] J.H. Applegate, C.J. Hogan, R.J. Scherrer, Phys. Rev. D **35** (1987) 1151

[2] P.E. Koehler, S.M. Graff, Phys. Rev. C 44 (1991) 2788

* Los Alamos National Laboratory, Los Alamos, New Mexico

** University of Notre Dame, Notre Dame, Indiana

*** Ruhr-Universität Bochum

3.1.4 A MEASUREMENT OF THE $^{22}Ne(n, \gamma)^{23}Ne$ CAPTURE CROSS SECTION AT A STELLAR TEMPERATURE OF kT = 25 keV[1)]

H. BEER, G. RUPP, F. VOß, F. KÄPPELER

The capture cross section of ^{22}Ne has been determined by a fast cyclic activation technique. The measurements were carried out at the Karlsruhe 3.75 MV pulsed Van de Graaff accelerator using the $^{7}Li(p,n)$ reaction close to the reaction threshold to generate neutrons with a distribution resembling a Maxwell spectrum of kT = 25 keV. The activation samples consisted of a mixture of enriched ^{22}Ne (99.9%) and natural Kr-gas contained in stainless steel spheres (20 mm diameter and 0.5 mm wall thickness). The activity of the samples was counted with a high-resolution Ge(Li) detector via the characteristic 439 keV ^{23}Ne γ-ray line. The ^{22}Ne capture cross section at kT = 25 keV was found to be 66.0 ± 5.0 μb.

1) published in the Astrophysical Journal, 379 (1991) 420

3.1.5 THE s-PROCESS BETWEEN A = 120 AND 124 : SIGNATURE OF THE NEUTRON DENSITY IN RED GIANTS

W. SCHANZ, F. KÄPPELER, K. WISSHAK, G. REFFO*

The mass region between tin and tellurium is of relevance for s-process nucleosynthesis, since the s-only isotopes ^{122}Te, ^{123}Te, and ^{124}Te provide for a sensitive test of the neutron density during helium burning in Red Giant stars. The neutron capture flow through this region is sketched in fig.1. Provided that the neutron density at the stellar site is low enough, the s-process reaction chain arriving at ^{120}Sn will completely follow the route via ^{121}Sb to ^{122}Te as indicated by the thick lines. In that case, the "local approximation" predicted by the classical approach to yield for neighboring nuclei

$$\sigma N = \text{const.}$$

can sensitively be tested at the example of the three s-only nuclei ^{122}Te, ^{123}Te, and ^{124}Te, which are shielded against the r-process by their stable isobars in Sn and Sb.

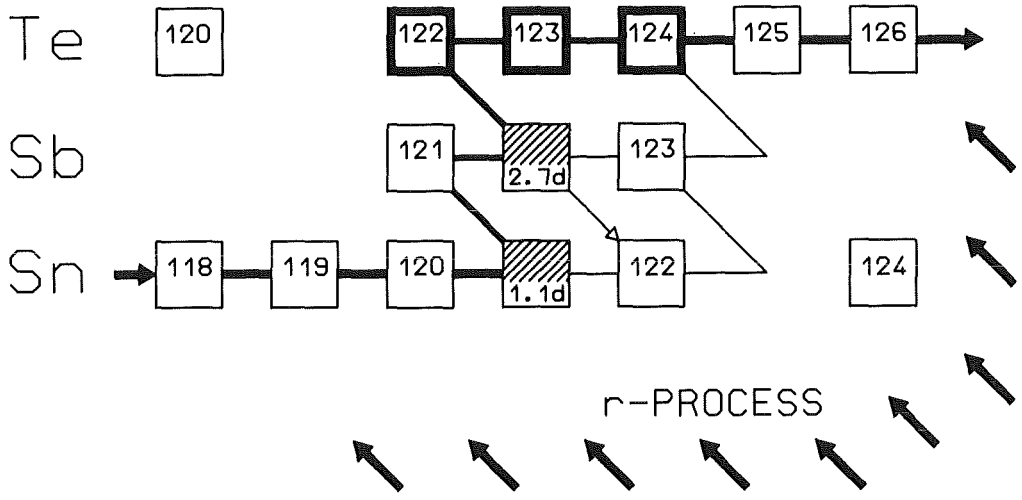

Fig.1 : The s-process neutron capture flow in the mass region 118 < A < 126.

This relation is the consequence of the fact that the s-process abundances are inversely proportional to the stellar (n,γ) cross sections of the respective isotopes.

Since the isotopic abundance ratio within a given element is well defined - to better than 0.1% in case of tellurium - the experimental cross section ratios are the decisive quantities for that test. Recent experiments have led to an enormous improvement of these ratios which are known to ±1.2% by now [1]. The reduced uncertainties did not only allow for an impressive confirmation of the local approximation predicted by the classical approach, but indicated also the possibility for identifying a small p-process contribution to the observed ^{122}Te abundance. This feature is important for a quantitative discussion of the p-process, which so far could only be characterized by the neutron-deficient p-only nuclei such as ^{120}Te. In contrast to their compatibility with the classical approach, the new tellurium cross sections gave rise to inconsistencies in the frame of current stellar s-process models, which may bear interesting consequences.

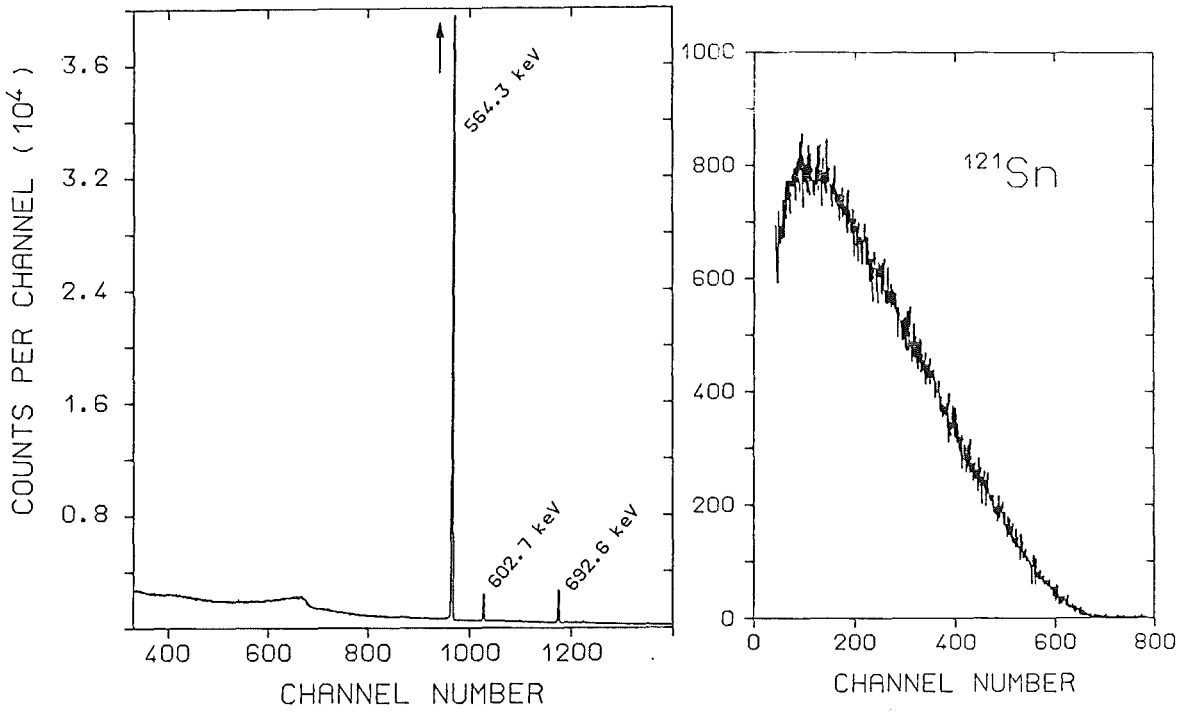

Fig.2: Typical spectra taken from the activated samples. *Left* : A γ-ray spectrum taken from a Sb sample of natural composition, showing the lines associated with the decay of ^{122}Sb (564.3 keV) and of ^{124}Sb (602.7 keV). *Right*: The electron spectrum of an activated ^{120}Sn sample.

In addition to the very accurate cross sections that are available for these s-only nuclei, complementary measurements are reported on ^{120}Sn, ^{121}Sb, ^{123}Sb, and ^{128}Te for an improved analysis of the s-process flow. The measurements were carried out via the activation technique in a quasi-stellar neutron spectrum for kT=25 keV, using gold as a cross section standard. In case of the antimony cross sections the induced activities could be determined via well known γ-ray

transitions in the decay of the respective product nuclei by means of a calibrated HPGe detector. For ^{120}Sn and ^{128}Te such γ-transitions were either missing or unreliable. Therefore, the activities were determined by counting the β-decay electrons directly with a spectrometer consisting of two Si(Li) detectors in close geometry. The 97% efficiency of that spectrometer compensated for the fact that thin samples had to be used with this set-up in order to avoid sizable self-absorption corrections. Fig.2 shows examples for the spectra taken with the two detection methods. In order to study the systematic uncertainties in the present measurements, a whole series of activations was carried out with modified experimental parameters.

The cross sections of the unstable isotopes, ^{121}Sn and ^{122}Sb, were determined by statistical model calculations. The reliability of these results were considerably improved compared to previous calculations by establishing a consistent systematics for the relevant model parameters for all stable nuclei in the mass range of interest. The parameters for the unstable branch points were then inferred from this systematics by interpolation. Uncertainties of $<4\%$ and $<30\%$ were obtained for the measured and calculated results, respectively. Based on these data, s-process analyses are presently be carried out by means of the classical approach and with a stellar model for low mass stars.

[1] K. Wisshak, F. Voss, F. Käppeler, G. Reffo, Report KfK 4899 (1991), Kernforschungszentrum Karlsruhe; Phys. Rev. C (in press)

* ENEA, Laboratorio Dati Nucleari, Bologna Italy

3.1.6 CAPTURE CROSS SECTION MEASUREMENTS OF KRYPTON AND XENON ISOTOPES AND THE FUNDAMENTAL PARAMETERS OF THE s-PROCESS[1)]

H. BEER

The capture cross sections of Kr and Xe isotopes have been determined by a fast cyclic activation technique. The data were used to perform s-process calculations with phenomenological models. The weak and the main s-process component were studied. Astrophysical parameters were determined in the frame

of the model, i.e., iron seed abundance, the neutron exposure, average number of neutrons captured by the iron seed, the temperature dependence of the neutron exposure, neutron density, temperature, and electron density. The solar abundances of Kr and Xe were determined. From the ^{85}Kr branching the pulse width of a pulsed s-process was estimated. The isotopic anomaly Xe-S, s-process Xe, was investigated.

1) published in the Astrophysical Journal, **375** (1991) 823

3.1.7 AN ADC SYSTEM FOR MEASUREMENTS WITH THE KARLSRUHE 4π BaF_2 DETECTOR

K. GUBER, K. WISSHAK

An ADC system has been added to the electronic equipment of the Karlsruhe 4π Barium Fluoride Detector [1]. It allows to store for each event the gamma-ray energy and time-of-flight (TOF) information of the individual detector modules. A special preprocessing unit rejects events in selectable sum energy and TOF regions. The decision whether an event is accepted is made within 4μs. The system is based on CAMAC modules of type FERA (Le Croy). The hardware trigger is realised by a combination of ALU- (arithmetic logic unit) and MLU- (multiplicity logic unit) modules. Accepted events are transmitted from a data stack to a set of two memorys that are mutually used for input and output. The ADC-system in conjunction with the preprocessing is able to accept a count rate up to 60 kHz.

The purpose of the ADC system is : (i) to measure capture gamma-ray spectra, necessary to determine the detector efficiency for capture events, which are presently taken from theoretical calculations [2], (ii) to allow for a deeper understanding of the capture process, e.g. by determining angular or multiplicity distributions of capture gamma-rays, (iii) to reduce significantly the recorded event rate by rejecting those events that are not needed for the evaluation of the cross section e.g. low sum energies and large TOFs, (iv) to improve the resolution in gamma-ray sum energy by off-line correction of the nonlinearity of the individual detector modules.

The data acquisition is schematically shown in fig.1. The events from one sample are stored on-line as a diskfile using a MV 4000 computer. After an

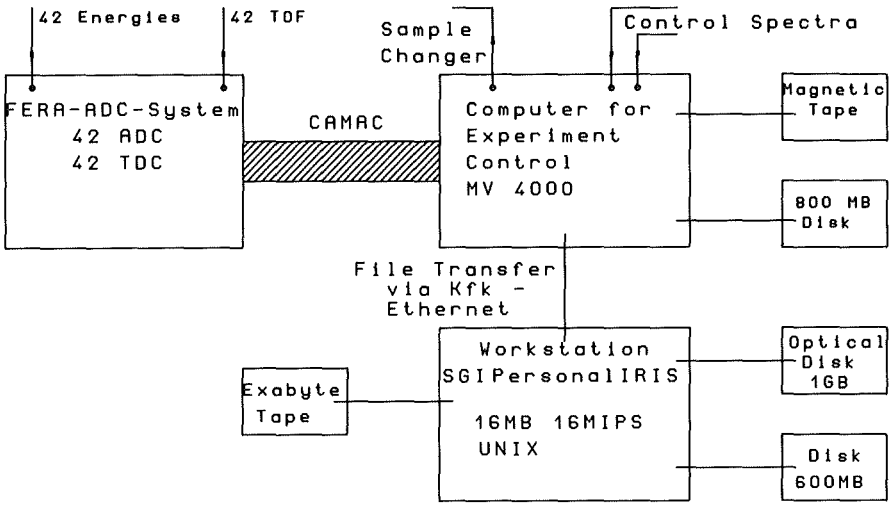

Fig. 1: Schematic view of the data acquisition of the Karlsruhe 4π BaF_2 detector using an ADC system.

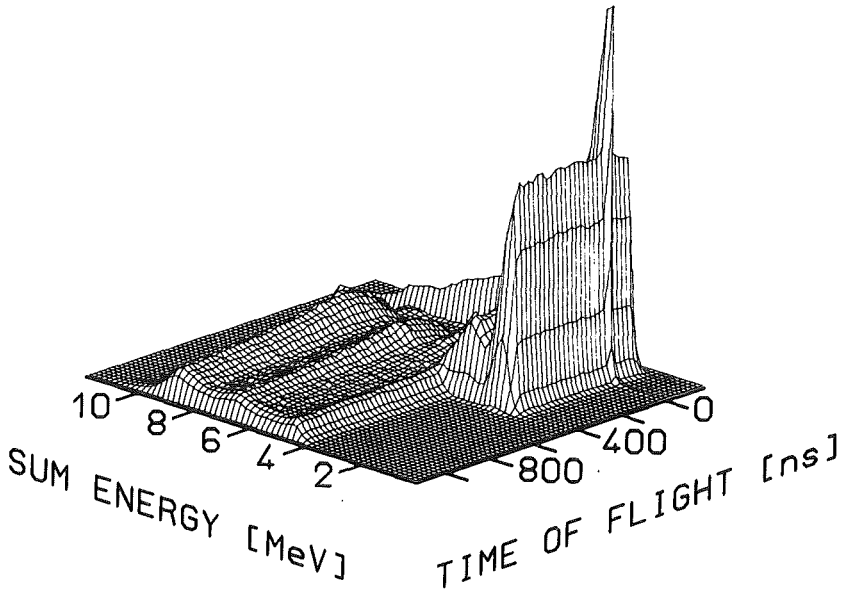

Fig. 2: Two-dimensional sum energy versus TOF spectrum as calculated from the events recorded with the ADC system. About 50% of the countrate located at low sum energy and large TOF are suppressed by the hardware trigger.

acquisition time of ~10 min, while the data of the next sample are recorded, the file is transferred via Ethernet to a Silicon Graphics workstation where they are finally stored either on optical disk or on an Exabyte tape. The workstation is lateron used to sort the individual events into two-dimensional sum energy versus TOF spectra dependent on detector multiplicity. An example of such a spectrum is shown in fig.2. Background events at low sum energy and large TOF are completely suppressed by the hardware trigger. The sorting procedure on the

workstation is faster by a factor of 18 compared to the respective step of data evaluation on the MV 4000 computer used in previous experiments [2].

The ADC system was used in a first experiment on samarium isotopes. The evaluated cross sections agreed with the respective data measured with the old acquisition system [2] well within the statistical uncertainties.

[1] K. Wisshak, K. Guber, F. Käppeler, J. Krisch, H. Müller, G. Rupp, F. Voß, Nucl. Instr. Meth. **A292**, (1990) 595

[2] K. Wisshak, F. Voß, F. Käppeler, G. Reffo, Phys. Rev. **C42** (1990) 1731

3.1.8 NEUTRON CAPTURE IN ^{148,150}Sm : A SENSITIVE PROBE OF THE s-PROCESS NEUTRON DENSITY

K. GUBER, K. WISSHAK, F. KÄPPELER, F. VOß

The neutron capture cross sections of ^{147,148,149,150,152}Sm have been measured in the energy range from 3 to 225 keV at the Karlsruhe Van de Graaff accelerator

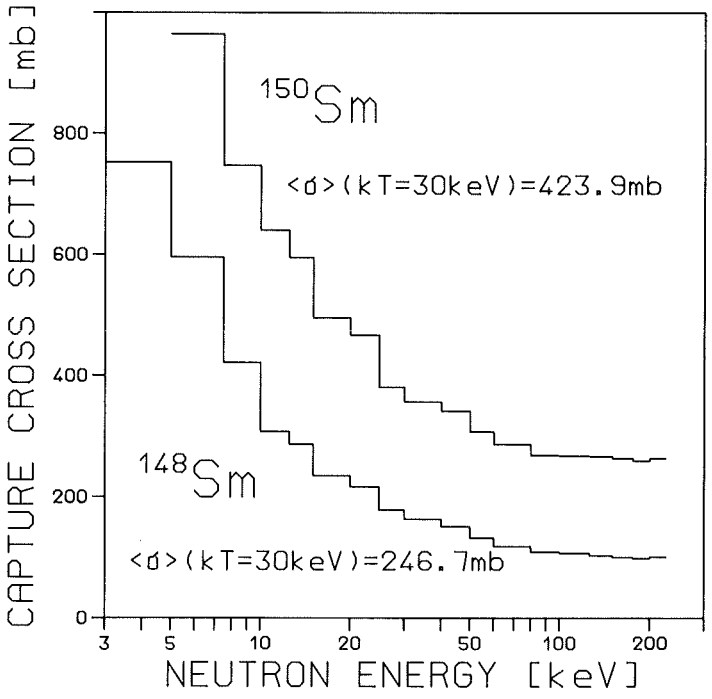

Fig.1 : The neutron capture cross section of the two s-only isotopes ^{148,150}Sm in the energy range from 3 to 225 keV (preliminary values).

using gold as a standard. Neutrons were produced via the ^{7}Li(p,n)^{7}Be reaction by

bombarding metallic Li targets with a pulsed proton beam. Capture events were registered with the Karlsruhe 4π Barium Fluoride Detector. Several sets of measurements have been performed under different experimental conditions to study the systematic uncertainties in detail. For the first time, in one of the measurements an ADC system was used for data acquisition that registers separately gamma-ray energy and time-of-flight of all detector modules. The cross section ratios σ(Sm)/σ(Au) were determined with an overall uncertainty of ~1%. This is an improvement by a factor 4 compared to the best experiment performed so far [1]. A preliminary result for the capture cross sections of the two s-only isotopes ^{148,150}Sm is shown in fig.1.

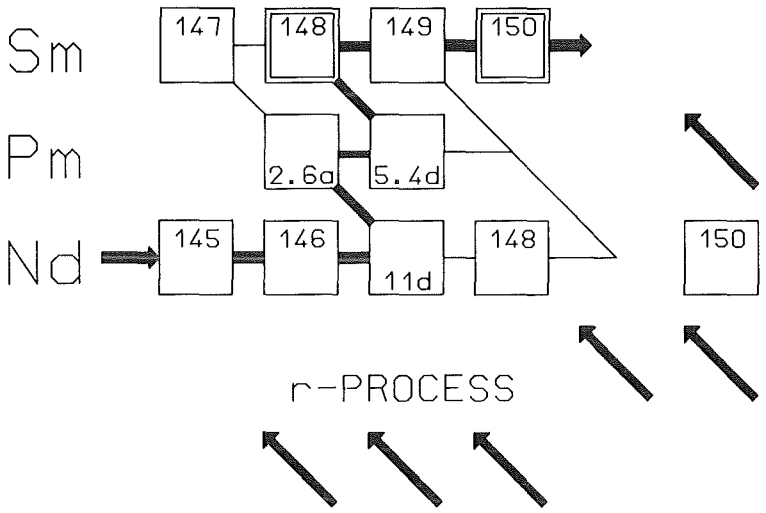

Fig.2 : The s-process path in the region of the samarium isotopes.

Maxwellian averaged neutron capture cross sections were calculated for thermal energies between kT=10 and 100 keV. In the energy range not covered by the present experiment, resonance parameters from literature and model calculations were used. As a preliminary result, the ratio of s-process abundance N_s times stellar cross section $<\sigma>$ of ^{148}Sm and ^{150}Sm, was determined (kT=30 keV) :

$$R = N_s <\sigma> (^{148}\text{Sm}) / N_s <\sigma> (^{150}\text{Sm}) = 0.887 \pm 0.008.$$

This result is in agreement with the number quoted in ref. 1, but the uncertainty has been improved by a factor 4. The deviation of R from unity indicates that the "local approximation" of the s-process ($N_s <\sigma> =$const.), which was well established for the tellurium isotopes [2] is violated in case of samarium due to a significant branching of the s-process path at the unstable isotopes ^{147}Nd, ^{147}Pm and ^{148}Pm (see fig.2). This branching is very sensitive to the s-process neutron density n_n. A first analysis in the framework of the classical model [3]

yields a neutron density $n_n = (3.3 \pm 0.3) \cdot 10^8$ cm^{-3}. This is the most stringent limitation for n_n which has been obtained so far.

[1] R.R. Winters, F. Käppeler, K. Wisshak, A. Mengoni, G. Reffo, Astrophysical Journal **300** (1986) 41

[2] K. Wisshak, F. Voß, F. Käppeler, G. Reffo, Report KfK 4899 (1991), Kernforschungszentrum Karlsruhe; Phys. Rev. C (in press)

[3] F. Käppeler, R. Gallino, M. Busso, G. Picchio, C.M. Raiteri, Astrophysical Journal **354** (1990) 630

3.1.9 STELLAR PRODUCTION CROSS SECTION OF $^{176}Lu^m$ [1)]

W.R. ZHAO*, F. KÄPPELER

The partial neutron capture cross section of ^{175}Lu to the isomer $^{176}Lu^m$ has been measured at kT = 25 keV via the activation technique. Systematic uncertainties were carefully evaluated by two independent methods for determination of the induced activities and by variation of the relevant experimental parameters. The final cross section of 1135 ± 30 mb was derived from six different activations. With this result, the production of the long-lived ground state $^{176}Lu^g$ ($t_{1/2}$ = 41 Gyr) by s-process neutron captures would not be sufficient to account even for the observed lutetium abundance. Consequently, other mechanisms, e.g., thermally induced transitions from the isomer to the ground state must have enhanced the yield of $^{176}Lu^g$ during the s-process.

1) published in Phys. Rev. C 44 (1991), 506

* On leave from Institue of Atomic Energy, Beijing

3.1.10 NUCLEAR STRUCTURE OF ^{176}Lu AND ITS ASTROPHYSICAL CONSEQUENCES. I. LEVEL SCHEME OF ^{176}Lu[1)]

N. KLAY, F. KÄPPELER, H. BEER, G. SCHATZ, H. BÖRNER*, F. HOYLER*, S.J. ROBINSON*, K. SCHRECKENBACH*, B. KRUSCHE*, U. MAYERHOFER**, G. HLAWATSCH**, H. LINDNER**, T. VON EGIDY**, W. ANDREJTSCHEFF***, P. PETKOV***

Excited states of the deformed odd-odd nucleus ^{176}Lu have been investigated by the following experiments : measurement of the ^{175}Lu(n,γ)^{176}Lu reaction with high resolution crystal spectrometers and of the ^{175}Lu(n, e$^-$)^{176}Lu reaction with a double focusing magnet-spectrometer. In total, 509 gamma transitions could be identified in ^{176}Lu, and multipolarities were determined for 228 of these transitions. Additionally, a measurement of γ-γ coincidences after neutron capture and an investigation of the ^{175}Lu(d,p)^{176}Lu transfer reaction were also performed. Information on the lifetimes of relevant levels was obtained by the technique of delayed coincidences, and, in one case, by the Doppler shift attenuation method. With these results, a level scheme was established, comprising 97 energy levels connected by 270 gamma transitions. About 30 Nilsson configurations and corresponding rotational bands were identified. The comparison with model calculations indicates that the level scheme comprises all excited states with spins $1<I<8$ up to 900 keV. In particular, this scheme contains transitions that connect the $I^\pi=7^-$ ground state with the 1^- isomer via mediating levels at higher excitation energy. From this coupling, the excitation energy of the isomer was precisely defined to 122.855 ± 0.009 keV. Accordingly, the neutron separation energy of ^{176}Lu could be revised to 6287.91 ± 0.15 keV. Based on the fact that more than 90% of the observed intensities could be placed in the level scheme, an isomeric ratio, $\sigma_p^{is}/\sigma_{tot} = 0.870\pm0.025$, was deduced for the fractional population of the isomer by thermal neutron captures.

1) published in Phys. Rev. C 44 (1991) 2801

* Institut Laue-Langevin, 38042 Grenoble, France

** Phys. Dept., Technische Universität München, Garching bei München

*** Institute for Nuclear Research and Nuclear Energy, Bulgarian Academy of Sciences, 1784 Sofia, Bulgaria

3.1.11 NUCLEAR STRUCTURE OF ^{176}Lu AND ITS ASTROPHYSICAL CONSEQUENCES. II. ^{176}Lu, A THERMOMETER FOR STELLAR HELIUM BURNING[1)]

N. KLAY, F. KÄPPELER, H. BEER, G. SCHATZ

On the basis of the improved level scheme of ^{176}Lu it is demonstrated that the stellar s-process production as well as the stellar beta decay rate of that nucleus depend strongly on temperature. This behavior results from the completely different half-lives of the ground state and the isomer; since these states are coupled by induced transitions in the hot stellar photon bath, the effective half-life of ^{176}Lu is drastically reduced. The 5^- state at 838.64 keV was identified as the most efficient mediating level. Consequently, ^{176}Lu can no longer be considered as a chronometer for the age of the s-process; instead, it can be interpreted as an s-process thermometer yielding a temperature range between $2.4 \cdot 10^8$ to $3.6 \cdot 10^8$ K.

1) published in Phys. Rev. C 44 (1991) 2839

3.1.12 ORIGIN OF ^{180}Ta^m AND THE TEMPERATURE OF THE s-PROCESS

ZS. NEMETH*, F. KÄPPELER, G. REFFO**

Despite of numerous studies over the past decade, the origin of ^{180}Ta^m, the rarest isotope in nature, has not been revealed yet. This isotope is so much less abundant than the typical yields of all processes contributing to this mass region, that it probably owes its existence to a delicate interplay between the nuclear physics and the physical condition during its production. It is this sensitivity,

which makes the origin of $^{180}Ta^{m}$ an important probe for a variety of nucleosynthesis sites.

The proposed mechanisms for producing $^{180}Ta^{m}$ are summarized in fig.1. The two light arrows from the right indicate the claims for an origin $^{180}Ta^{m}$ by the p- and ν-processes. While $^{180}Ta^{m}$ is generally not obtained in p-process calculations using parametrized scenarios, a more recent study [1] of a realistic model for the type II supernova SN1987A indicates for the first time a significant p-process yield of $^{180}Ta^{m}$. On the other hand, calculations of neutrino-induced nucleosynthesis in SN II explosions do also show $^{180}Ta^{m}$ production [2].

At present, reliable predictions can only be made for a possible neutron capture origin of $^{180}Ta^{m}$ (indicated by heavy arrows in fig.1), due to the availability of relevant experimental information. There are three ways of producing $^{180}Ta^{m}$ by neutron capture processes :

(i) A small fraction of the r-process beta decay chain at A = 180 feeding the 8^{-} isomer in ^{180}Hf could, in principle, result in sufficient $^{180}Ta^{m}$ production. However, there is ample experimental evidence that the corresponding branching in the decay of ^{180}Lu is compatible with zero, thus excluding an r-process origin of $^{180}Ta^{m}$.

(ii) Following the s-process path through the hafnium isotopes, Beer and Ward [3] suggested to produce $^{180}Ta^{m}$ by feeding the 8^{-} isomer in ^{180}Hf via s-process neutron captures in ^{179}Hf. Also this route was shown to be not efficient enough, yielding at most 22% of the observed $^{180}Ta^{m}$ abundance.

(iii) An important alternative was proposed by Yokoi and Takahashi [4], who found that ^{179}Hf becomes unstable under s-process conditions against beta decay from excited states. This results in a finite $^{179}Ta/^{179}Hf$ ratio, that is determined by the temperature (via the beta decay rate of ^{179}Hf) and the electron density in the stellar plasma (via the electron capture rate of ^{179}Ta). Neutron captures on ^{179}Ta lead then partly to $^{180}Ta^{m}$ and partly to the short-lived ground state of ^{180}Ta. Through the second path, this scenario provides also an s-process contribution to ^{180}W, that was previously considered as a pure p-process isotope. Normalizing the s-process flow to the observed abundances of ^{180}W and $^{180}Ta^{m}$ could, therefore, constrain neutron density, temperature, and electron density in the s-process.

In the present work, two crucial aspects of the solution proposed by Yokoi and Takahashi [4] are investigated. First, the question is addressed whether $^{180}Ta^{m}$ can survive under s-process conditions or whether it might be quickly destroyed by equilibration with the short-lived ground state. It was found by photoexcitation measurements, that thermal equilibration between the short-

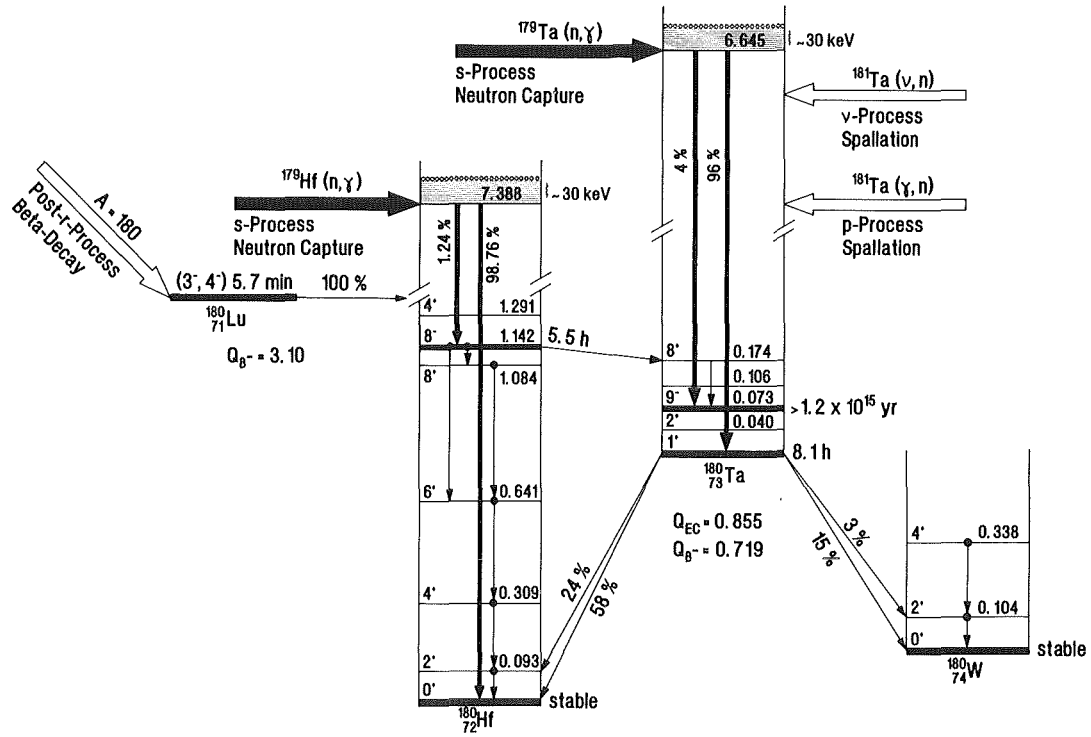

Fig.1: Level structure of the relevant A=180 isobars and the possible production processes of $^{180}Ta^{m}$ (energies are given in MeV). The r-process does not contribute the to the abundance of $^{180}Ta^{m}$ since $^{180}Hf^{m}$ is not populated in the β-decay of ^{180}Lu.

lived ground state and the almost stable isomer is **not** achieved for temperatures lower than $5 \cdot 10^{8}$ K. This means, that $^{180}Ta^{m}$ is practically stable under all plausible s-process conditions of relevance for the mass region beyond A=90.

Secondly, the stellar neutron capture rates are calculated with a refined statistical model approach in order to quantify the s-process flow to $^{180}Ta^{m}$ and ^{180}W. These calculations include the total (n,γ) cross sections of ^{179}Ta and $^{180}Ta^{m}$.

These results allowed for a considerably refined description of the s-process flow in the mass region 178<A<184, which is characterized by the important branching at A=179. The classical approach has been shown to yield ambiguous solutions for the production of $^{180}Ta^{m}$, even if the additional constraint is met, that not more than about 30% of the ^{180}W abundance should be produced in the s-process. It was found that there is a rather sharp temperature limit at $3 \cdot 10^{8}$ K : For *lower* temperatures, the branching at A=179 remains unimportant, resulting in a marginal production of $^{180}Ta^{m}$. This solution is compatible with the predictions of current stellar models for low mass stars of low metallicity. At temperatures slightly *higher* than $3 \cdot 10^{8}$ K, $^{180}Ta^{m}$ can efficiently be produced in the s-process. Such temperatures, which are expected for stars of higher

metallicity, are obtained from the s-process branchings, which can be interpreted as thermometers.

A distinction between the two possible interpretations of the origin of $^{180}Ta^{m}$ and the related consequences would require either reliable and quantitative p- and/or ν-process calculations (which can hardly be expected in the near future), or a further improvement of the temperature estimates via the classical model. Given the recent progress in experimental techniques, the second possibility may be more promising. For the case of the branching at A = 179 further efforts have to concentrate on the experimental determination of the neutron capture rates of ^{179}Ta and $^{180}Ta^{m}$, on a critical assessment of the stellar beta decay rates, in particular the of ^{179}Hf, and on a measurement of the branching ratio in the decay of the 8^{-} isomer in ^{180}Hf. With these improvements, the origin of $^{180}Ta^{m}$ will be an important clue to the identification of the s-process site, and will allow to establish constraints for the p-and ν-processes, as well.

[1] N. Prantzos, M. Hashimoto, M. Rayet, M. Arnould, Astron. Astrophys. **238** (1990) 455

[2] S.E. Woosley, D.H. Hartmann, R.D. Hoffman, W.C. Haxton, Astrophysical Journal **356** (1990) 272

[3] H. Beer, R.A. Ward, Nature **291** (1981) 308

[4] K. Yokoi, K. Takahashi, Nature **305** (1983) 198

* Institute of Isotopes, Budapest, Hungary

** ENEA, Laboratorio Dati Nucleari, Bologna, Italy

3.1.13 MEASUREMENT OF THE ^{180}W (n, γ) ^{181}W CROSS SECTION

H. BEER, F. KÄPPELER

The origin of ^{180}W is traditionally ascribed to p-process nucleosynthesis. However, according to Yokoi and Takahashi [1], a significant s-process contribution is also possible by a branching at ^{179}Hf via the sequence

$$^{179}Hf(\beta^{-})\,^{179}Ta\,(n,\gamma)\,^{180}Ta^{g}(\beta^{-})\,^{180}W$$

provided the s-process conditions (temperature, neutron- and electron density) allow for the β decay of the terrestrially stable isotope ^{179}Hf [2].

For a quantitative determination of the s-process part of the ^{180}W abundance, the ^{180}W destruction rate is needed. This quantity was measured by the activation technique at the Karlsruhe 3.75 MV Van de Graaff accelerator. For this purpose a 100 mg ^{180}W sample (enrichment 13.5%) was irradiated over a period of 7 days. The produced ^{181}W activity was counted with a HPGe detector via a γ-ray line at 152.21 keV [intensity per decay = (0.084 + 0.003) %].

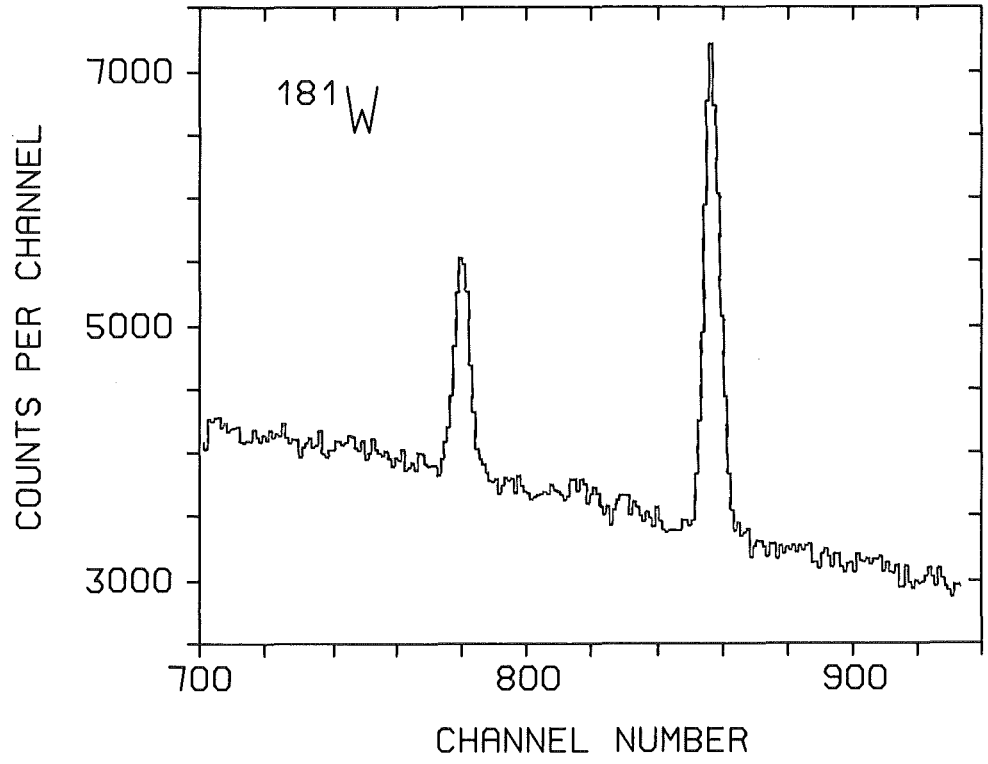

Fig.1: The γ ray lines of the ^{181}W decay at 136.17keV and 152.21 keV, respectively, counted after the activation.

The cross section was determined relative to the ^{197}Au standard. The sample was sandwiched between two thin Au foils which were exchanged after three days of irradiation by fresh foils to avoid saturation of the Au activity. In fig.1, two characteristic γ-ray lines from the ^{181}W decay are shown.

In order to check the measurements for systematic uncertainties, three additional activations on ^{186}W were performed with tungsten of natural isotopic composition using the same conditions for neutron irradiation. Two of these

measurements were carried out with thin metallic foils, and in the third measurement 100 mg of natural W powder was used simulating exactly the ^{180}W measurement.

For ^{180}W we derived a Maxwellian averaged capture cross section $\sigma = 624 \pm 29$ mb at 25 keV. This result is within quoted uncertainties in agreement with the respective value $\sigma = 603 \pm 27$ mb, calculated from the time-of-flight data of Bokhovko et al. [3] for kT = 25keV.

[1] K. Yokoi, K. Takahashi, 1987, Nature, **305** (1987), 198

[2] Zs. Németh, F. Käppeler, Astrophysical Journal (in press)

[3] M.V. Bokhovko, L.E Kazakov, V.N. Kononov, Problems of Atomic Sci. and Technology, Series on Nuclear Constants, Moscow (1986), No. 1, p. 39

3.1.14 AN UPDATED TABLE OF STELLAR (n, γ) CROSS SECTIONS

Z. Y. BAO, H. BEER, F. KÄPPELER, F. VOß, K. WISSHAK

An updated version of the compilations of Maxwellian averaged capture cross sections reported by Bao and Käppeler [1] is being prepared. The new table includes all recent publications and improved recalculations of Maxwellian averaged capture cross sections of older data. These improvements consider the following aspects :

- The normalization to a standard cross section is checked, and a renormalization is performed if necessary. Most of these changes refer to the improved capture cross section of ^{197}Au [2].
- The influence and origin of the thermal cross sections is studied in terms of bound state capture, positive resonance tails and direct capture.
- Resolved resonance data are reexamined. In particular it is checked whether the approximate treatment of resonances as delta functions can be applied or if instead a sum of Breit-Wigner resonance shapes has to be used.
- Incomplete experimental data have been supplemented by statistical model calculations.

- If cross sections were averaged over large energy bins before calculating the Maxwellian average, the error introduced by this early smoothing procedure was investigated.

In addition, it is intended to present Maxwellian average cross sections for the entire range of astrophysically relevant temperatures, from He-burning with the $^{13}C(\alpha,n)^{16}O$ neutron source (kT=12 keV) up to carbon burning in massive stars (kT~100 keV).

[1] Z.Y. Bao, F. Käppeler, Atomic Data and Nuclear Data Tables, **36** (1987) 411

[2] W. Ratynski, F. Käppeler, Phys. Rev. C **37** (1988) 595

3.1.15 AN ANALYTICAL FORMULATION OF THE DOUBLE-PULSE s-PROCESS MODEL[1)]

H. BEER

Recent studies of the astrophysical site of the s-process suggest a double-pulse s-process in the He-burning shell of low-mass asymptotic giant branch stars, where the $^{13}C(\alpha,n)$ and the $^{22}Ne(\alpha,n)$ neutron sources are active as well. Previous analyses have been performed in terms of a pulsed neutron s-process from intermediate-mass stars. The periodic neutron bursts were ascribed to the $^{22}Ne(\alpha,n)$ reaction only. The current effort is to reformulate the mathematics of the s-process to study the combined effect of repeated double pulses with different properties. Similar to the model of a single-pulse s-process, the effect of the pulses for the double-pulse model shows up at the branchings but, in contrast to the single-pulse model, also at the unbranched s-process path and at isomeric states populated by neutron capture. The new model contains the simpler models as special cases, and it is able to overcome difficulties associated with the single-pulse model.

1) published in the Astrophysical Journal, **379** (1991) 409

3.1.16 STELLAR (n, γ)-CROSS SECTIONS OF SHORT-LIVED NUCLEI[1)]

F. KÄPPELER

Stellar neutron capture cross sections are the essential input for investigating the element production via the slow neutron capture process (s-process). With the availability of accurrate cross sections for the stable s-process isotopes, analyses of the abundance patterns in the various branchings of the s-process flow require also reliable cross sections for unstable nuclei with stellar half-lives down to a few days. This contribution deals with the question to which extent existing techniques can be applied for these cases, and whether a future radioactive ion beam could be used for the preparation of suited samples. As an example, recent measurements of the stellar (n, γ) cross section of ^{147}Pm ($t_{1/2}$ = 2.6 yr) are discussed.

1) published in Radioactive Nuclear Beams, ed. Th. Delbar, Adam Hilger, Bristol-Philadelphia-New York 1991, p. 305

3.1.17 THE s-PROCESS: BRANCHINGS AND CHRONOMETERS[1)]

F. KÄPPELER

The abundance patterns in s-process branchings represent the most important reservoir of information on nucleosynthesis during stellar helium burning in red giant stars. The stellar temperatures and neutron fluxes obtained from their detailed analysis are required as the basis for investigating the various s-process chronometers. This interplay will be illustrated with examples of the chronometers associated with the unstable isotopes ^{99}Tc, ^{176}Lu, and ^{187}Re. In this discussion, the classical s-process approach as well as the stellar model for low mass stars of low metallicity are considered.

1) published in Nuclei in the Cosmos, ed. H. Oberhummer, Springer, Berlin-Heidelberg-New York 1991, p. 179

3.2 NUCLEAR REACTIONS

3.2.1 INVESTIGATION OF THE SEQUENTIAL BREAK-UP MODE $^{6}Li \rightarrow {}^{6}Li^{*}(3_1^{+}) \rightarrow \alpha + d$ OF 156 MeV ^{6}Li PROJECTILES ON ^{208}Pb IN THE VERY FORWARD ANGULAR HEMISPHERE[1)]

J. KIENER, G. GSOTTSCHNEIDER, H. J. GILS, H. REBEL, V. CORCALCIUC, S. K. BASU, G. BAUR*, J. RAYNAL**

The sequential break-up of 156 MeV ^{6}Li projectiles colliding with ^{208}Pb has been investigated in the very forward angular hemisphere in order to explore the role of the Coulomb and nuclear interaction in inducing projectile break-up processes. The experiments use the Karlsruhe spectrograph "Little John" with a newly developed technique to detect efficiently break-up pairs of α-particles and deuterons emitted with small relative energies and within a small opening angle. The observed differential cross section for the projectile excitation $^{6}Li \rightarrow {}^{6}Li^{*}$ ($I = 3_1^{+}$) has been analysed (together with forward elastic scattering) by a coupled channel approach, and various sensitivities to the nuclear potential and other ingredients have been studied. We conclude, that in the angular region below half the grazing angle the excitation is completely due to the Coulomb force. This feature is a basis for an application of the disintegration approach for studies of radiative capture cross section of astrophysical interest.

1) published in Z. Phys. A **339** (1991) 489

* Forschungszentrum Jülich, Institut für Kernphysik, 5170 Jülich,

** Service de Physique Théorique, CE-Saclay, 91191 Gif-sur-Yvette Cedex, France

3.2.2 MEASUREMENTS OF THE COULOMB DISSOCIATION CROSS SECTION OF 156 MeV ^{6}Li PROJECTILES AT EXTREMELY LOW RELATIVE FRAGMENT ENERGIES OF ASTROPHYSICAL INTEREST[1)]

J. KIENER, H. J. GILS, H. REBEL, S. ZAGROMSKI, G. GSOTTSCHNEIDER, N. HEIDE, H. JELITTO, J. WENTZ, G. BAUR*

Coulomb dissociation of light nuclear projectiles in the electric field of heavy target nuclei has been experimentally investigated as an alternative access to radiative capture cross sections at low relative energies of the fragments, which are of astrophysical interest. As a pilot experiment the break-up of 156 MeV ^{6}Li projectiles at ^{208}Pb with small emission angles of the α-particle and deuteron fragments has been studied. Both fragments were coincidentally detected in the focal plane of a magnetic spectrograph at several reaction angles well below the grazing angle and with relative angles between the fragments of 0°-2°. The experimental cross sections have been analyzed on the basis of the Coulomb break-up theory. The results for the resonant break-up give evidence for the strong dominance of the Coulomb dissociation mechanism and the absence of nuclear distortions, while the cross section for the nonresonant break-up follows theoretical predictions of the astrophysical S-factor and extrapolations of corresponding radiative capture reaction cross section to very low c.m. energies of the α-particle and deuteron. Various implications of the approach are discussed.

1) published in Phys. Rev. C 44 (1991) 2195

* Forschungszentrum Jülich, Institut für Kernphysik, 5170 Jülich,

3.2.3 COINCIDENCE CROSS SECTIONS WITHIN THE QUASI FREE BREAK-UP MODEL FOR ELASTIC PROJECTILE BREAK-UP[1)]

V. CORCALCIUC, H. JELITTO

Scrutinizing the basic break-up model of Serber we show that it is possible to derive the triple differential cross sections for particle-particle coincidences in analytical form. An alternative interpretation within the opaque version of the model suggests to assign these cross sections to the elastic nonresonant projectile break-up due to the nuclear interaction. Distortion effects by the Coulomb field of the target are included in analogy to the Serber model. Beside the well known single maximum in the break-up spectra double and triple peak structures appear for certain combinations of the observation angles. The model yields reasonable agreement to the given experimental data, concerning the multiple peak structure as well as the order of magnitude for the absolute normalisation. Its application comprise the region of forward emission angles, especially the angular range of the classical Coulomb deflection.

1) published as KfK Report 4660 (1991)

3.2.4 (^{6}Li. ^{6}He) MEASUREMENTS AS AN ALTERNATIVE CALIBRATION FOR SOLAR NEUTRINO DETECTORS[1)]

A. ASCHENAUER*, H. DENNERT*, W. EYRICH*, A. LEHMANN*, M. MOOSBURGER*, H. WIRTH*, H. J. GILS, H. REBEL, S. ZAGROMSKI

The (^{6}Li, ^{6}He) reaction was studied on the nuclei ^{37}Cl and ^{71}Ga at $E_{^{6}Li}$ = 156 MeV at extreme forward angles including zero degree. Gamov-Teller strength and the corresponding B (GT) values were extracted. It is shown that these measurements provide an alternative method to calibrate solar neutrino detectors.

1) published in Phys. Rev. C44 (1991) 2771

* Physikalisches Institut der Universität Erlangen-Nürnberg

3.2.5 ANGULAR RESOLVED COINCIDENT MEASUREMENT OF DECAY PROTONS FOLLOWING THE REACTION $^{12}C(^{6}Li,^{6}He)^{12}N$

N. SCHOLZ*, H. DENNERT*, H.J. GILS, A. LEHMANN*, M. MOOSBURGER*, H. REBEL, H. WIRTH*, S. ZAGROMSKI

In the course of the coincident measurement observing the reaction (^{6}Li, ^{6}He p) the analysis of the system $^{12}C \rightarrow ^{12}N$ has been continued. More precise information completing the results of earlier singles measurements [1] referring to the structure of the nucleus ^{12}N can be obtained by means of the coincident, angular resolved detection of the decay protons.

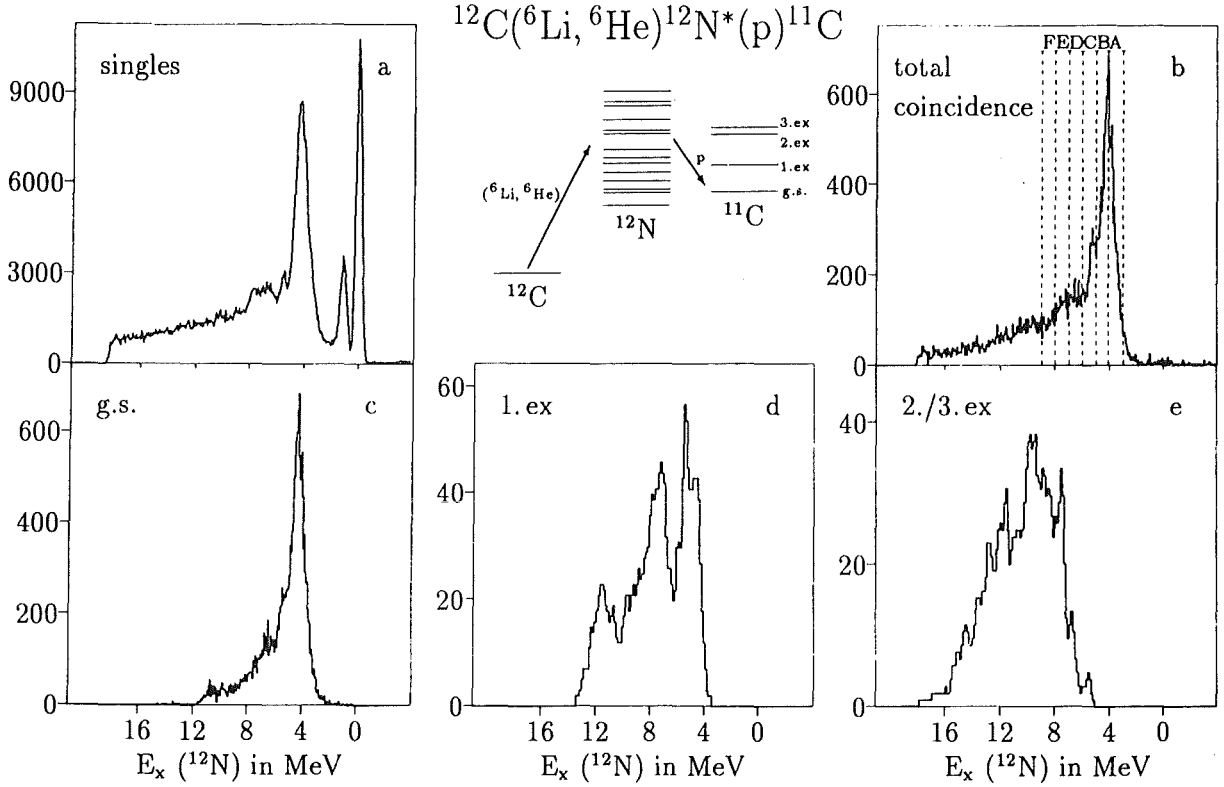

Fig.1 : Singles (a) and coincident (b-e) spectra of the reaction ^{12}C (^{6}Li, ^{6}He) ^{12}N(p) ^{11}C for $E_{6_{Li}} = 156$ MeV and $\Theta_{6_{He}} = 0°$.

The experiment has been performed at the $^{6}Li^{3+}$-beam of the Karlsruhe Isochronous Cyclotron with an energy of $E_{^{6}Li}=156$ MeV. While the ^{6}He-ejectiles were detected at 0° using the magnetic spectograph "Little John", the decay protons were analysed under backward angles between 100° and 170° with an arrangement of large area ion implanted semiconductor strip detectors, covering a total solid angle of 330 msr. They allowed for the angular resolved measurement of decay particles under 40 separate angles, simultaneously. A detailed review of the employed detector set up as well as more detailed specifications are given in ref. [2].

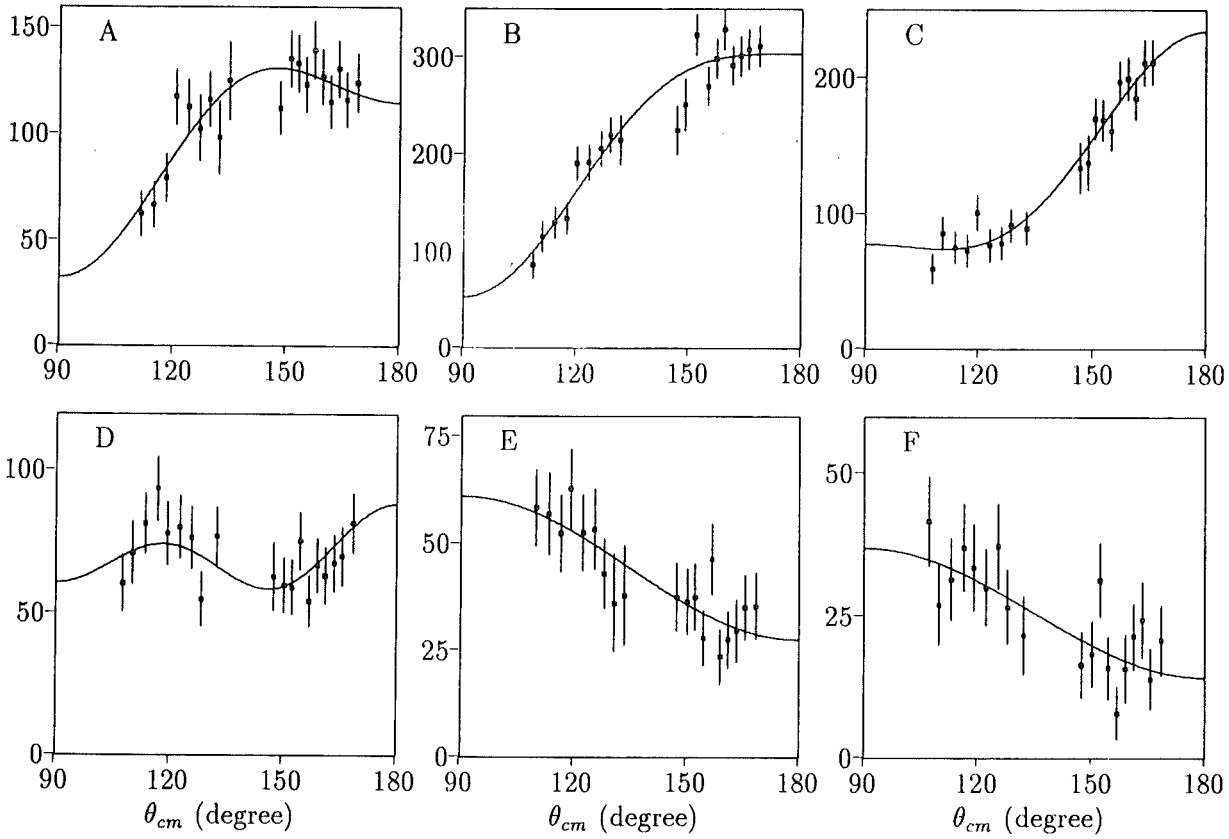

Fig.2 : Angular correlation functions for the decay to the ^{11}C-ground state for six different energy regions. The solid line represents a Legendre polynomial fit.

In addition to the singles spectra (fig.1a) already presented in [3], the analysis of the coincident ^{6}He-spectra reveals the excitation of ^{12}N levels decaying via proton emission. In the considered energy region the proton emission is the only possible particle decay mode of the excited nucleus. Besides the dominant proton decay leading to the ground state of ^{11}C, the decay to the first excited state at $E_x=2.00$ MeV and to unresolved higher lying states ($E_x=4.33$ MeV and 4.80

MeV) was observed. The extracted coincident ^{6}He-spectra of these three decay channels are separately shown in fig.1c-d. Comparing the spectra of coincident data with the singles measurement significant structures of unresolved states appear to be pronounced for higher excitation energies.

Further information about the proton decay of the nucleus ^{12}N could be obtained by an analysis of the angular correlation function of different decay modes. For the decay to the ^{11}C-ground state the extracted angular correlations are shown in fig.2 for six different energy regions, indicated in fig.1b. The experimental data were fitted to the form $W(\Theta) = A_0(1 + a_2 P_2(\cos\Theta) + a_4 P_4(\cos\Theta))$ by a least-squares procedure. The different energy ranges show specific angular dependences restricting the multipolarities of the decay modes.

[1] M. Moosburger, E. Aschenauer, H. Dennert, W. Eyrich, A. Lehmann, R. Rudeloff, H. Schlösser, H.J. Gils, H. Rebel, S. Zagromski, Phys. Rev. C 41 (1990) 2925

[2] N. Scholz, H. Dennert, W. Eyrich, A. Lehmann, M. Moosburger, H. Wirth, Nucl. Instr. and Meth. A 313 (1992) 233

[3] M. Moosburger, N. Scholz, H. Dennert, W. Eyrich, A. Lehmann, H. Wirth, H.J. Gils, H. Rebel, S. Zagromski, Report KfK 4875 (1991), eds. H. Beer, J. Wochele, Kernforschungszentrum Karlsruhe, p. 43

* Physikalisches Institut, Universität Erlangen-Nürnberg

3.2.6 DECAY OF THE GAMOW TELLER GIANT RESONANCE IN THE SYSTEM $^{90}Zr \rightarrow ^{90}Nb$

M. MOOSBURGER*, H. DENNERT*, W. EYRICH*, H.J. GILS, A. LEHMANN*, H. REBEL, N. SCHOLZ*, H. WIRTH*, S. ZAGROMSKI

The investigation of excitation and decay of giant resonances is a very sensitive way to explore the mechanisms of nuclear reactions. The selectivity of the (^{6}Li, ^{6}He) charge transfer reaction to the excitation of spin-isospin modes ($\Delta S = \Delta T = 1$) and measurements at extreme foreward angles establish the (^{6}Li, ^{6}He) reaction as an appropriate tool for the investigation of Gamow Teller (GT) resonances [1, 2]. We studied the reaction ^{90}Zr(^{6}Li, ^{6}He)^{90}Nb and the subsequent decay via proton emission to ^{89}Zr in order to study the damping processes of the GT giant resonance in ^{90}Nb.

The experiments were performed at the 156 MeV ^{6}Li-beam of the Karlsruhe isochronous cyclotron. The magnetic spectrograph "Little John" was used for the measurement of the ^{6}He ejectiles at extreme forward angles including zero degree. An arrangement of large area semiconductor strip detectors was built up within the target chamber for the detection of decay protons [3]. Eight strip detectors were combined to four counter telescopes and mounted symmetrically to the beam axis. Ten separate strips per detector allowed simultaneous measurements of emitted protons at 40 different decay angles with a angular resolution better than $\pm 3°$.

Fig.1 presents first results of the (^{6}Li, ^{6}He p) correlation measurements in the system $^{90}Zr \rightarrow ^{90}Nb \rightarrow ^{89}Zr$. In the upper part singles measurements at 0° and 2° are compared to coincidence spectra, when ^{6}He particles have been detected in coincidence with a decay proton. In the region of the GT giant resonance, just located between the Coulomb barrier for proton emission and the threshold for neutron decay the dominance of the proton channel is evident. The decay spectra of protons from the GT giant resonance region to final states in the residual nucleus ^{89}Zr are presented in the lower part of fig.1. A decay to low lying n-hole states (indicated by gaussian shapes) could be found. The population of the $9/2^+$ ground state appears to be nearly unchanged between zero and two degrees observation. The $1/2^-$ state at $E_x = 0.59$ MeV, however, is much more populated in the 0°- than in the 2°-spectrum. So, we conclude that the Gamov-Teller giant resonance in ^{90}Nb ($J^\pi = 1^+$) is decaying with preference to low spin states in ^{89}Zr.

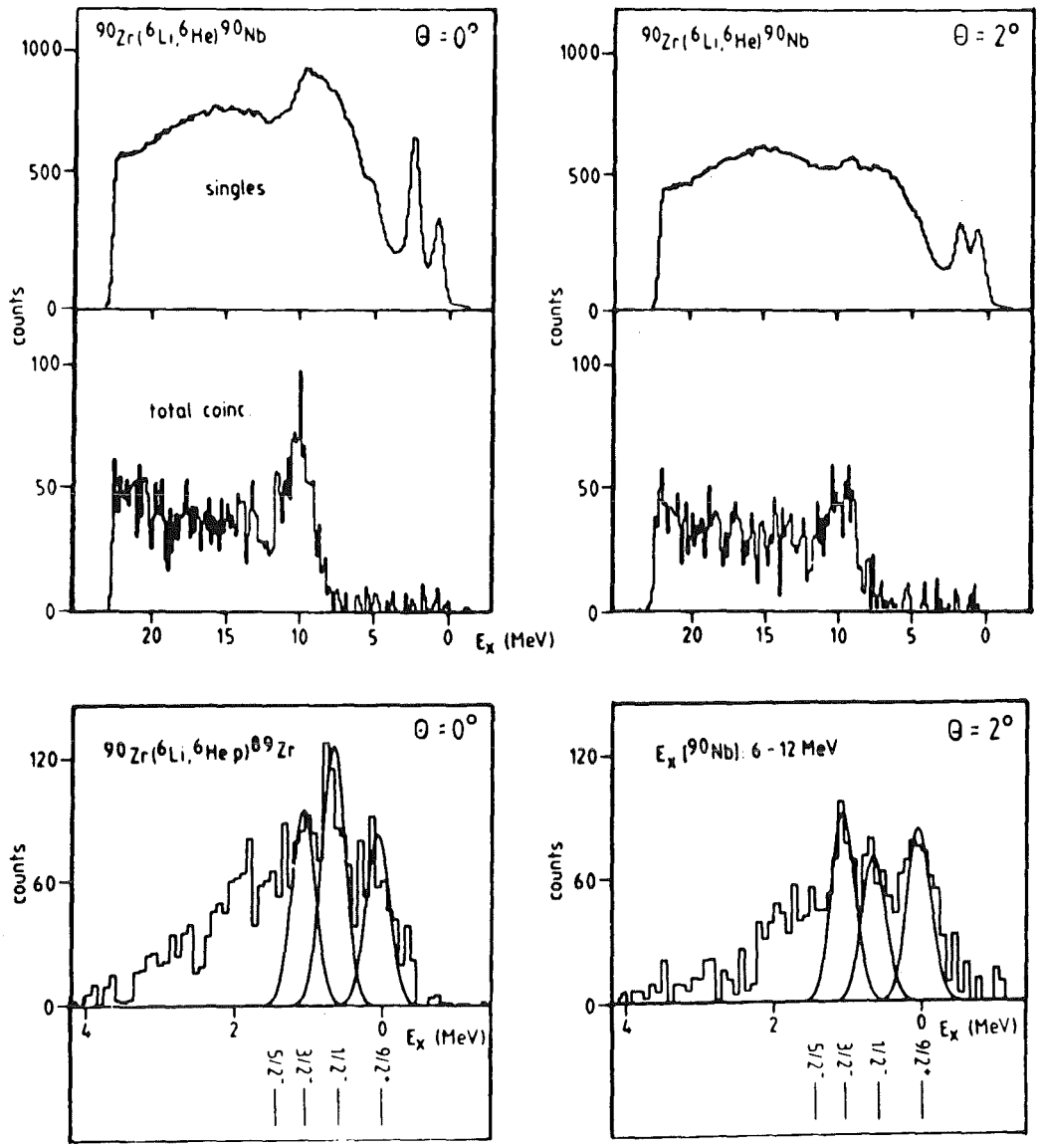

Fig.1 : Singles and total coincidence spectra of the reaction ^{90}Zr(^{6}Li, ^{6}He) ^{90}Nb at 0° and 2° (upper part).

Spectra of the proton decay from the GT giant resonance region in ^{90}Nb (lower part).

In contrast, the underlying physical continuum - probably a superposition with higher multipolarities, too - is able to decay to all states, also to higher-spin states like the $9/2^+$ ground state. This is mainly due to the fact that low energetic protons emitted from the GT giant resonance region induce only small transfer of angular momentum. Moreover, the feature tentatively favours a dominant statistical decay of the GT giant resonance in ^{90}Nb.

* Physikalisches Institut der Universität Erlangen-Nürnberg

[1] M. Moosburger, E. Aschenauer, H. Dennert, W. Eyrich, A. Lehmann, R. Rudeloff, H. Schlösser, H.J. Gils, H. Rebel, S. Zagromski, Phys. Rev. C 41 (1990) 2925

[2] H. Wirth, E. Aschenauer, W. Eyrich, A. Lehmann, M. Moosburger, H.J. Gils, H. Rebel, S. Zagromski, Phys. Rev. C 41 (1990) 2698

[3] N. Scholz, H. Dennert, W. Eyrich, A. Lehmann, M. Moosburger, H. Wirth, Nucl. Instr. Meth. A 313 (1992) 233

3.2.7 EXCITATION OF ISOSCALAR GIANT MONOPOLE RESONANCE IN ^{24}Mg USING ^{6}Li - SCATTERING

H. DENNERT*, E. ASCHENAUER*, W. EYRICH*, H. J. GILS, A. LEHMANN*, M. MOOSBURGER*, H. REBEL, N. SCHOLZ, H. WIRTH*, S. ZAGROMSKI

The incompressibility of nuclear matter is directly related to the excitation energy of the isoscalar giant monopole resonance (GMR), the so-called "breathing mode". To extract the compression modulus (K_∞) more precisely, measurements over a wide mass range of nuclei are of considerable interest. Compared to the situation for heavy and medium mass nuclei where the GMR is well established, only few experiments found a larger amount of the E0-EWSR (energy-weighted sum rule) in light nuclei and determined accurately the excitation energy .

For light nuclei the width of the E0-strength is more extended and fragmentated. In order to discriminate clearly the GMR from other multipolarities, measurements under extreme forward angles are required. With the advantages of the 156 MeV ^{6}Li-beam of the Karlsruhe Isochronous Cyclotron and using additional devices in the beamline, in particular, the magnetic spectrograph "Little John" the experimental difficulties could be efficiently reduced.

Figs.1a-c show three spectra between the first maximum and the first minimum of the GMR angular distribution. Based on the theoretical angular distribution the enhancement in the energy region between 10 and 23 MeV

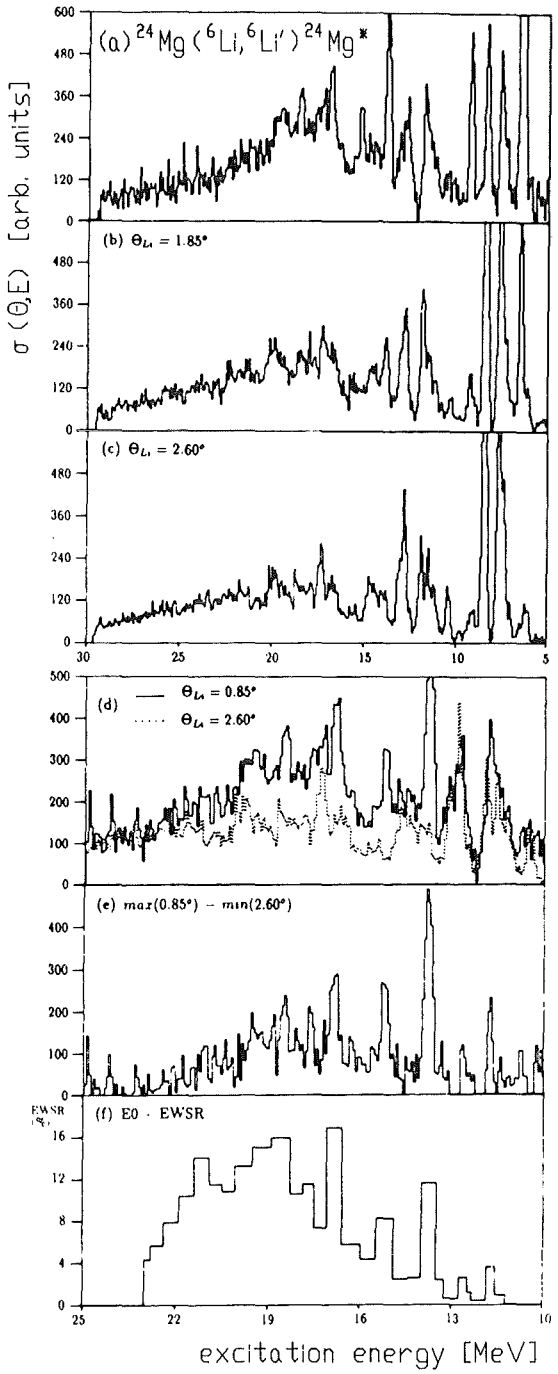

Fig. 1 :

(a-c) Spectra of the reaction ^{24}Mg(^{6}Li, ^{6}Li)^{24}Mg' at 0.85° and 2.60°.

(d) Maximum (0.85°) and minimum (2.60°) of the excited E0-strength in the high energy region of the spectra.

(e) Difference of maximum (0.85°) and minimum (0.60°).

(d) E0-distibution in percentage of EWSR.

reveals the GMR pattern. The region of the GMR is plotted in fig.1d for the maximum (0.85°) and the minimum (2.60°). The difference of the spectra

("maximum-minimum method") shows (fig. 1e) a fragmented GMR with the same shape of the distribution of the E0-strength between 10 and 20 MeV as found by Lu et al. [1], and some additional strength between 20 and 23 MeV. The E0-strength extracted by an energy weighted analysis (fig.1f) is 97.15±10% of the EWSR with a width of the distribution of about 7 MeV, centered at $E_x = 18.4 \pm 0.5$ MeV. This value is significantly higher than the result of ref.[1] ($E_x = 17.2 \pm 0.5$ MeV).

[1] H.J. Lu, S. Brandenburg, R. De Leo, M.N. Harakeh, T.D. Poelhekken, A. van der Woude, Phys. Rev. C33 (1986) 1116

* Physikalisches Institut, Universität Erlangen-Nürnberg

3.2.8 NEUTRON-PROTON CAPTURE USING POLARIZED NEUTRONS FROM 19 TO 50 MeV[1)]

G. FINK, P. DOLL, S. HAUBER, M. HAUPENTHAL*, H.O. KLAGES, H. SCHIELER, F. SMEND*, G.D. WICKE*

A polarized neutron beam has been used to determine the differential cross section and the analyzing power for neutron-proton capture at laboratory angles of 55°, 90° and 125° and neutron energies from 19 to 50 MeV. Capture photons were identified by measuring the time-of-flight and employing pulse-shape discrimination in the NaI detectors. Multiple scattering effects in the NE213 target were studied. The differential cross sections and analyzing powers are compared to modern nucleon-nucleon potential calculations including meson-exchange currents.

1) published in Nucl. Phys. A 530 (1991) 331

* Physikalisches Institut, Universität Göttingen

3.2.9 RADIATIVE CAPTURE OF POLARIZED NEUTRONS BY ^{12}C IN THE ENERGY RANGE E_n = 20 - 35 MeV[1)]

G.D. WICKE*, G. MONDRY, F. SMEND*, G. FINK, P. DOLL,
S. HAUBER, M. HAUPENTHAL*, H.SCHIELER, H.O. KLAGES

Radiative capture of polarized neutrons by ^{12}C was investigated using a scintillating NE-213 target and three NaI detectors. Angular distributions of the capture gamma photons and analyzing powers were measured at laboratory angles of 55°, 90° and 125° and neutron energies E_n = 20 to 35 MeV. Capture photons and recoil nuclei were detected in coincidence, the photons being identified by measuring the time of flight and analyzing the pulse shape in the NaI detectors. In the energy range above the centre of the GDR in ^{13}C, a pronounced rise of the forward-backward asymmetry for the $^{12}C(n,\gamma_0)^{13}C$ reaction was observed indicating the presence of E2 capture interfering with direct and collective E1 capture. The direct-semidirect (DSD) model of radiative capture does not give a satisfactory description of the experimental results.

1) published in Z. Phys. A 341 (1992) 453

* Physikalisches Institut, Universität Göttingen

3.2.10 CHARGE CHANGING CROSS SECTIONS

P. DOLL, H.J. CRAWFORD*

The 'transport collaboration' [1] provides accurate charge changing fragmentation cross sections which can be used to develop and refine models for galactic cosmic-ray propagation. We investigated the strong energy dependence of these cross sections for collisions with hydrogen for nuclei ranging from ^{12}C to ^{58}Ni, in the energy range from 300 to 2000 MeV/nucleon, and we studied the influence of the Δ excitations of nucleons. Already in 1975 P.J. Karol [2] has derived an analytical expression for the total nuclear reaction cross section for high energies, which was based on the semi-classical optical model. In the present model we go along the same line, introducing the free nucleon-nucleon cross

sections in order to determine the mean-free-path for protons entering the target nuclei. The use of the free nucleon-nucleon cross sections [3] for calculating the mean-free-path with an average nuclear density of $\rho_0 = 0.16$ fm^{-3} is probably justified because of the reduced nuclear density in the outer hemisphere of the nucleus, where the fragmentation dominantly takes place.

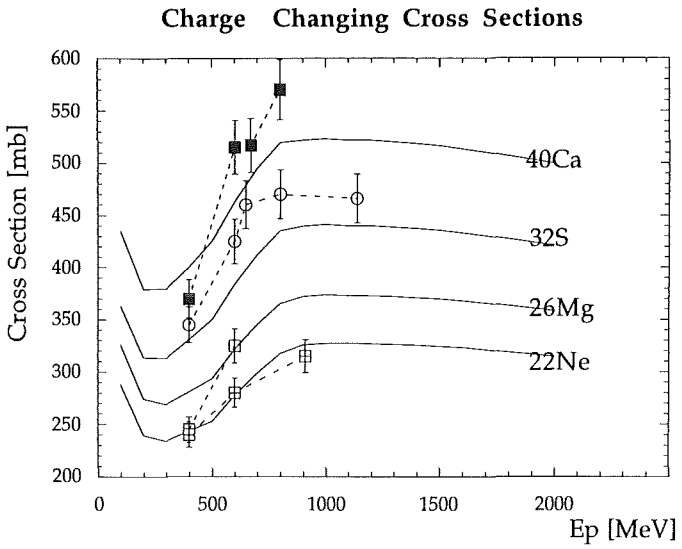

Fig.1: Total charge changing cross sections as a function of proton energy E_p for the present calculations (solid line) and data from Chen et al. [1] for the nuclei ^{40}Ca, ^{32}S, ^{26}Mg and ^{22}Ne.

These cross sections exhibit with the usual 1/k dependence at low momenta k an increase at around a nucleon momentum of 1GeV/c which is associated to the excitation of the Δ-resonances and other excitations of the nucleon. Below 1GeV/c the proton-neutron cross sections are almost three times larger than the proton-proton or neutron-neutron cross sections due to the $^3S_1$ or $^1S_0$ spin- and isospin-structure of the systems, respectively.

Fig.1 compares with the recent HISS data [1] for the nuclei ^{22}Ne, ^{26}Mg, ^{32}S and ^{40}Ca, additionally including some data from Webber et al. [4] for ^{32}S and ^{40}Ca. It reveals that the new data rise very fast at around 600 MeV. This is very interesting as neither Pauli blocking and nor Fermi motion of the nucleons inside the nucleus are explicitely taken into account in the calculations. Especially the Fermi motion is assumed to soften the energy dependence. The semi-empirical calculations by Letaw et al. [5] do not show such a strong threshold dependence. We find indications that the delta-isobar excitations provide the doorway state through which the excitation within the nucleus propagates towards various fragmentation channels.

[1] C.-X. Chen et al., Proc. 22 Int. Cosmic Ray Conf., Dublin, Ireland 11-23. August, 1991, Contr. OG 8.3-6

[2] P.J. Karol, Phys. Rev. 11C (1975) 1203

[3] Review of Particle Properties, Particle Data Group, Phys. Lett. **239B** (1990) III. 82

[4] W.R. Webber, J.C. Kish and D.A. Schrier, Phys. Rev. C41 (1990) 520

[5] J.R. Letaw, R. Silberberg and C.H. Tsao, Astrophys. Jour. Suppl. **51** (1983) 271

* Space Science Laboratory, University of California, Berkeley, Berkeley, California

3.2.11 INVESTIGATION OF LARGE-AREA SEMICONDUCTOR STRIP DETECTORS FOR USE IN LOW-ENERGY NUCLEAR PHYSICS[1)]

N. SCHOLZ*, H. DENNERT*, W. EYRICH*, A. LEHMANN*, M. MOOSBURGER*, H. WIRTH*

Commercial large area ion implanted semiconductor strip detector were investigated in respect of depletion behaviour, using the 8 MeV-proton beam of the Erlangen Tandem Accelerator. A characteristic resistivity profile of the n-type silicon detector material was observed. The semiconductor counters were used in a coincidence experiment for detection charged decay particles from the (^{6}Li, ^{6}He p) reaction on ^{12}C. Covering a total solid angle of 330 msr, they allow the simultaneous measurements of a considerably large number of angles.

1) published in Nucl. Instr. Meth. A 313 (1992) 233

* Physikalisches Institut, Universität Erlangen-Nürnberg

3.2.12 SUPERCONDUCTING ALUMINIUM TUNNEL JUNCTIONS WITH INDIUM ABSORBERS FOR LOW-ENERGY X-RAY SPECTROSCOPY[1)]

F. FINKBEINER, A. HAHN, W. HEERINGA, P. JANY,
H.O. KLAGES, T. STROBELT

We report here on studies of the preparation of and on measurement with an absorber-type tunnel junction detector ($Al/Al_2O_3/Al/In$) suitable for low-energy X-ray spectroscopy. With a ^{55}Fe source of 6 keV the energy resolution was determined to be 3.3% at a temperature of 276 mK. The experiments indicate that mainly phonons with $E \geq 2\Delta_{Al}$, generated in the indium absorbers, contribute to the observed detector signals.

1) published in Nucl. Instr. Meth. **A 306** (1991) 215

4. LASERSPECTROSCOPY

4.1 ISOTOPES SHIFTS AND HYPERFINE STRUCTURE IN POLONIUM ISOTOPES BY ATOMIC-BEAM LASER SPECTROSCOPY[1)]

D. KOWALEWSKA, K. BEKK, S. GÖRING, A. HANSER,
W. KÄLBER, G. MEISEL, H. REBEL

Laser-induced fluorescence spectroscopy in a collimated atomic beam has been applied to determine isotope shifts and the hyperfine structure of an isotopic chain of the radioactive element polonium (^{200}Po, ^{202}Po, $^{204-210}$Po). The relative isotope shifts show a striking similarity with results for other elements in the vicinity of Pb, even reproducing details of the odd-even staggering.

1) published in Phys. Rev A 44 (1991) 1442

4.2 TWO-STEP OPTICAL EXCITATION FOR DOPPLER LINEWIDTH REDUCTION AND MOTION STUDY OF IONS STORED IN A PAUL TRAP[1)]

W. KÄLBER, G. MEISEL, J. RINK, R.C. THOMPSON*

Atomic thorium ions were stored in an r.f. quadrupole trap and excited by tunable laser light. One-step and two-step excitation schemes were applied; a four to eightfold reduction of the Doppler linewidth is obtained for the two-step scheme with essentially no loss in signal strength. The Doppler-free two-photon transition was also observed. The lineshapes were calculated using a simple model; the observed profiles were well reproduced proving that the velocity and acceleration features of stored ions are properly accounted for. A further reduction of the Doppler linewidth is expected for the two-step method if a short lived intermediate level is used.

1) published in J. Modern Optics 39 (1992) 335

* Blackett Laboratory, Imperial College, London, England

4.3 OPTICAL ISOTOPE SHIFT MEASUREMENT OF ^{172}Hf

J. RINK, B. GORSKI*, W. KÄLBER, G. MEISEL, H.J. MIELKE, H. REBEL, M. SCHUBERT

In the course of preparing experiments with the long-lived isomer ^{178m2}Hf (Karlsruhe-Dubna collaboration), optical isotope shifts for the stable Hf isotopes and for ^{172}Hf were measured. The particular interest in hafnium arises from the existence of a unique range of high K isomers, the investigation of which may provide some insight into the competition between quasi-particle and collective behaviour of the nucleons. There has been considerable progress in producing relatively large samples of long-lived isomers as, e.g., ^{178m2}Hf [1].

Since Hf is a refractory element, the conventional atomic beam method cannot be applied. Instead, we use an rf trap to store atomic ions of Hf to investigate their spectra. For this purpose hafnium is deposited onto a tantalum wire as volatile $HfCl_4$. Upon heating the wire, the compound is vaporized; a very small but sufficiently large number of Hf^+ ions is produced by bombardment with electrons simultaneously emitted by the wire. To avoid chemical reactions between stored Hf^+ ions and residual gas contaminants, the vacuum system is thoroughly cleaned resulting in storage lifetimes of many hours.

Optical resonance fluorescence is induced by ultraviolet light at $\lambda = 301.2$ nm; it is generated by frequency doubling in a lithium iodate crystal mounted inside a modified type 699 cw dye laser. After optical excitation and emission of fluorescence radiation the ions reach metastable states. To prepare them for further excitations, the vacuum chamber is filled with hydrogen gas at a pressure of 10^{-4} mbar so that the ions are collisionally quenched back to the ground state. A signal photon count rate of 1 MHz is obtained if the trap is filled to the space charge limit with a nuclear spin $I = 0$ Hf isotope.

Because of their fast motion the stored ions exhibit a wide optical Doppler broadening which limits the resolution. For linewidth reduction the light is switched on only while the rf voltage is close to its peak value. The overall sensitivity is such that about 100 stored $I = 0$ ions are sufficient to record smooth spectra within minutes if no overlap with optical features of other isotopes occurs;

the sample size required to obtain 100 stored Hf ions is $2 \cdot 10^9$ Hf atoms (or 0.6 pg of Hf) on the Ta wire.

To have a dependable set of reference data, the isotope shifts were determined for all stable isotopes. To test our methods under realistic conditions, we have performed experiments with ^{172}Hf (I = 0, $T_{1/2}$ = 1.87 a). It was produced by irradiation of $^{171}Yb_2O_3$ with α particles at an energy of about 37 MeV. Hf was separated chemically from the $^{171}Yb_2O_3$ target by selective extraction chromatography with TOPO. The spectrum (fig.1) obtained from a sample containing ^{172}Hf shows a strong contamination with other hafnium isotopes.

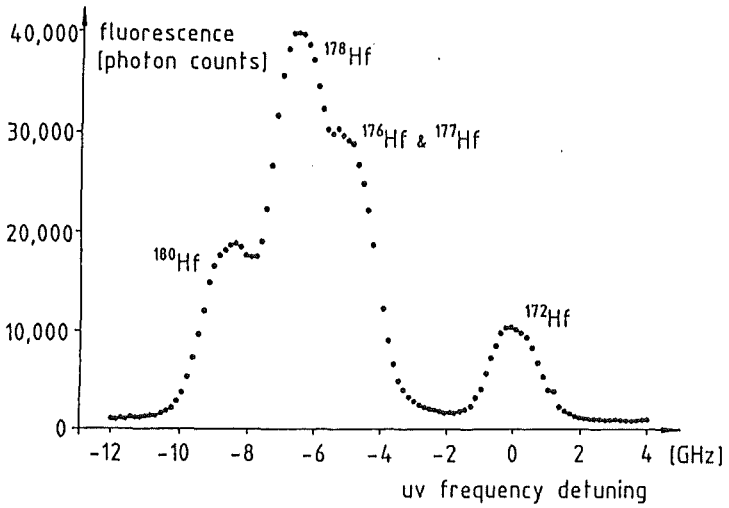

Fig.1 : Spectrum for the resonance line λ = 301.3 nm for Hf^+. The ion cloud contained several stable Hf isotopes and a small fraction of radioactive ^{172}Hf.

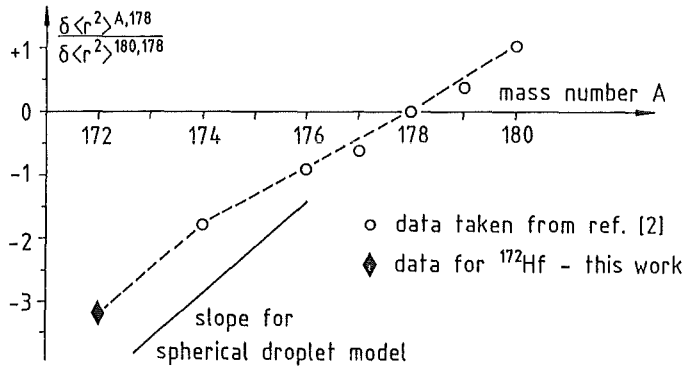

Fig.2 : Relative $\delta\langle r^2\rangle$ values as function of mass number.

All relative $\delta\langle r^2\rangle$ values known so far for Hf are diplayed in fig.2. For the stable isotopes they were taken from [2]. We have added our result for ^{172}Hf. The

errors are too small to be displayed in the Figure. For comparison the results obtained from the spherical droplet model were included. For the stable isotopes, the model slope differs somewhat from the experimental results. The discontinuity in the experimental curve at A = 174 may indicate a change of deformation at this mass number.

In order to deduce an absolute value $\delta\langle r^2\rangle$ for ^{172}Hf, we combine the nuclear parameter $\lambda^{180,178} = -0.072(4)$ fm^2 [3] with our isotope shift data and find $\lambda^{180,178} = -0.230(15)$ fm^2. This can be converted to a $\delta\langle r^2\rangle$ result applying a correction factor K = 0.95 [2,4] : $\delta\langle r^2\rangle^{172,178} = -0.242(16)$ fm^2.

Experiments are in progress to reduce the contamination of the Hf^+ cloud with stable Hf isotopes and to improve the resolution by optical two-step excitation.

[1] Y.T. Oganessian, S.A. Karamian, Ch. Briançon, H.J. Wollersheim, R. Kulessa, Nuclear Physics News 1 (1991) 28

[2] P. Aufmuth, K. Heilig, A. Steudel, Atomic Data and Nuclear Data Tables 37 (1987) 455

[3] P. Aufmuth, I. Henneberg, A. Siminski, A. Steudel, Z. Phys. D 18 (1991) 107

[4] G. Tarbohm, B. Fricke, A. Rosén, Phys. Rev. A 31 (1985) 2038

* JINR Dubna, Russia

4.4 EXPANDED DYNAMIC RANGE FOR A LASER WAVEMETER

R. SCHRUFT, G. MEISEL

A fast reading wavemeter for the determination of laser frequencies has been built and tested [1-4]. It is based on interferograms that are picked up by photodiode arrays. The interferometer pattern are processed on-line resulting in a 20 Hz readout rate. The instrument is applied to measure and to control the actual operating frequencies of five cw dye lasers. It is calibrated by a stabilized HeNe

laser. The laser beams are fed into the wavemeter via single mode fibers. A fiber switch is used to change from one laser to another one.

The practical use of this instrument, however, was limited by the poor quality of the diode arrays. A key parameter is the saturation signal compared to the dark signal and its noise. For the array used so far (model RL 1024 G by EG & G Reticon) the saturation to dark charge ratio is only 1.6 for 50 msec integration time. The dark current also varies for different diodes of the array. The high dark signal required that the interferogram illumination is very carefully adjusted for uniformity and intensity which usually is difficult to realize.

An considerable improvement was possible by replacing the diode arrays by the type RL 1024 SB (also by EG & G Reticon) which has a saturation-to-dark ratio of 70 for our repetition rate of 20 Hz.

A further improvement is obtained making use of the fact that the dark signal is relatively stable with time though it varies from diode to diode ("fixed pattern dark signal"). This dark signal is determined occasionally and stored for continuous subtraction from the incoming data. With this method the fast fluctuations of the dark signal set a lower limit for the signals that can be detected. For the new diode arrays the dynamic range (i.e. the ratio of the saturation signal to the peak-to-peak fluctuations for the dark signal for a single diode of the array) was increased to 4000.

With the new detector system the interferometers accept laser beams that are just coarsely aligned making it a handy instrument requiring a minimum of attention.

[1] R. Schruft, W. Kälber, D. Kowalewska, G. Meisel, Report KfK 4875 (1991), eds. H. Beer, J. Wochele, Kernforschungszentrum Karlsruhe, p. 112

[2] A. Fischer, R. Kullmer, W. Demtröder, Opt. Comm. 39, 277 (1981)

[3] A. Steiger, Report KfK 3820 (1984), Kernforschungszentrum Karlsruhe

[4] R. Schruft, G. Meisel, K. Bekk, Report KfK 4660 (1990), eds. G. Drexlin, H.J. Gils, Kernforschungszentrum Karlsruhe, p. 95

4.5 TEST OF A MULTISTEP PROCEDURE FOR OPTICAL FREQUENCY METROLOGY

H. BOSCHERT, W. KÄLBER, G. MEISEL, K. MÜLLER

A method for precise and accurate frequency measurements [1-4] has been tested to determine its statistical and possible systematic errors. For this purpose the multistep method was performed starting from the frequency of an iodine stabilized HeNe laser. After a number of steps the step direction was reversed returning to the starting frequency. The beat frequencies for all signed steps were summed up and compared with the expected null result.

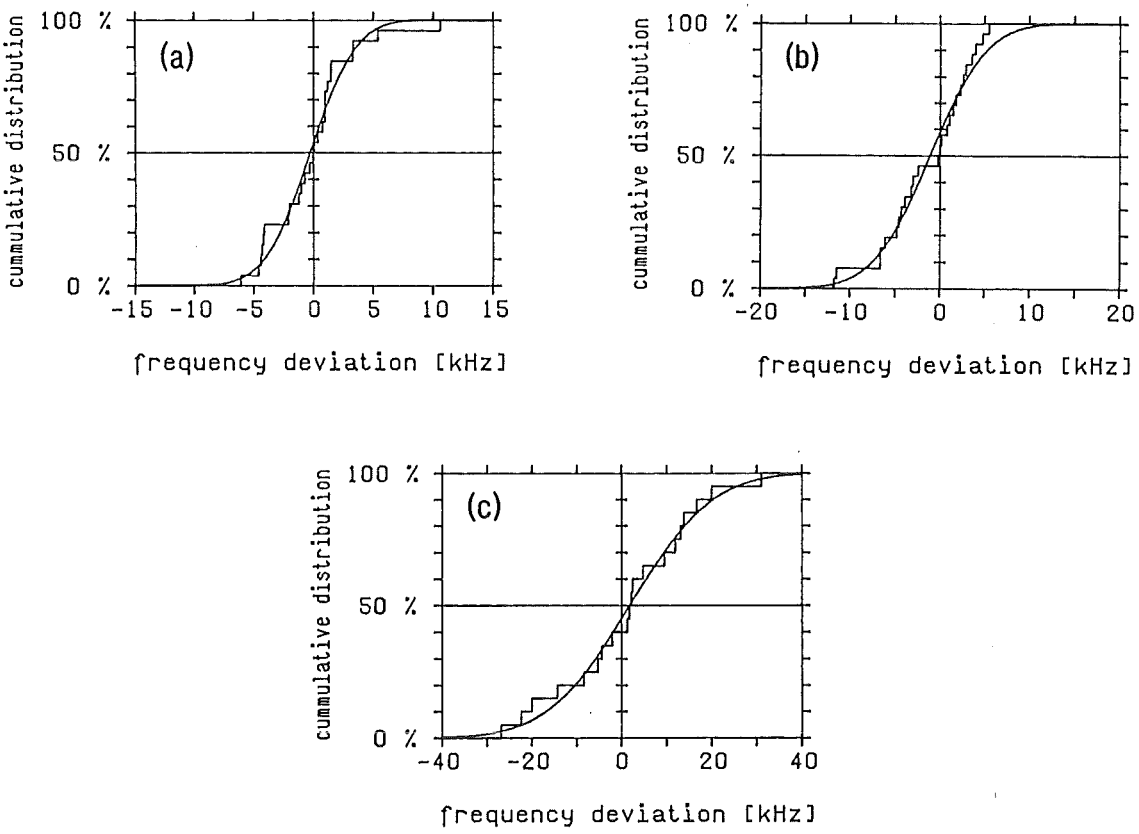

Fig.1 : Results for multi-step round-trip measurements. a : 12 steps, b : 32 steps, c : 100 steps. The expected result is zero. The figure diplays the experimental cummulative distribution (step function) and a best fitting cummulative normal distribution.

The round trips were performed with a stepwidth of about 4 GHz and a total of 12, 32 and 100 steps; they were repeated 20 to 26 times. The average duration for one step was 6 seconds. The experimental results are displayed in fig.1. They were evaluated by fitting a normal distribution to the data. For the results see Table 1.

Table 1 : Round trip results for 12, 32 and 100 steps. The round trip procedure was repeated 26, 26 and 20 times for 12, 32 and 100 steps, respectively.

Quantity	Number K of steps :		
	K=12	K=32	K=100
Median [kHz]	0.	−0.15	+1.9
Mean value [kHz]	−0.15	−1.46	+1.24
Standard deviation for mean value [kHz]	0.7	0.9	3.4
Standard deviation for single round trip [kHz]	3.5	4.6	15.0
Standard deviation for single step [kHz]	1.0	0.8	1.5

Fig.1 shows that the experimental data follow a normal distribution fairly well, i.e. the scatter appears to be mainly of statistical nature. The median and mean both are close to zero and to each other (lines 2 and 3 of table 1). The standard deviation of the mean value (line 4 of table 1) shows that the means are fairly compatible with the expected zero result. Line 5 of table 1 gives the uncertainty for a single round trip. It increases with the number of steps; if this uncertainty is divided by the square root of the step number K the single-step uncertainties in the last line of table 1 result. To the extent the numbers in this

line are considered constant, the error for a round trip increases with the square root of the step number.

With the present step width of 4 GHz, a 100 step unidirectional procedure would allow to determine differences of optical frequencies 400 GHz apart to about ± 5 kHz. If one of the frequencies is an optical standard to which an unknown frequency is traced, the relative error contribution of the multi-step procedure alone is 10^{-11}. The range of the method can be extended by either performing even more steps or by taking higher beat frequencies of, e.g., 80 GHz [2,5] so that differences of many THz can be bridged.

[1] W. Kälber, A. Dorn, G. Meisel, Report KfK 4875 (1991), eds. H. Beer, J. Wochele, Kernforschungszentrum Karlsruhe, p. 117

[2] B. Burghardt, H. Hoeffgen, G. Meisel, W. Reinert, B. Vowinkel, Precision Measurement and Fundamental Constants II, B.N. Taylor, W.D. Phillips, eds. Natl. Bur. Stand. (U.S.), Sprec. Publ. 617, 49 (1984)

[3] A. Dorn, G. Meisel, Report KfK 4508 (1989), eds. P. Doll, G. Meisel, Kernforschungszentrum Karlsruhe, p. 77

[4] A. Dorn, W. Kälber, G. Meisel, Report KfK 4709B (1990), Kernforschungszentrum Karlsruhe

[5] B. Burghardt, H. Hoeffgen, G. Meisel, W. Reinert, B. Vohwinkel, Appl. Phys. Lett. 35 (1979) 498

5. APPLICATIONS

5.1 ANALYSIS OF Th-U, U-Pu AND Pu SOLUTIONS WITH A HYBRID K-EDGE / XRF ANALYZER [1)]

H. OTTMAR, H. EBERLE, N. DOUBEK*, W. RAAB*, J. PARUS*

The Safeguards Analytical Laboratory (SAL) of the IAEA has been equipped with a hybrid K-edge/XRF analyzer for the measurement of nuclear materials in liquors. The purpose of the instrument is to establish at SAL the technical capability to provide IAEA inspectors with experimental support and training in the use of such instrumentation for in-field measurements. Typical performance data for different applications are presented and discussed. The work presented is done in the frame of the Joint Programme of the IAEA and the Federal Republic of Germany for the Development of Safeguards.

1) published in EUR-13686-EN (1991) 149

* International Atomic Energy Agency, Safeguards Analytical Laboratory, Vienna, Austria

5.2 THE HYBRID K-EDGE / K-XRF DENSITOMETER : PRINCIPLES - DESIGN - PERFORMANCE [1)]

H. OTTMAR, H. EBERLE

The Euratom Safeguards Directorate (ESD) has recently installed a hybrid K-edge/K-XRF densitometer in a commercial reprocessing plant for the safeguarding of nuclear materials. This instrument, developed at KfK Karlsruhe, offers for the first time analytical measurement capabilities for timely on-site input accountancy verification. Lectures providing informations on measurement principles, instrument design features and performance data have been given to inspectors of ESD to make them familiar with the new instrument. The report summarizes the essential material presented during these courses.

1) published as KfK Report 4590 (1991)

5.3 ESARDA PERFORMANCE VALUES OF NON-DESTRUCTIVE ASSAY TECHNIQUES APPLIED IN SAFEGUARDS [1)]

S. GUARDINI*, G. BIGNAN**, R. S. J. HARRY***, H. OTTMAR, B. G. R. SMITH****, G. WELLS*****

The Working Group on Non-Destructive Assay (NDA) Techniques and Standards of ESARDA (European Safeguards R and D Association) is currently discussing the assessment of NDA Performance Values, i. e. the "knowledge of the overall uncertainty and error sources associated with NDA measurement systems". The group has devoted great attention to determine the error structure of the different techniques and the error propagation patterns. The paper presents a compilation of NDA Performance Values for some techniques : High Resolution Gamma Spectrometry (HRGS) on PuO_2 and MOX ; calorimetry on PuO_2; passive and active neutron techniques on Pu/U samples; K-edge and X-ray fluorescence densitometry; gamma and neutron techniques on spent fuels.

1) published in 4th Internat. Conf. on Facility Operations-Safeguards Interface, Albuquerque, N. M., September 29 - October 4, 1991
Transactions of the American Nuclear Society **63**, Suppl. 1 (1991) 66

* Institute of Safety Technology, JRC-Ispra, Italy

** DER/SSAE, CEN Cadarache, France

*** Stichting Energieonderzoek Centrum Netherland, Petten, The Netherlands

**** CEC, Euratom Safeguards Directorate, Luxembourg

***** AEA Technology, ANMCO, Harwell, UK

5.4 ON-SITE ANALYTICAL MEASUREMENTS FOR INPUT ACCOUNTANCY VERIFICATION IN A LARGE REPROCESSING PLANT BY HYBRID K-EDGE [1)]

H. G. WAGNER*, J. GÖRTEN*, P. LOUIS*, W. PÖRSCH*, R. SCHENKEL*, L. KOCH**, M. OUGIER**, H. OTTMAR, H. EBERLE, R. SCHOTT***, P. GRISON***, J. SALAÜN***, P. COURVOISIER***

Independent, accurate, effective and efficient verification of the flow of special nuclear materials in large reprocessing plants is an important task for the Euratom Safeguards Directorate (ESD). Traditionally this has been effected by taking readings of the operator's tank instrumentation and by shipping samples taken from the accountancy tanks off-site to Euratom laboratories for chemical analysis. After discussions between Cogema, the French government and ESD, the Euratom Safeguards Directorate decided to install a hybrid K-edge instrument for non-destructive, on-site analysis in the analytical laboratories of Cogema La Hague. This paper lists the reasons for this decision, discusses the design and installation of the instrument, it describes the measurement procedure followed and it reviews the measurement performance. The operational experience since the installation of the instrument in November 1989 shows that uranium and plutonium concentrations in undiluted samples of input liquor can be determined to 0.3 % and 0.7 %, respectively.

1) published in 4th Internat. Conf. on Facility Operations-Safeguards Interface, Albuquerque, N. M., September 29 - October 4, 1991
Transactions of the American Nuclear Society **63**, Suppl. 1 (1991) 22

* CEC, Euratom Safeguards Directorate, Luxembourg

** CEC, European Institute for Transuranium Elements, Karlsruhe

*** COGEMA, Etabl. de la Hague, Cherbourg, France

5.5 CONSEQUENCES OF THE PRESENCE OF NEPTUNIUM IN Pu BEARING SAMPLES FOR SAFEGUARDS VERIFICATION MEASUREMENTS [1)]

O. CROMBOOM*, J. I. GARCIA ALONSO*, L. KOCH*, J. GÖRTEN**, E. ROESGEN**, H. G. WAGNER**, H. OTTMAR, H. EBERLE

The presence of neptunium in safeguards samples containing plutonium interferes with the determination of the plutonium concentration in different ways, depending on the analytical method employed. This paper presents results of five different analytical methods obtained from samples specially prepared from pure plutonium solution and pure neptunium metal.

Further, the prepared Pu-Np reference samples were also used for the purpose of testing different analytical techniques for their capabilities to determine neptunium in a plutonium matrix. The techniques investigated were Inductively Coupled Plasma-Mass-Spectrometry (ICP-MS), K-Edge Densitometry (KED), X-Ray Fluorescence (XRF) and Gamma-Spectrometry (GS).

1) published in 4th Internat. Conf. on Facility Operations-Safeguards Interface, Albuquerque, N. M., September 29 - October 4, 1991
Transactions of the American Nuclear Society **63**, Suppl. 1 (1991) 69

* CEC, European Institute for Transuranium Elements, Karlsruhe

** CEC, Euratom Safeguards Directorate, Luxembourg

5.6 A COMPACT K-EDGE DENSITOMETER FOR URANIUM [1)]

P. MATUSSEK, I. MICHEL-PIPER, H. OTTMAR

A compact K-edge densitometer has been designed for the use by safeguards inspectors to verify the uranium concentration in product solutions from a reprocessing plant. The densitometer is based on multi-energy transmission measurements near the uranium K-absorption edge using a single isotopic source (^{57}Co) in conjunction with a uranium converter foil. The compact set-up is easily coupled to standard high-resolution spectroscopy systems. The measurement accuracy achieved in a counting time of 1000 seconds is about 0.2-0.3% at concentration levels typical for product solutions.

An approach to determine the ^{235}U enrichment from aliquots of less than 5 ml with an accuracy of better than 1% within the same measurement time is also discussed.

1) published in EUR-13686-EN (1991) 329

5.7 DETERMINATION OF SAMARIUM ISOTOPE QUANTITIES BY K-EDGE DENSITOMETRY

H. EBERLE, K. WISSHAK

The technique of K-edge densitometry was applied to verify the content of Sm isotopes in samples of Sm-oxide (Sm_2O_3). The analysis was carried out in support of the Van de Graaff group at our laboratory, where the Sm isotopes were used as target material for neutron capture cross-section measurements. The purpose of the present analysis was to assure that the quantities of the Sm isotopes ($^{147,148,149,150,152}Sm$) as determined from the weight of the highly enriched samples have not been invalidated by a possible take-up of moisture or by an incorrect stochiometric sample material.

K-edge densitometry is preferably applied as a method for the determination of element concentrations in liquid samples. Therefore the Sm isotopes were separately dissolved in a defined volume (10ml) of 1.5n HNO_3. An aliquot of about 2ml was filled into a quartz cell of well-defined path length (2cm) for the energy-

differential photon transmission measurements near the K-absorption edge of Sm at 46.85 keV. A highly collimated X-ray beam from an X-ray tube operated at 53 kV was utilized for the transmission measurements. Fig. 1 shows the energy distribution of the transmitted X-ray beam as recorded with a HpGe detector. The discontinuity of the photon transmission at the K-edge energy of Sm clearly shows up.

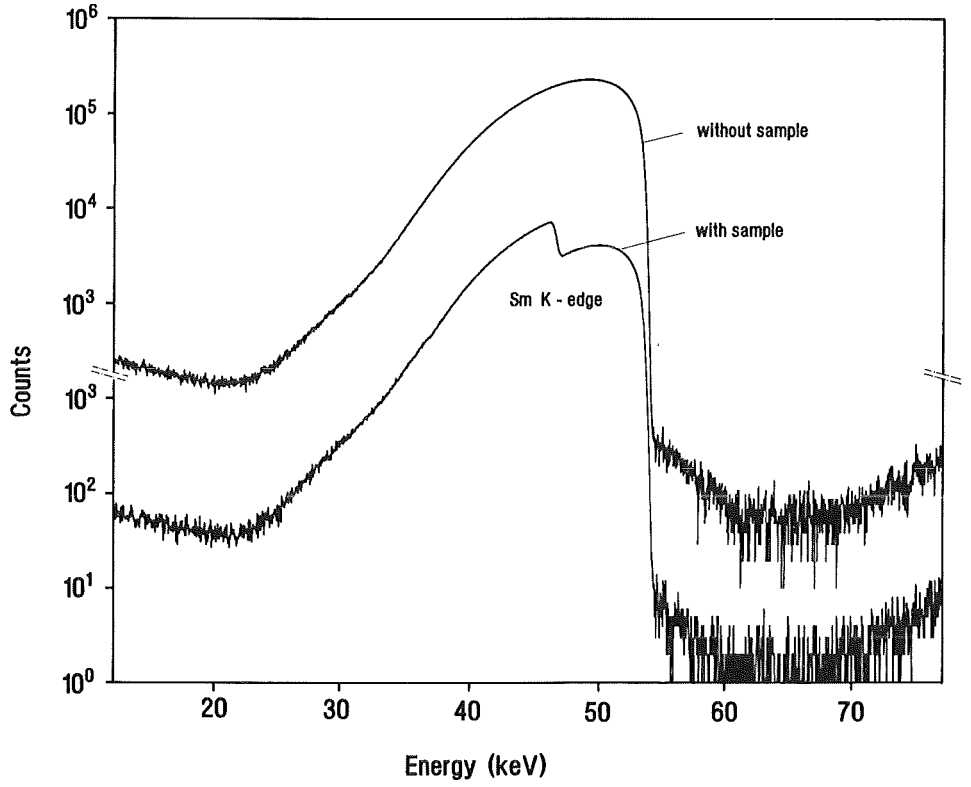

Fig.1 : Discontinuity of the photon transmission at the K-edge energy of Sm.

The concentration of the Sm atoms was simply determined from the change of the photon transmission across the absorption edge. This determination requires a single calibration factor which describes the change of the mass attenuation coefficient of the analyte at its K-edge energy. The calibration factor was derived from comparison measurements on reference samples of natural Samarium (metallic Sm and Sm_2O_3) with known Sm content. The photon transmission was determined at energies slightly displaced (46.1 and 48.0 keV) from the Sm K-edge. The results of the measurements yielded isotope concentrations for the five Sm isotopes 147, 148, 149, 150 and 152, which were on the average 0.34% higher (standard deviation = 0.55%) than the declared values.

5.8 AN ANALYZER FOR SIMULTANEOUS PLUTONIUM ELEMENT AND ISOTOPE CONCENTRATION MEASUREMENTS

H. OTTMAR

A measurement system has been designed for the simultaneous determination of plutonium element and isotope concentrations in liquid samples. The instrument is designated for an on-site analytical laboratory to be installed and operated by the Euratom Safeguards Directorate (ESD) in the new reprocessing plant at Sellafield, England. The on-site laboratory, starting operation in 1994, will host a number of automated analysis systems for timely verification measurements on process samples taken from the facility by inspectors of ESD.

The present analyzer utilizes the proven technique of K-edge densitometry (KED) to measure the plutonium element concentration, and passive gamma spectrometry to determine its isotopic composition. The arrangement of the basic components, which are located underneath of a glovebox, is shown in fig.1.

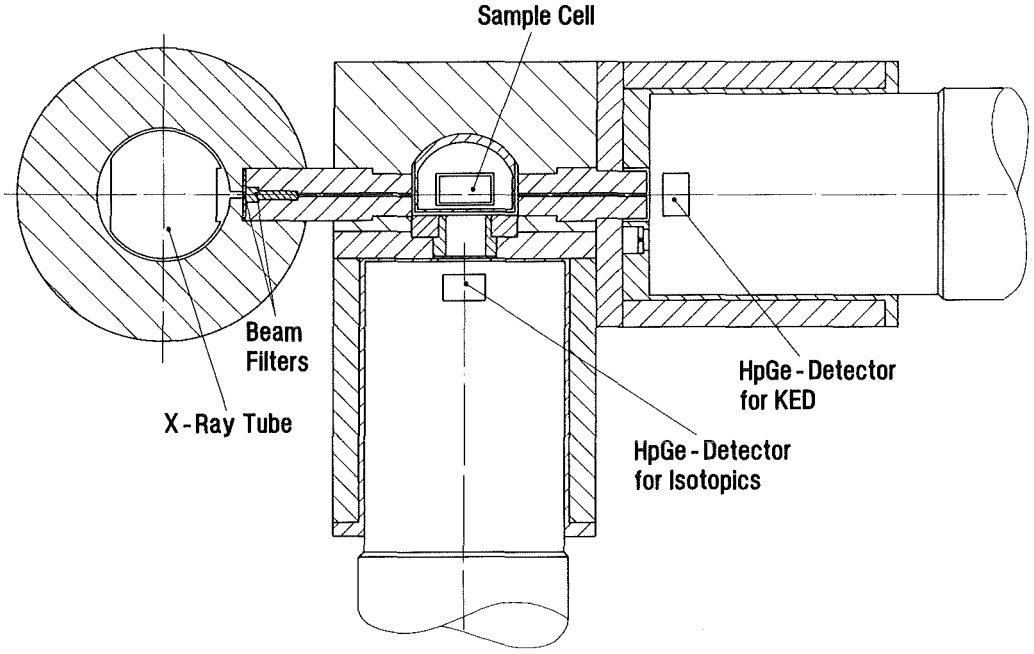

Fig.1 : Set-up of the basic instrument components (horizontal cross-section).

The vertically mounted sample cavity is coupled to the bottom of the glovebox. It will receive by means of a robot system a single sample cell (glass vial) for the two types of measurement done in parallel. The level of the horizontal beam axis for the KED measurement, which uses a tailored and highly collimated

X-ray continuum from an X-ray tube, is positioned at about 15 cm below the bottom of the glovebox. The detector axis of the detector for the isotopic measurement, positioned at 90° relative to the beam axis for KED, views the sample through a collimator 1.5 cm above the transmitted X-ray beam. It has been verified from test measurements that with this configuration the scattered radiation generated by the highly intense X-ray beam contributes a negligible fraction (about 0.1%) to the background of the passive spectrum for the isotopic analysis. The latter analysis will be based on the analysis code MGA developed at the Livermore National Laboratory [1].

[1] R. Gunnink, "MGA, A Gamma-Ray Spectrum Analysis Code for Determining Plutonium Isotopic Abundances", UCRL-LR-103220, Vol. 1 and 2 (1990)

5.9 CALCIFICATION OF AORTIC WALL IN CHOLESTEROL-FED RABBITS[1)]

E. ROKITA*, T. CICHOCKI**, D. HECK, L. JARCZIK*, A. STRZALKOWSKI*

Development of the mineralization process in the course of atherogenesis was studied using the cholesterol-fed rabbit model. The aorta samples were investigated by means of proton and electron microprobes, infrared spectroscopy and X-ray diffraction as well as selected histochemical staining. Blood serum was analysed every 2 weeks tot determine the content of cholesterol, triglycerides, inorganic phosphorus, ionized calcium, elemental composition as well as activity of alkaline phosphatase. It was found that the administered diet did not disturb the calcium and phosphorus homeostasis. Histochemical findings confirmed the formation of lipid-rich lesions blocking the lumen of the vessel. The dystrophic calcification was observed only in the atheroma, while in the tunica media a slight mineralization similar to that found in controls was observed after 210 days of the diet. In the atheroma the only phase detected was a defective hydroxyapatite. The perfection of the crystals, as well as the diameter of the deposits, increased during the courses of the diet reaching about 2 μm after 210 days. The crystals were not contaminated with carbonate groups regardless of the duration of the diet.

1) published in Atherosclerosis 87 (1991) 183

* Institute of Physics, Jagellonian University, Poland

** Department of Histology, Academy of Medicine, Poland

5.10 TOXIC ELEMENTS IN TISSUE SECTIONS DETECTED BY PROTON INDUCED X-RAY EMISSION (MICRO-PIXE)[1)]

A. OCHS*, D. HECK, H.E. SCHÄFER**, W. GEROK***

All diseases mentioned here (idiopathic hereditary hemochromatosis, Wilson's desease, primary biliary cirrhosis, Thorotrast-induced malignancies) are characterized by metal or elemental deposits or overload. In contrast, the diagnosis of element deficiency at the at the trace- or ultratrace-element level is almost impossible considering substantial contamination by the biopsy needles (Versieck et al. 1973). The objective of this study was to evaluate existing procedures for the diagnosis of elemental overload and to offer alternative if tissues necessary for those procedures were not available. We used Micro-PIXE, a method combining the spatial resolution of histochemistry with exact quantitation of the elements of interest.

1) published in Progr. Histo- and Cytochemistry 23 (1991) 164

* Albert Einstein College of Medicine, USA

** Pathologisches Institut,Freiburg

*** Medizinische Klinik II der Universität Freiburg

6. LIST OF PUBLICATIONS

6.1 PUBLICATIONS AND REPORTS

ASCHENAUER, E.; DENNERT, H.; EYRICH, W.; LEHMANN, A.; MOSSBURGER, M.; WIRTH, H.; GILS, H.J.; REBEL, H.; ZAGROMSKI, S.
(^{6}Li, ^{6}He) measurements as an alternative calibration for solar neutrino detectors
Physical Review C, 44, 6 (1991) p. 2771-2775

BEER, H.
An analytical formulation of the double-pulse s-process model
The Astrophysical Journal, 379 (1991) p. 420-23

BEER, H.; RUPP, G.; VOß, F.; KÄPPELER, F.
A measurement of the ^{22}Ne (n, γ) ^{23}Ne capture cross section at a stellar temperature of kT = 25 keV
The Astrophysical Journal, 379 (1991) p. 420-23

BEER, H.; WOCHELE, J.
Annual report on nuclear physics activities July 1, 1989 - December 31, 1990
KfK-4875 (Mai 1991)

BIGMAN,G.; GUARDINI, S.; OTTMAR, H.; SMITH, B. G. R.,; HARRY, R. J. S.; WELLS, G.
ESARDA performance values of nondestructive assay techniques applied in safeguards
4th Internat. Conf. on Facility Operations-Safeguards Interface, Albuquerque, N. M, September 29 - October 4, 1991
Transactions of the American Nuclear Society, 63 (1991) Suppl. 1, p. 66-67

CORCALCIUC, V.; JELITTO, H.
Coincidence cross sections within the quasi free break-up model for elastic projektile break-up
KfK-4960 (November 1991)

CROMBOOM, O.; GARCIA-ALONSO, J. I.; KOCH, L.; GÖRTEN, J.; ROESGEN, E.; WAGNER, H. G.; OTTMAR, H.; EBERLE, H.
Consequences of the presence of neptunium in Pu-bearing samples for safeguards verification measurements
4th Internat. Conf. on Facility Operations-Safeguards Interface, Albuquerque, N. M., September 29 - October 4, 1991
Transactions of the American Nuclear Society, 63 (1991) Suppl. 1, p. 69

FINK, G.; DOLL, P.; HAUBER, S.; HAUPENTHAL, M.; KLAGES, H. O.; SCHIELER, H.; SMEND, F.; WICKE, G. D.
Neutron-proton capture using polarized neutrons from 19 to 50 MeV
Nuclear Physics A, 530 (1991) p. 331-46

FINKBEINER, F.; HAHN, A.; HEERINGA, W.; JANY, P.; KLAGES, H. O.; STROBELT, T.
Superconducting aluminium tunnel junctions with indium absorbers for low-energy X-ray spectroscopy
Nuclear Instruments and Methods A, 306 (1991) p. 215-19

GERSTENHÖFER, T. W.; KÄPPELER, F.; WISSHAK, K.; REFFO, G.
^{147}Pm - an experimental stellar cross section for a short-lived s-process branching point
In : Cierjacks, S. [Hrsg.]
Progress Report on Nuclear Data Research in the Federal Republic of Germany for the Period April 1, 1990 to March 31, 1991
NEANDC (E)-322 U Vol. 5 (July 1991) p. 8-10
INDC (Ger)-36/LN + Special
KfK-4953

GILS, H. J.
Die Karlsruher Detektoranlage KASCADE zur Elementanalyse ultra-hochenergetischer Kosmischer Strahlung
KfK-Nachrichten, 22 (1990) p. 222-33

GILS, H. J.
KASCADE - eine Detektoranlage zur Analyse hochenergetischer kosmischer Strahlung
Physikalische Blätter, 47 (1991) p. 313-14

GILS, H. J.; TESCH, S.
Blick in die Tiefen des Universums : KASCADE
Wissenschaft und Fortschritt, 41 (1991) p. 235-38

JAAG, S.; KÄPPELER, F.
The stellar cross section of ^{209}Bi : implications for the s-process
In : Cierjacks, S. [Hrsg.]
Progress Report on Nuclear Data Research in the Federal Republic of Germany for the Period April 1, 1990 to March 31, 1991
NEANDC (E)-322 U Vol. 5 (July 1991) p. 12-13
INDC (Ger)-36/LN + Special
KfK-4953

KÄPPELER, F.; JAAG, S.; BAO, Z. Y.; REFFO, G.
The s-process branchings at ^{185}W and ^{186}Re
The Astrophysical Journal, 366 (1991) p. 605-16

KARMEN-COLLABORATION
First observation of the neutral current nuclear excitation ^{12}C (ν, ν') ^{12}C (1^+, 1)
KfK-4893 (Juni 1991)

KIENER, J.; GILS, H. J.; REBEL, H.; ZAGROMSKI, S.; GSOTTSCHNEIDER, G.; HEIDE, N.; JELITTO, H.; WENTZ, J.; BAUR, G.
Measurements of the Coulomb dissociation cross section of 156 MeV ^6Li projectiles at extremely low relative fragment energies of astrophysical interest
Physical Review C, 44 (1991) p. 2195-2207
KfK-4870 (April 1991)

KIENER, J.; GSOTTSCHNEIDER, G.; GILS, H. J.; REBEL, H.; CORCALCIUC, V.; BASU, S. K.; BAUR, G.; RAYNAL, J.
Investigation of the sequential break-up mode $^6Li \rightarrow {}^6Li\,(3_1^+) \rightarrow \alpha + d$ of 156 MeV ^6Li projectiles on ^{208}Pb in the very forward angular hemisphere
Zeitschrift für Physik A, 339 (1991) p. 489-91

KOWALEWSKA, D.
Laserspectroscopic investigations of isotope shifts and hyperfine structure of polonium isotopes
KfK-4802 (Juni 1991)

KOWALEWSKA, D.; BEKK, K.; GÖRING, S.; HANSER, A.; KÄLBER, W.; MEISEL, G.; REBEL, H.
Isotope shifts and hyperfine structure in polonium isotopes by atomic-beam laser spectroscopy
Physical Review A, 44 (1991) R 1442-R 1445

MATUSSEK, P.; MICHEL-PIPER, I.; OTTMAR, H.
A compact K-edge densitometer for uranium
Proc. of the 13th Annual Symp. on Safeguard and Nuclear Material Management, Avignon, F, May 14-16, 1991
Luxembourg : Commission of the European Communities, 1991. p. 329-35
ESARDA-24
EUR-13686-EN

MEISEL, G.; KÄLBER, W.; RINK, J.
Verfahren zur Reduktion der spektralen Linienbreite des von angeregten und in einer Paulschen Ionenfalle elektrodynamische gespeicherten Gasionen emittierten Lichtes
DE-OS 39 11 052 (11.10.1990)
DE-PS 39 11 052 (08.07.1991)

MEISEL, G.; KÄLBER, W.; RINK, J.
Verfahren zur Reduktion der spektralen Breite von Anregungsspektrallinien
DE-OS 40 06 790 (12.09.1991)

NEMETH, Z.
Low-spin levels of $^{111, 113}Cd$
KfK-4888 (Juli 1991)

NEUBERGER, D.; KÄPPELER, F.
^{87}Rb : s-Process nucleosynthesis at N = 50
In : Cierjacks, S. [Hrsg.]
Progress Report on Nuclear Data Research in the Federal Republic of Germany for the Period April 1, 1990 to March 31, 1991
NEANDC (E)-322 U Vol. 5 (July 1991) p. 1-2
INDC (Ger)-36/LN + Special
KfK-4953

OCHS, A.; HECK, D.; SCHÄFER, H. E.; GEROK, W.
Toxic elements in tissue sections detected by proton-induced X-ray emission. (Micro-PIXE)
Graumann, W. [Hrsg.]
Histo- and Cytochemistry as a Tool in Environemental Toxicology
Stuttgart [u. a.] : Gustav Fischer Verl., 1991
p. 164-77

OTTMAR, H.; EBERLE, H.
The hybrid K-edge/K-XRF densitometer : principles - design - performance
KfK-4590 (Februar 1991)

OTTMAR, H.; EBERLE, H.; DOUBEK, N.; RAAB, W.; PARUS, J.
Analysis of Th-U, U-Pu and Pu solutions with a hybrid K-edge/XRF analyzer
Proc. of the 13th Annual Symp. on Safeguards and Nuclear Material Management, Avignon, F, May 14-16,1991
Luxembourg : Commission of the European Communities, 1991. - p. 149-57
ESARDA-24
EUR-13686-EN

OTTMAR, H.; EBERLE, H.; SCHOTT, R. M.; SALAÜN, J.; GRISON, P.; OUGIER, M.; WAGNER, H. G.; GÖRTEN, J.; BALLETTE, G.; LOUIS, P.
The use of the hybrid K-edge densitometer for routine analysis of safeguards verification samples of reprocessing input liquor
Proc. of the 13th Annual Symp. on Safegueards and Nuclear Material Management, Avignon, F, May 14-16, 1991
Luxembourg : Commission of the European Communities, 1991. - p. 337-44
ESARDA-24
EUR-13686-EN

ROKITA, E.; CICHOCKI, T.; HECK, D.; JARCZYK, L.; STRZALKOWSKI, A.
Calcification of aortic wall in cholesterol-fed rabbits
Arteriosclerosis, 87 (1991) p. 183-93

SCHATZ, H.; RUPP, G.; KÄPPELER, F.
The stellar cross sections of ^{120}Sn, ^{121}Sb, ^{123}Sb, and ^{128}Te - a study of possible s-process branchings at A = 121, 122
In: Cierjacks, S. [Hrsg.]
Progress Report on Nuclear Data Research in the Federal Republic of Germany for the Period April 1, 1990 to March 31, 1991
NEANDC (E)-322 U Vol. 5 (July 1991) p. 2-4
INDC (Ger)-36/LN + Special
KfK-4953

SUPPER, R.
Untersuchung und Erklärung des Signal-verhaltens von Flüssigkeitsionisationskammern für stark ionisierende Teilchen und Entwicklung einer Rekombinationstheorie
KfK-4666 (Dezember 91)

TEPE, M.; KÄPPELER, F.
The stellar (n, γ) cross sections of ^{192}Pt - a new constraint for the s-process
In: Cierjacks, S. [Hrsg.]
Progress Report on Nuclear Data Research in the Federal Republic of Germany for the Period April 1, 1990 to March 31, 1991
NEANDC (E)-322 U Vol. 5 (July 1991) p. 10-11
INDC (Ger)-36/LN + Special
KfK-4953

WISSHAK, K.; VOß, F.; KÄPPELER, F.; REFFO, G.
Neutron capture of $^{122, 123, 124}$Te : a critical test for s-process studies
KfK-4899 (November 1991)

WISSHAK, K.; VOß, F.; KÄPPELER, F.; REFFO, G.
Measurement of the keV neutron capture cross sections of $^{122, 123, 124, 125, 126}$Te with the Karlsruhe 4π BaF_2 detector
In: Cierjacks, S. [Hrsg.]
Progress Report on Nuclear Data Research in the Federal Republic of Germany for the Period April 1, 1990 to March 31, 1991
NEANDC (E)-322 U Vol. 5 (July 1991) p. 5-6
INDC (Ger)-36/LN + Special
KfK-4953

XIA, Y.; GERSTENHÖFER, T. W.; JAAG, S.; KÄPPELER, F.; REFFO, G.; WISSHAK, K.
Neutron capture cross sections of ^{122}T, ^{123}T, and ^{124}Te at low energies
In: Cierjacks, S. [Hrsg.]
Progress Report on Nuclear Data Research in the Federal Republic of Germany for the Period April 1, 1990 to March 31, 1991
NEANDC (E)-322 U Vol. 5 (July 1991) p. 7
INDC (Ger)-36/LN + Special
KfK-4953

ZHAO, W. R.; KÄPPELER, F.
The stellar production cross section of ^{176}Lu^{m}
Phys. Rev. C, 44 (1991) p. 506-13

ZIMMERMANN, R.; TILLMANNS,H.; BUBECK, B.; NEUMANN, F. J.; ERNST, A.; BIHL, H.; HANSER, A.; KÜBLER, W.
Non-invasive detection of reduced regional myocardial perfusion at rest in patients with unstable angina pectoris : increased regional ^{81m}Kr deposition following intravenous injection of ^{81}Rb
Nuclear Medizin, 30 (1991) p. 125-31

6.2 CONFERENCE CONTRIBUTIONS

6th Workshop on Nuclear Astrophysics, Ringberg Castle, Bad Wiessee, February 18-23, 1991

BEER, H.
Parametric s-process studies using an analytical formulation of the double pulse model

WISSHAK, K.; VOß, F.; KÄPPELER, F.; REFFO, G.
Neutron capture of ^{122,123,124}Te : a critical test for s-process studies

GALLINO, R.; BEER, H.; BUSSO, M.; CORCIONE, L.; RAITERI, C. M.
s-processing in low mass stars from the combined operation of the ^{13}C and ^{22}Ne neutron sources

Frühjahrstagung DPG, Physik der Hadronen und Kerne, Darmstadt, 11-15. März 1991
Verhandlungen der Deutschen Physikalischen Gesellschaft, R. 6, Bd. 26 (1991)

BODMANN, B.; BURTAK, F.; FINCKH, E.; HANIKA, T.; HOESSL, J.; KRETSCHMER, W.; MEYER, R.; SCHILLING, F.; MASCHUW, R.
Untergrundunterdrückung mit den Antizählern des KARMEN-Experiments

BOLZ, J.; ENGLER, J.; GILS, H. J.; KEIM, H.; MIELKE, H. H.; REBEL, H.; SUPPER, R.; ZIEGLER, P.
Untersuchungen zum Signalverhalten von Raumtemperatur-Flüssigkeitsionisationskammern

BRANCUS, I. M.; REBEL, H.; WENTZ, J.; CORCALCIUC, V.
Extended sum-rule model for dissipative processes

CORCALCIUC, V.; REBEL, H.; KIENER, J.; GSOTTSCHNEIDER, G.; GILS, H. J.; RAYNAL, J.; BAUR, G.
Analysis of the sequential break-up ^{6}Li → ^{6}Li (3_1^+) → α + d of 156 MeV ^{6}Li projectiles on ^{208}Pb observed in the very forward angle hemisphere

DENNERT, H.; ASCHENAUER, E.; EYRICH, W.; LEHMANN, A.; MOSSBURGER, M.; SCHOLZ, N.; WIRTH, H; GILS, H. J.; REBEL, H.; ZAGROMSKI, S.
Anregung der isoskalaren Monopolriesenresonanz in ^{90}Zr und ^{208}Pb durch ^{6}Li-Streuung

DENNERT, H.; EYRICH, W.; LEHMANN, A.; MOSSBURGER, M.; SCHOLZ, N.; WIRTH, H; GILS, H. J.; REBEL, H.; ZAGROMSKI, S.
Grossflächige Halbleiterstreifendetektoren zur Spektroskopie geladener Zerfallsteilchen aus der (^{6}Li, ^{6}He p)-Reaktion

KARMEN-COLLABORATION; MASCHUW, R.
Erste Ergebnisse vom Neutrinoexperiment KARMEN

MONDRY, G.; SMEND, F.; DOLL, P.; KLAGES, H. O.; SKACEL, H.
Ein szintillierendes Flüssig-Neon-Target für neutronen-induzierte Reaktionen

NEMETH, Z.; KÄPPELER, F.; REFFO, G.
^{180}Ta (γ, γ') ^{180}Ta bei 1.33 und 4.0 MeV : Konsequenzen für den s-Prozess

NEMETH, Z.
Zustände in ^{111}Cd und ^{113}Cd mit niedrigem Spin

PARLOG, M.; POPESCU, D.; WENTZ, J.; ZAGROMSKI, S.; BRANCUS, I. M.; CORCALCIUC, V.; DUMA, M.; GILS, H. J.; REBEL, H.
Intermediate-mass fragment emission induced by 104 MeV alpha particles

RINK, J.; GORSKI, B.; HANSER, A.; KÄLBER, W.; MEISEL, G.; MIELKE, H.; OGANESSIAN, Y.; REBEL, H.
Laserspektroskopie an gespeicherten Ionen in einer Paul'schen Falle

SCHOLZ, N.; DENNERT, H.; EYRICH, W.; LEHMANN, A.; MOSSBURGER, M.; WIRTH, H.; GILS, H. J.; REBEL, H.; ZAGROMSKI, S.
Anregung und Zerfall von Spin-Isospin Moden bei der Reaktion ^{12}C (^{6}Li, ^{6}He p)

WISSHAK, K.; VOß, F.; KÄPPELER, F.
Die (n, γ)-Querschnitte der Tellurisotope : ein Test für die stellare Elementsynthese

MONDRY, G.; SMED, F.; DOLL, P.; KLAGES, H. O.; SKACEL, H.
Ein szintillierendes Flüssig-Neon-Target für neutronen-induzierte Reaktionen

Frühjahrstagung DPG, Atomphysik, Massenspektrometrie, Molekülphysik, Quantenoptik, Freiburg 11-15. März 1991 Verhandlungen der Deutschen Physikalischen Gesellschaft, R. 6, Bd. 16 (1991)

RINK, J.; GORSKI, B.; HANSER, A.; KÄLBER, W.; MEISEL, G.; MIELKE, H.; OGANESSIAN, Y.; REBEL, H.
Laserspektroskopische Messungen an gespeicherten Hafnium-Ionen

Frühjahrstagung DPG, Teilchenphysik, Aachen, 12.15. März 1991 Verhandlungen der Deutschen Physikalischen Gesellschaft, R. 6, Bd. 26 (1991)

BOLZ, J.; ENGLER, J.; GILS, H. J.; KEIM, H.; REBEL, H.; SUPPER, R.; VATER, G.; ZIEGLER, P.
Signaldämpfung für stark ionisierte Teilchen in Flüssigkeitsionisationskammern

DAUMILLER, K.; DOLL, P.; KLAGES, H. O;
Untersuchungen zum Streamermechanismus

EITEL, K.; GEMMEKE, H.; MASCHUW, R.; RAPP, J.; WOLF, J.
Lischtausbeute- und Absorptionsmessungen von organischen Flüssigszintillatoren

ENGLER, J.; GETTERT, M.; KEIM, H.; KNAPP, J.; TREZECIAK, R.
Energiebestimmung von kosmischen Myonen im Bereich 1 bis 10 TeV mit Kalorimeter

ENGLER, J.; GETTERT, M.; KEIM, H.; KNAPP, J.; MIELKE, H. H.
TMS-Kalorimeter mit Fe, Pb und U-Absorbern

GABRIEL, P.; GILS, H. J.; HECK, D.; KNAPP, J.; OEHLSCHLÄGER, J.; REBEL, H.; SCHATZ, G.; THOUW, T.
Simulation von Luftschauern mit dem Programm CORSIKA

KARMEN-COLLABORATION; WÖLFLE, S.
Test und Eichung des Neutrinoexperiments KARMEN mit myoninduzierten Reaktionen

LEICH, H.; MEYER, U.; GILS, H. J.
Der Transputer-VME-Controller (TVC) für KASCADE

MAYER, H. J.; KLAGES, H. O.
Messung der myonischen Komponente von ausgedehnten Luftschauern mit dem KASCADE Array

VÖLKER, G.; BAUER, F.; DOLL, P.; GILS, H. J.; HAUNSCHILD, D.; MAYER, H. J.; KLAGES, H. O.; KRIEGLEDER, W.; KRÖNER, F.; SCHMALZ, G.; SIMONIS, J.; WETZEL, Y.
Erstes Cluster des KASCADE Detektor-Arrays, Statusbericht und erste Ergebnisse

Jahrestagung der Deutschen Gesellschaft für Nuklearmedizin, Tübingen, 11-13. April 1991

STOLL, H. P.; BAY, W.; VOGEL, W.; HANSER, A.; OBERHAUSEN, E.; SCHIEFFER, H.; HARBAUER, G.
Messung der spezifischen Myokardperfusion am isolierten Kaninchenherzen unter Verwendung von Rb-81/Kr-81m

16th General Assembly of the European Geophysical Society, Wiesbaden, April 22-26, 1991

BEER, H.
Double pulse s-process nucleosynthesis and the solar abundances

WISSHAK, K.; VOß, F.; KÄPPELER, F.
The neutron capture cross sections of Te isotopes : a test of the classical s-process model

Internat. Conf. on Nuclear Data for Science and Technology, Jülich, May 13-17, 1991

GERSTENHÖFER, T. W.; KÄPPELER, F.; WISSHAK, K.; REFFO, G.
^{147}Pm - an experimental stellar cross section for a short-lived s-process branching point

NEUBERGER, D.; TEPE, M.; KÄPPELER, F.
The stellar (n, γ) cross sections for ^{87}Rb and ^{192}Pt

WISSHAK, K.; VOß, F.; KÄPPELER, F.; REFFO, G.
Measurements of keV neutron capture cross sections of $^{122, 123, 124, 125, 126}Te$ with 4π barium fluoride detector

Proc. of a Specialists' Meeting on Neutron Cross Section Standards for the Energy Region above 20 MeV, Uppsala, S, May 21-23, 1991 NEANDC-305 U (1991) p. 13

DOLL, P.; EBERHARD, V.; FINK, G.; HANSMEYER, J.; HEERINGA, W.; KLAGES, H. O.; KRUPP, H.; WILCZYNSKI, J.; WOELFL, C.;
Status of neutron-proton scattering in the energy range from 20-70 MeV

5th Pisa Meeting on Advanced Detectors, Pisa, I, May 26-31, 1991

ENGLER, J.; GETTERT, M.; KEIM, H.; KNAPP, J.; MIELKE, H.; KAMYSHKOV, Y.; SHEVCHENKO, V.; SHMAKOV, K.
Calorimeter studies with liquid ionization chambers

Proc. of the 1st Kiev Internat. School on Nuclear Physics, Kiev, SU, May 28 - June 8, 1990 - Kiev, Nemets O. H. [Hrsg.], Naukova Dumka, 1991 p. 83-171

REBEL, H.; SRIVASTAVA, D. K.
Mechanism of Li-projectile break-up.

Workshop on Future Experiments at ISOLDE, Leysin, CH, May 29 -June 1, 1991

KÄPPELER, F.; WIESCHER, M.; KOEHLER, P. E.
Application of radioactive ion beams to s-process nucleosynthesis

Conf. on Nuclear Shapes and Nuclear Structure at Low Excitation Energies, Cargese, F, June 3-7, 1991

KOWALEWSKA, D.; BEKK, K.; GÖRING, S.; HANSER, A.; KÄLBER, W.; MEISEL, G.; REBEL, H.
Isotope shifts and hyperfine structure in polonium isotopes by atomic-beam laser spectroscopy

International Workshop on Unstable Nuclei in Astrophysics, Tokio, J, June 7-8, 1991

AGUER,P.; BAUR, G.; BIMBOT, R.; BOGAERT, G.; CLAPIER, F.; COC, A.; CORCALCIUC,V.; DISDIER, D.; FORTIER, S.; GILS, H. J.; GSOTTSCHNEIDER, G.; KIENER, J.; KRAUS, L.; LEFEBVRE, A.; LINCK, I.; PASQUIER, G.; REBEL, H.; STEPHAN, C.; TASSAN-GOT, L.; THIBAUD, J. P.
Astrophysical interesting information for the α + d and the p + ^{13}N capture reactions by the Coulomb dissociation appproach

6th Internat. Conf. on Nuclear Reactions Mechanisms, Villa Monastero, Varenna, I, June 10-15, 1991

REBEL, H.
Application of Coulomb breakup in nuclear astrophysics

Internat. Conf. on New Nuclear Physics with Advanced Techniques, Iarapetra, GR, June 23-29, 1991

KÄPPELER, F.
Astrophysics with the Karlsruhe 4π BaF_2 detector

Gordon Research Conf. 'Frontiers of Science', New London, N. H., June 24-28, 1991

REBEL, H.
The elemental composition of ultrahigh energy cosmic rays from extensive air shower studies

Joint Internat. Lepton-Photon Symp. and Europhysics Conf. on High Energy Physics, Geneve, CH, July 25 - August 1, 1991

MASCHUW, R.
Status of v-oscillations

3rd Internat. Conf. on Haemachromatosis, Düsseldorf, 25-26 July 1991

OCHS, A.; HECK, D.; SCHAEFER, H. E.; MAIER, K. P.; GEROK, W.;
Iron determination in a single histological section of liver biopsies in haemachromatosis by proton induced X-ray emission

13th Congress of the European Society of Cardiology, Amsterdam, NL, August 18-22, 1991

STOLL, H. P.; BAY, W.; VOGEL, W.; HANSER, A.; OBERHAUSEN, E.; SCHIEFFER, H.; HARBAUER, G.
Specific myocardial perfusion measured by the count rate ratio between rubidium-81 and krypton-81m in the isolated working rabbit heart

Internat. Conf. on Radioactive Nuclear Beams, Louvain-La-Neuve, B, August 19-21, 1991

WIESCHER, M.; AZUMA, R. E.; BARNES, C. A.; BEER, H.; GOERRES, J.; KÄPPELER, F.; THIELEMANN, F. K.
Capture reactions on ^{14}C in inhomogeneous big bang nucleosynthesis

KÄPPELER, F.;
Stellar (n, γ) cross sections of short-lived nuclei

Applications of Transputers 3 : Proc. of the 3rd Internat. Conf. on applications of Transputers, Glasgow, GB, August 28-30, 1991

BEKK, K.; GILS, H. J.; KEIM, H.; KLAGES, H. O.; SCHIELER, H.; LEIC, H.; MEYER, U.; SCHWENDICKE, U.; WEGNER, P.
The application of transputers in an aire shower experiment
Vol. II p. 412-17
Amsterdam [u. a.] : IOS Pr., 1991

Recent Advances in Nuclear Structure : Proc. of a Symp., Predeal, R, August 28 - September 8, 1990, Bucurescu, [Hrsg.]
Singapore [u. a.] : World Scientific, 1991
p. 479

REBEL, H.
Contemporary interest in cosmic rays. Aspects of the KASCADE project

General Conf. of the Balkan Physical Union, Thessaloniki, GR, September 26-28, 1991

BRANCUS, I. M.; REBEL, H.; WENTZ, J.
Analysis by extended sum rule model of particle emission from dissipative processes

10th Internat. School on Nuclear Physics, Varna, BG, October 14-19, 1991

KÄPPELER, F.
s-process nucleosynthesis in red giant stars

KÄPPELER, F.
Laboratory studies for the s-process

1991 Annual Fall Meeting of the APS Division of Nuclear Physics, East Lansing, Mich, October 23-27, 1991

GÖRRES, J.; WIESCHER, M.; BEER, H.; KÄPPELER, F.; KÖHLER, P.;
^{14}C (n, γ) in nonstandard big bang nucleosynthesis

Workshop on Applications of Lasers in Nuclear Physics, Dubna, SU, December 18-21, 1990, G. Ganskry [Hrsg.], Dubna 1991

MEISEL, G.; KOWALEWSKA, D.; HANSER, A.; KÄLBER, W.; REBEL, H.
Variation of the ms nuclear charge radii of polonium isotopes by atomic beam laser spectroscopy

MEISEL, G.; RINK, J.; GORSKI, B.; HANSER, A.; KÄLBER, W.; MIELKE, H.; OGANESSIAN Y.; REBEL, H.
Laser spectroscopic investigations of radioactive ions in a Paul rf trap

6.3 SEMINAR TALKS

BEER, B.
Fortschritte in der Theorie der s-Prozess Nukleosynthese und bei der Messung von stellaren Einfangraten
Vortr. :Universität Stuttgart, 27. Juni 1991

BEER, H.
New perspectives in s-process nucleosynthesis and the implications for stellar neutron capture rates
Vortr. : Central Bureau for Nuclear Measurements, Euratom, Geel, B, 29. Januar 1991

ENGLER, J.
Calorimeter configurations with Fe, Pb and U absorbers and liquid ionization chambers
Vortr. : DESY, Hamburg, 19. November 1991

GEMMEKE, H.
Neutrinophysik mit KARMEN
Vortr. : ZfK Rossendorf, Dresden, 10. Oktober 1991

GILS, H. J.
KASCADE : a detector system for the elemental analysis of high energetic cosmic rays
Vortr. : ILL, Grenoble, F, 20. März 1991

KÄPPELER, F.
Experimental studies of stellar (n, γ) rates - status and perspectives
Vortr. : Université Louvain-La-Neuve, B, 2. Mai 1991

KLAGES, H. O.
Messung und Analyse ausgedehnter Luftschauer mit dem KASCADE Detektorsystem
Vortr. : ZfK Rossendorf, Dresden, 20. Juni 1991

MASCHUW, R.
KARMEN - Neutrinophysik zwischen 5 und 50 MeV
Vortr. : DESY, Hamburg, 7. Mai 1991
Vortr. : ILL, Grenoble, F, 15 Mai 1991
Vortr. : MPI für Kernphysik, Heidelberg, 27. Juni 1991

MASCHUW, R.
KARMEN - Neutrinophysics at ISIS
Vortr. : Queen Mary and Westfield College Physics Department, 9. November 1991

MEISEL, G.; KÄLBER, W.
Genaue Heterodyn-Frequenzmessungen mit Farbstofflasern
Vortr. : Universität Heidelberg, 24. April 1991

MEISEL, G.; RINK, J.; KÄLBER, W.
Untersuchung der Kernradien radioaktiver Isotope in Ionenfallen
Vortr. : Universität Mainz, 28. November 1991

REBEL, H.
Break-up of light projectiles as a source of astrophysical information
Vortr. : Kolloquium, Universität Tübingen, 31. Januar 1991

REBEL, H.
Das KASCADE-Experiment zur Untersuchung der ultrahochenergetischen Höhenstrahlung
Kolloquium im Rahmen der AGF-Ausstellung, TU Dresden, 20. Juni 1991

REBEL, H.
Laserspectroscopic studies of nuclear structure using a Paul ion trap
Vortr. : State University of New York, Stony Brook, N. Y., 1. Juli 1991

SCHATZ, G.
Das KASCADE-Höhenstrahlexperiment
Vortr. : Universität Giessen, 24 Juni 1991

ZEITNITZ, B.
Das Neutrinoexperiment
Vortr. : HMI, Berlin, 21 Januar 1991

7. PERSONNEL

Head of the Institute, sec. IK I

Prof. Dr. B. Zeitnitz

Scientific and Technical staff:

Bauer, F.[1]

Bolz, J.[1]

Csabo, Th.

Daumiller, K.[1]

Deutsch, G., Mrs.

Dittmann, R.

Doll, P., Dr.

Drexlin, G., Dr.

Eberhard, V., Dipl.-Phys.[2]

Eitel, K., Dipl.-Phys.[2]

Engler, J., Dr.

Föller, M., Mrs.[1]

Foltin, G.[1]

Gabriel, P., Dipl.-Phys.[2]

Gemmeke, H., Prof. Dr.

Gettert, M., Dipl.-Phys.[2]

Glasstetter, R.[1]

Grandegger, W., Dipl.-Phys.[2]

Grundel, G., Mrs.

Gumbsheimer, R., Dipl.-Ing.

Hahn, A.[1]

Haunschild, D.[1]

Heneka, B., Mrs.

Hucker, H.

Hüther, H., Dipl-Ing.

Husson, L., Ing.

Keim, H., Ing.

Kern, H.

Klages, H.O., Dr.

Kleifges, M., Dipl.-Phys.[2]

Kleinfeller, J., Dr.

Knapp, J., Dr.

Kriegleder, W., Dipl.-Phys.[2]

Kröner, F.,

Maschuw, R., Dr.

Mayer, H,-J., Dr.

Mitschke, C.[1]

Mondry, G., Dr.

Müller, H., Ing.

Paulus, W.

[1] Student

[2] Graduate Student

Plischke, P. Dr.

Rämer, Chr., Mrs., Ing.

Rapp, J., Dipl.-Phys.[2]

Rininsland, A.,Mrs.

Schieler, H., Dipl.-Phys.[2]

Schmalz, G., Dipl.-Ing.

Schmidt, F.K., Dr.

Seufert, I., Mrs.

Simonis, H.-J., Dr.

Skacel, H.

Spohrer, G.

Stark, B.

Treceziak, R.[1]

Vater, G., Mrs.[1]

Völker, G., Dr.

Wetzel, Y., Mrs.[1]

Wochele, J., Dr.

Wölfle, S., Mrs., Dipl.-Phys.[2]

Wolf, J., Dipl.-Phys.[2]

Ziegler, P.

[1] Student

[2] Graduate student

Head of the Institute, sec. **IK III**

Prof. Dr. G. Schatz

Scientific and technical staff:

Antoni, I., Mrs.

Beer, H. Dr.

Bekk, K., Dr.

Bollmann, E., Dipl.-Phys.

Boschert, H.[1]

Burkhardt, S., Mrs.

Corcalciuc, V., Dr.

Eberle, H., Ing.

Emmler, J., Mrs.[1]

Engster, J.

Feurer, B.

Furler, E.[1]

Gerstenhöfer, Th., Dipl.-Phys.[2]

Gils, H.J. Priv.-Doz., Dr.

Grill, A.[1]

Gsottschneider, G.[1]

Guber, K., Dipl.-Phys.[2]

Hanser, A., Dr.

Heck, D., Dr.

Herm, F.[1]

Jaag, S.[1]

Kälber, W., Dr.

Käppeler, F., Dr.

Kaltenbaek, J.

Klay, N., Dipl.-Phys.

Kölmel, U.[1]

Kowalewska, D., Mrs, Dipl.-Phys.[2]

Kretschmer, M.[1]

Masuch, V.

Mathes, H., Dipl.-Phys.[2]

Matussek, P., Dipl.-Phys.[2]

Meisel, G., Priv.-Doz., Dr.

Michel-Piper, I., Mrs., Dipl.-Ing.

Mielke, H.[1]

Müller, H.

Müller, K.[1]

Neuberger, D.[1]

Neumann, R.[1]

Oehlschläger, J., Dipl.-Math.

Ottmar, H., Dr.

Rämer, Chr., Mrs., Dipl.-Ing.

Rebel, H., Prof. Dr.

Rink, J., Dipl.-Phys.[2]

Rupp, G.

[1] Student

[2] Graduate student

Schatz, H.[1]

Schmalz, G., Dipl.-Ing.

Schmidt, K.A., Dipl.-Phys.

Schöps, O.[1]

Schubert, M.[1]

Schulze, B., Mrs.[1]

Supper, R.[1]

Thouw, T., Dr.

Tepe, M.[1]

Völker, G., Dr.

Vos, C.[1]

Voß, F, Dr.

Weber, N.

Wentz, J., Dipl.-Phys.[2]

Wisshak, K., Dr.

Zagromski, S., Dipl.-Ing.

Zirker, A., Mrs.

[1] Student

[2] Graduate student

Guest Scientists :

Bao, Z.Y., Mrs., Prof. Dr.

Brady, P., Prof. Dr.

Brâncuş, I.M., Mrs., Dr.

Capdevielle, J.N., Prof. Dr.

Duma, M., Dipl.-Math.

Fomin, Yu., Prof. Dr.

Gangrsky, Yu, Prof. Dr.

Gorski, B., Mrs., Dr.

Kalmykov, N.N., Dr.

Kazakov, L., Dr.

Khrenov, B., Dr.

Koehler, P., Dr.

Koepernik, H., Dipl.-Ing.

Kornilov, N., Dr.

Miller, W., Ing.

Nemeth, Z., Dr.

Ostapchenko, S.S., Dr.

Pârlog, M., Dr.

Pascovici. G., Dr.

Petcu, M., Dipl.-Ing.

Proehl, D., Dr.

Trautvetter, H.-P., Prof. Dr.

Vedeneev O., Dr.

Wdowczyk, J., Prof. Dr.

Wegner, P., Dr.

Wibig, T., Dr.

Wiescher, M., Prof. Dr.

Wolf, A., Dr.

Xia, Y., Prof. Dr.

Zabierovski, J., Dr.

Zemlyanoi, S., Dr.

Zimmer, K.W., Dr.